Jet A Explosion Experiments: Laboratory Testing

Joseph E. Shepherd, J. Christopher Krok, and Julian J. Lee

Graduate Aeronautical Laboratories
California Institute of Technology
Pasadena, CA 91125

June 26, 1997 corrected on November 21, 1997

Explosion Dynamics Laboratory Report FM97-5

Prepared for and supported by the National Transportation Safety Board
Under Order NTSB12-97-SP-0127

Contents

List of Figures

List of Tables

1 Introduction

This report describes a series of experiments and analyses on the flammability of Jet A (aviation kerosene) in air. This is a progress report on ongoing work. The emphasis so far has been on measuring basic explosion parameters as a function of fuel amount and temperature. These parameters include vapor pressure, flammability limits, peak explosion pressure and pressure as a function of time during the explosion. These measurements were undertaken in order to clear up some fundamental issues with the existing data.

The report is organized as follows: First, we give some background with data from previous studies and discuss the fuel weathering issues. Second, we describe the facility used to do combustion experiments, the combustion test procedures and the results of the combustion experiments. Third, we give estimates of peak pressure, review the standard analysis of pressure histories and discuss the application to the present data. Fourth, we review the standard approach to flammability limits and the issues in determining Jet A flammability. Fifth, we discuss the problems associated with measuring vapor pressure and describe our results for Jet A. Sixth, we present a model for Jet A which illustrates the issues in analyzing multicomponent fuels. Finally, we apply these results to TWA 800 and summarize our conclusions to date.

2 Airplane Fuel Tank Explosions

The TWA 800 crash investigation is focusing on an explosion in the center fuel tank as a primary event in initiating the structural failure of the airplane. The Center Wing Tank (CWT) on a 747-100 is located within the fuselage between the wings, see Fig. 1. The upper and lower surfaces of the tank are extensions of the wing's upper and lower skin. The tank is approximately 21.25-ft (6.48 m) wide, 20.17-ft (6.15 m) long and 4 to 6.5-ft (1.2 to 1.65 m) high. Wing structural members, three spars and three spanwise beams, form the vertical surfaces that bound the tank and divide it into four compartments and a dry bay, see Fig. 2. The two rear compartments are further divided by a partial rib in the center of the structure. The total volume of the fuel-containing portion of the tank is about 50 m^3. The volumes of compartments containing fuel range from 4.9 to 15.4 m^3. The compartments communicate through a number of penetrations through the beams, spars and partial ribs. The total area of the communicating passageways between compartments ranges from 4.8×10^{-4} m^2 to 6.98×10^{-2} m^2. On some flights, this tank is often empty except for whatever residual fuel (50 to 100 gal) remains from the previous use. This was the case in TWA 800. The tank is vented to the atmosphere and the volume of the tank above the fuel (ullage) contains mainly air. The vaporization and mixing of the residual fuel into this air can result in the formation of an explosive mixture within the tank.

A main concern is the range of conditions under which Jet A-air mixtures can be ignited, i.e., are flammable. The standard method for describing flammability of aviation fuel is to use spark ignition sources in laboratory experiments to determine the altitude (pressure) and temperature boundaries for flame propagation. The results of previous

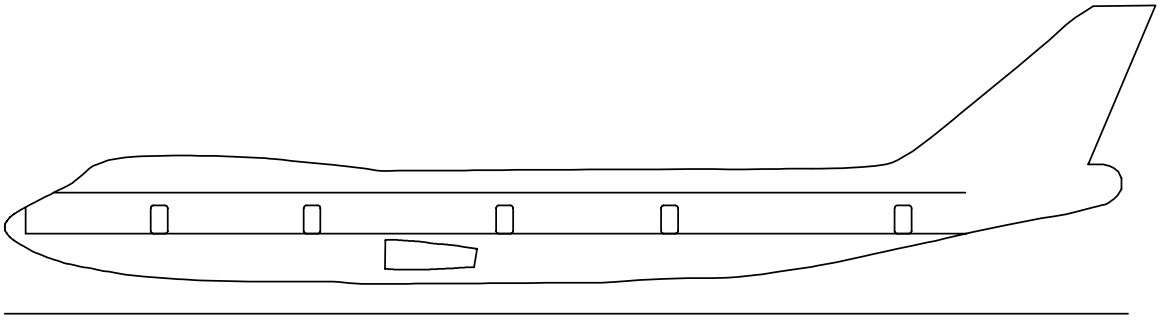

Figure 1: Schematic of 747-100 showing the location of Center Wing Tank.

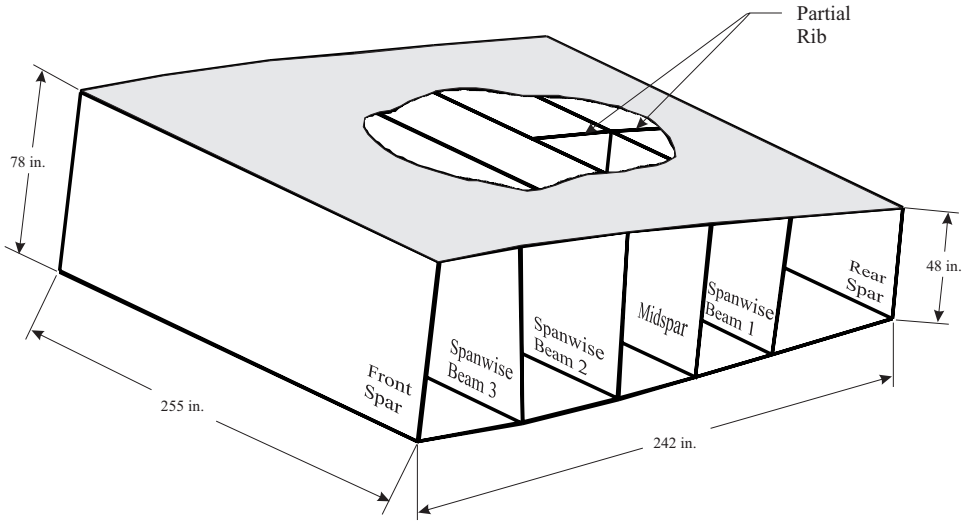

Figure 2: Perspective view of Center Wing Tank.

tests (described in detail in the next section) are summarized in Fig. 3. Mixtures within the shaded region between the solid lines are considered flammable. The static tests are carried out in situations for which the fuel vapor is created by evaporation of a large, stagnant mass of fuel into the air in the ullage. The air, fuel vapor and fuel liquid are all at a common temperature. In dynamic tests, the fuel tank is vibrated, resulting in fuel suspended as a mist, lowering the lean limit to the dashed line.

If the temperature is sufficiently high (above 35°C), then the mixture will be flammable. As discussed below, this appears to be the case in TWA 800. However, there are several problems with this representation of the flammability limit and its application to situations such as TWA 800. The contents of the tank in a climbing aircraft are not in equilibrium. In TWA 800, a very limited mass of fuel was present in the tank, rather than the large amounts considered in previous flammability tests. The residual fuel in the CWT of TWA 800 was subjected to extensive environmental effects, i.e., varying temperature and pressure, over the previous 15 hours. The fuel, air and surfaces of the CWT were all at different temperatures due to the presence of a large heat source under

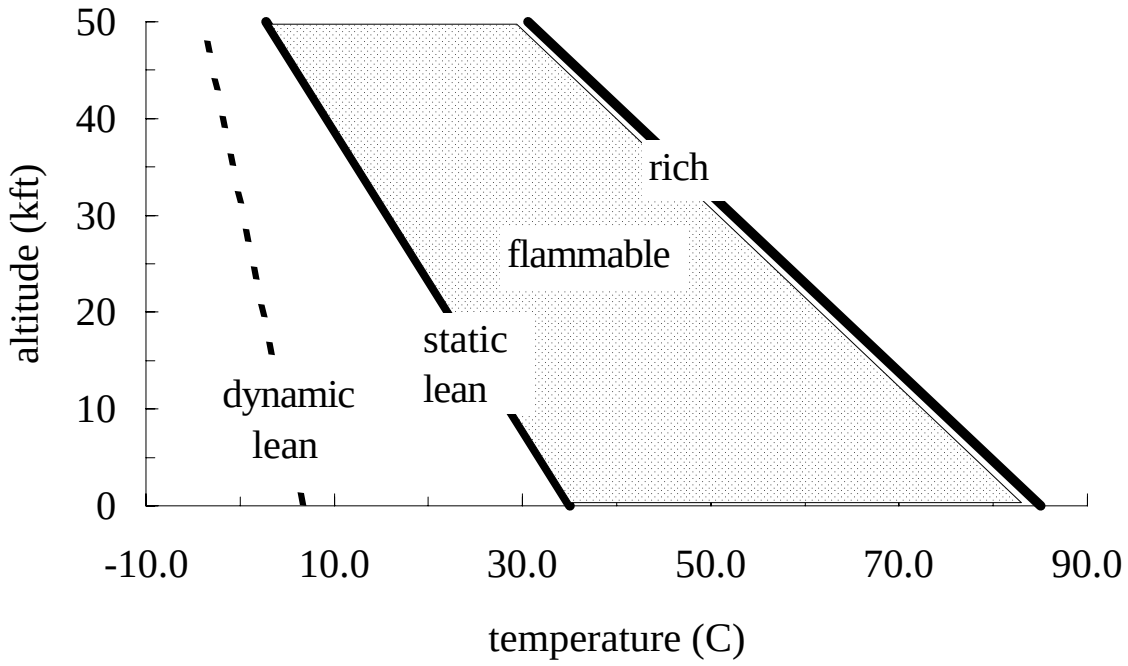

Figure 3: Flammability limits of Jet A in air in the standard representation of temperature vs altitude (CRC 1983).

the CWT. Each of these issues is discussed in this report.

2.1 Previous Studies

Although there are many reports on aircraft fire and explosion (Kuchta 1973, Kuchta 1975, Kuchta and Clodfelter 1985, Moussa et al. 1996, Moussa 1990), there is a limited amount of fundamental flammability data on Jet A. There is meager data in the standard references (Kuchta 1985, Zabetakis 1965) on explosion properties and much of the data cited in the industry standard publication (CRC 1983) is without direct attribution. All of the combustion data on Jet A appear to derive from three technical reports: Nestor (1967); Ott (1970); Kosvic et al. (1971).

Nestor (1967) and Ott (1970) both carried out experiments on the flammability of Jet A in air at various temperatures and pressures. The effects of altitude are simulated by varying the pressure within the fuel tank. Airplane fuel tanks are vented and the pressure within the tank is close to the ambient pressure, see Figs. 6 and 5 for the relationships between altitude and atmospheric temperature and pressure. Kosvic et al. (1971) carried out experiments on measuring composition of fuel vapor in the ullage (vapor volume) at various temperatures and pressures. Our test results are generally consistent with all of these but it is worthwhile examining each set of tests in more detail.

Nestor carried out the most extensive and careful work on the flammability of Jet A. He used two facilities to determine flammability limits and peak explosion pressures.

Limits to upward flame propagation were studied in a 4-in. diameter, 4-ft. long tube. A mixture was considered flammable if the flame propagated the entire length of tube.

Nestor's experiments were carried out with an ullage that was 87.5% of the total volume of the facility. Multiple electric sparks with energies of 5 and 20 J were used to initiate combustion. Three batches of Jet A were examined. Flammability limit pressures were found as a function of temperature (Fig. 4a, b). At sea level (1 bar), the mixtures were found to be flammable between 89 and 100°F (31.7 to 37.8°C). This range of temperatures is due to the variability between fuel batches. At a pressure equivalent to 15 kft, the mixtures were found to be flammable between 75 and 85°F (23.9 to 29.4°C). Although flammability limits did depend on the batch of fuel, they did not appear particularly sensitive to how the fuel was handled.

Nestor used a 2-1/2 gal. tank (9-in. diam. and 15-in high) to examine the effects of vibration and sloshing of the fuel. A 16 to 24 J spark ignition source was used above the surface of the liquid fuel and the fuel tank was vibrated at 15 Hz with an amplitude of 1/8-in. If the ignition sparks were outside the spray and mist produced by the motion of the fuel, there was no noticeable effect on the flammability limits. If the ignition sparks were inside the spray region, then a marked extension of the flammability limit occured. On the lean side, the temperatures could be decreased to 54°F (12.2°C) at sea level and ignition was still obtained.

Nestor used a pressure rise of about 4 psi (0.27 bar) as a flammability criterion. Pressure rises of up to 40 psi (2.72 bar) were observed near the "static" flammability limit temperature at sea level when spray combustion occurred. The "static" vessel data (Fig. 4c) are similar to the flame tube data (Fig. 4b) but the temperature limits are lower in the vessel than in the tube. There is substantial scatter in Nestor's "dynamic" data for peak pressure (see his Figs. 13 and 23). Data from different initial pressures have been combined on a single plot but the temperature axis has been scaled to reflect differences from a nominal flammability limit temperature. Presenting the data in this fashion, a unique upper bound to the peak pressure is not apparent as it is in Ott's presentation. The raw data is not given so it is impossible to reanalyze the data for trends in the peak pressure with initial temperature.

Ott's study is more useful from the viewpoint of peak pressure prediction. Ott used an 80 gallon tank (20-in diam and 60-in long) mounted horizontally on a slosh-vibration table. About 10 gallons of fuel (JP-8) were placed in the bottom of the tank and used for a number (2 to 8) of tests. His ignitor was a furnace system consisting of a high-voltage transformer that produced a moving arc (Jacob's ladder) between two 12-in long electrodes. Mixtures of JP-8 with air were determined to become flammable between 110 and 120°F (43.3 and 48.9°C) at sea level. At 8 psi (0.544 bar), the limiting temperature was between 90 and 95°F (32.2 and 35.0°C). Data for other pressures is not given explicitly, but can be deduced from his Fig. 7 and are consistently higher (Fig. 4d) than Nestor's data.

Ott found that sloshing decreased the flammability limit temperature from 110-120°F (43.3-48.9°C) to as low as 55-60°F (12.8-15.6°C). The maximum values of the peak pressure were bounded by a single curve that was proportional to the estimated vapor pres-

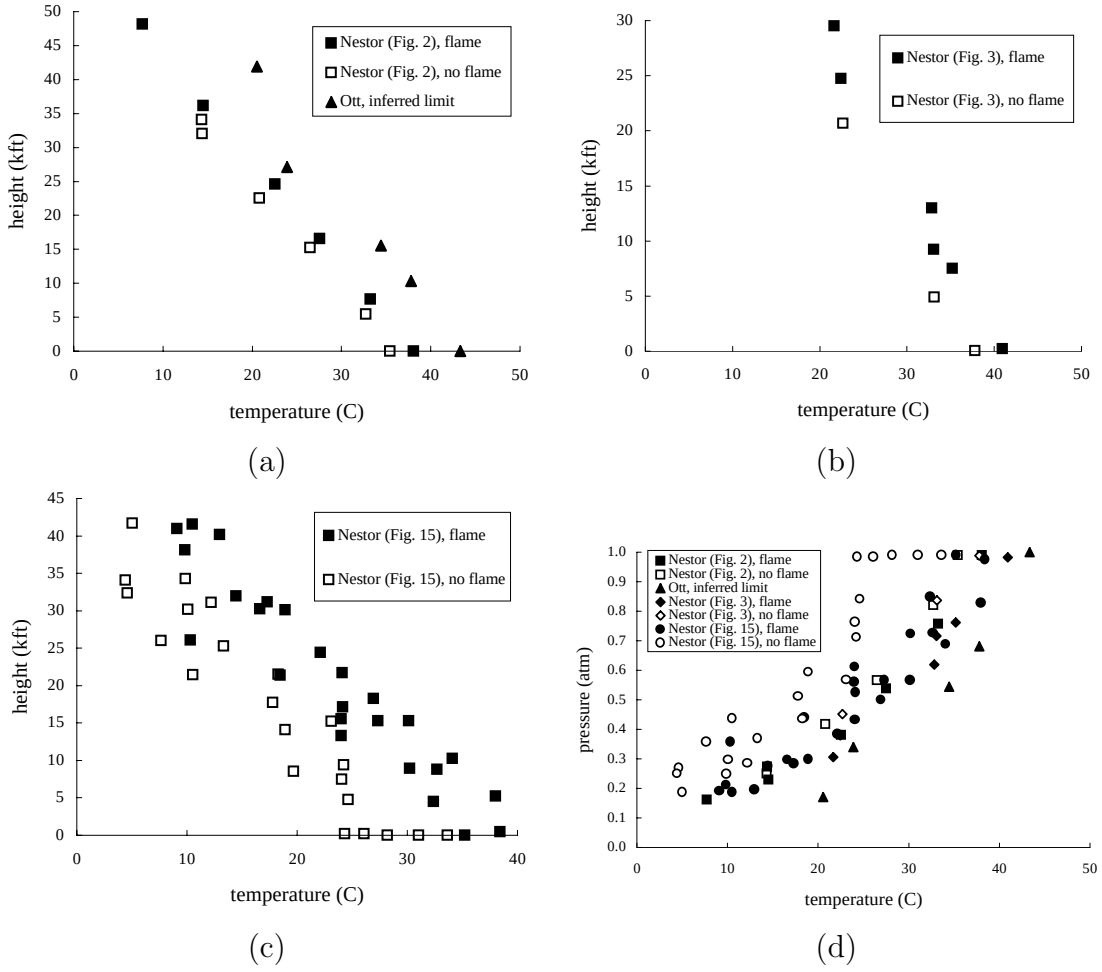

Figure 4: Lower (lean) flammability limits as determined by Nestor (1967). (a) Jet A tests with flammability limit tube (Fig. 2 of Nestor and Fig. 7 of Ott) (b) Jet A-1, batch 1 tests with flammability limit tube (Fig. 3 of Nestor) (c) Jet A-1, batch 2 tests with flammability limit vessel, static conditions (Fig. 15 of Nestor) (d) Comparison between Nestor and Ott limits in P-T coordinates.

sure. The peak change in pressure was apparently independent of the initial pressure in the tank. At 100°F (37.8°C), a peak pressure change of approximately 40 psi (2.72 bar) was observed.

Kosvic et al. (1971) used a 110 gallon tank (2-ft diam. and 5-ft long) containing 50 gallons of fuel. They studied the effect of altitude changes and fuel temperature on the vapor composition in the ullage. No combustion experiments were carried out but the gas concentration (in terms of total hydrocarbon content) was measured using a gas chromatograph with a flame ionization detector. The gas concentrations were measured as a function of time during simulated climbs at a rate of 2000 ft/min. Two key conclusions were: a) the ullage above the liquid Jet A would be flammable at sea

level at a temperature of 120°F; b) the vapor concentration would remain close to the "equilibrium" value for a climb or descent rate of 2000 ft/min. At sea level, a fuel/air mass ratio between .06 and .07 was measured for a fuel temperature of 120°F (48.9°C). At 14 kft, a fuel/air mass ratio of about 0.14 was measured for a fuel temperature of 120°F. These can be compared with their estimated flammability limits (fuel/air mass ratio) of 0.035 (lean) and 0.29 (rich). For reference, the stoichiometric ratio is in the range of 0.065 to 0.076 for typical hydrocarbon fuels (see the subsequent discussion on peak pressure).

We conclude that there is substantial variability in the measured flammability limits of Jet A. In terms of temperature conditions, Nestor's limits are lower than Ott's and the lower flammability limit is between and 38°C at sea level, 24 and 29°C at 15 kft. In order to interpret these in terms of mass or mole fraction, some assumptions about molar mass and vapor pressure have to be made, see Section 5. The presence of a mist extends the lower limit to much lower liquid temperatures if the igniter is located in the mist. Our observations of propagating flames in vapor-air mixtures at 40°C and 0.585 bar are consistent with the flammability limits obtained by Ott and Nestor. In the present phase of the study we have not systematically hunted for the lean limit but it is clearly at temperatures less than 40°C at a pressure of 0.585 bar.

All three authors note that the vapor composition and mean molar mass will be a function of temperature but did not quantify these effects. They also stated that the ratio of fuel mass to tank volume will have some influence on the vapor composition but did not study this issue either. These are key issues for interpreting the present experiments and understanding combustion in nearly empty fuel tanks.

2.2 Flight conditioning or "Weathering"

Fuel in an airplane is exposed to a range of conditions during flight. The pressure and the temperature in the atmosphere are a function of altitude as shown in Figs. 5 and 6. The pressure within the fuel tank is slightly less than ambient (the pressure differential is about .25 psi) when cruising since the vents are located in a low pressure region on the wing tips. The temperature of the fuel and vapor depends on the rate of heat transfer to the fuel from the surroundings. The fuel temperature is not normally measured in flight but can be estimated from a heat transfer model or measured in a special flight test. A heat transfer model must include heat transfer from the heated cabin (nominally at 70°F), heat transfer from the air packs (air cycle machines or ACM), heat losses through the rear spar to the ambient atmosphere in the wheel well, and heat transfer through the side-of-body ribs from the adjacent fuel in the wing. The amount of fuel in the tank, the rate at which fuel is removed and the rate of climb or descent are additional factors that must be considered in addition to the properties of the particular batch of fuel.

The effect of airplane operation on the fuel is important to address for the TWA 800 situation. The key question is: What was the composition and concentration of fuel vapor within the tank at the time of the explosion? The answer apparently depends on the entire history of the fuel up to the time of the explosion. There are four important

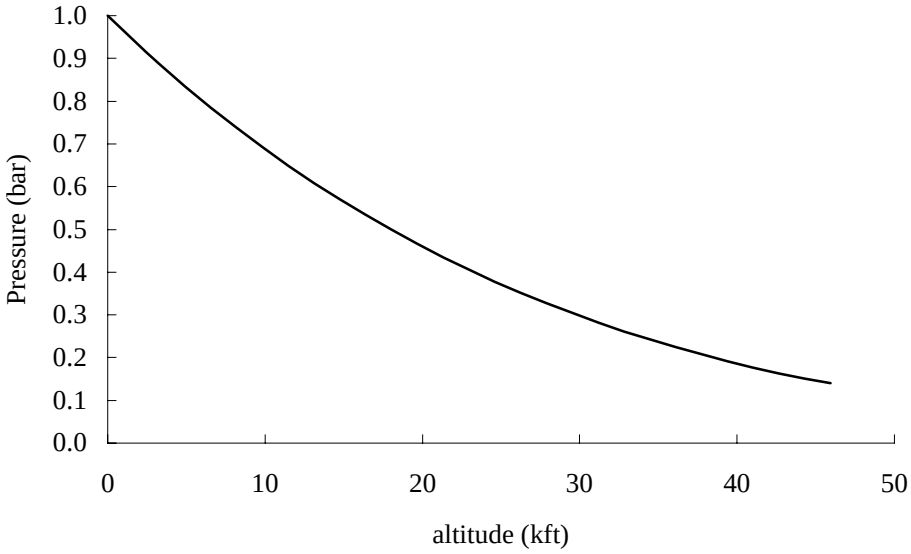

Figure 5: Pressure vs altitude, standard atmosphere.

aspects to this history of the fuel: 1) the properties of the batch of fuel loaded in Athens; 2) the effect of the flight from Athens; 3) the effect of ground operations at JFK airport in NY; 4) the effect of the climb up to 14 kft, where the explosion took place. The nominal history of the key CWT fuel parameters: pressure, temperature, and mass; are shown in Figs. 7-9. Note that the fuel temperature history is mainly conjecture at this point.

Samples of the fuel loaded at Athens have been examined by the NTSB. It has a flash point of 113°F (45°C) which is within the range usually reported for Jet A (see the subsequent discussion on flammability). Further characterization of the fuel is in progress.

The flight from Athens took about 10 hours and for most of this time, the airplane was at cruising altitude of 33 to 35 kft. The fuel in the center wing rank (CWT) was consumed first, and after the first several hours, it is believed that only 300 lb or slightly less than 50 gallons[1] remained in the tank. The temperature in the air at cruising altitude is quite low (-50°C), however the temperature in the tank is expected to be much higher due to the heat load from the ACMs, which can increase the air temperature under the CWT up to 150°F. The underside of the CWT is not insulated.

Nestor and Ott carried out a limited study of the effect of flight conditioning, i.e., cycling the fuel from sea level to 35 kft and back again. However, this was done with very large mass to volume ratios and prolonged exposure to high or low temperatures was not considered. The fuel was aged in a vented tank for four months and retested. There was no noticeable effect of aging but it is unclear how much vapor loss would occur in the configuration used in these tests. The experiments of Kosvic et al. indicate that when large fuel loadings are used, the fuel vapor concentration rapidly adjusts to changes

[1]The mass density of Jet A is nominally 6.74 lb/gal.

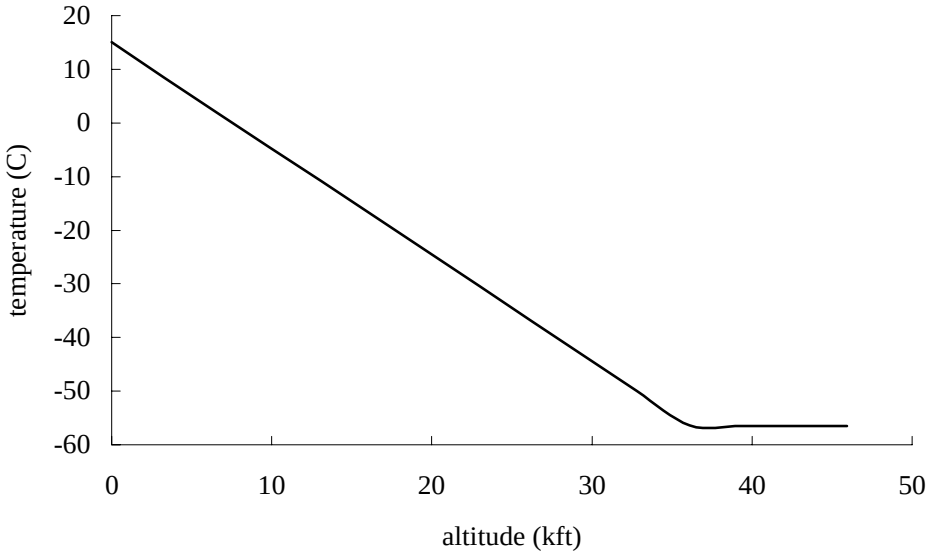

Figure 6: Temperature vs altitude, standard atmosphere.

Figure 7: Nominal fuel pressure history for TWA 800 CWT.

in pressure. Kosvic et al. developed a computer simulation to model the effects of fuel withdrawal, heat transfer, dissolved air, fuel evaporation and altitude changes to predict the fuel-air ratio within the fuel tank ullage. However, experiments indicate much more rapid equilibration than the models predict.

The CWT was not refilled at JFK and the airplane was on the ground for about 5 hours, 2 of this in a "gate hold". For some fraction of this time, one or more of the ACMs were operating. Fifty gallons in the CWT corresponds to a layer 3/16-in thick if spread uniformly over the bottom of the CWT. However, due to the varying elevation of the tank floor, the fuel was probably localized in a deeper puddle near the center of the tank. During the climb up in altitude after takeoff, the plane is at an angle of about 6° and

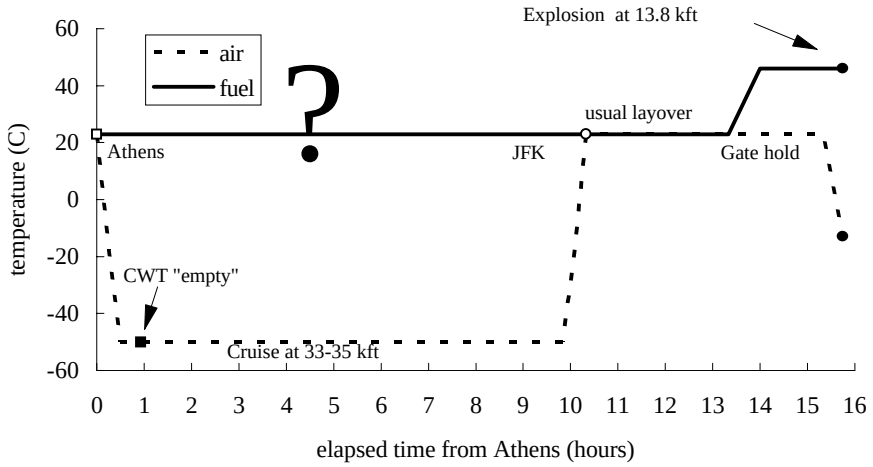

Figure 8: Conjectured fuel temperature history for TWA 800 CWT.

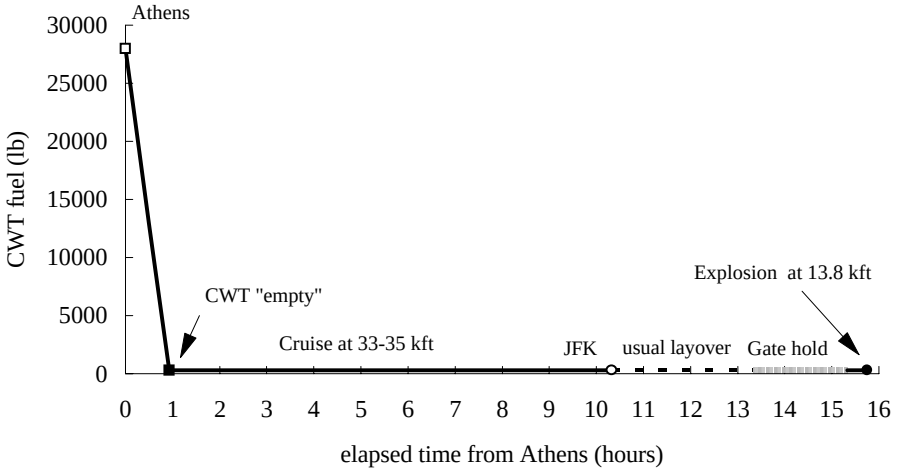

Figure 9: Nominal fuel mass history for TWA 800 CWT.

fuel moves to the rear of the tank to form a layer with a maximum thickness of about 4 in. at the rear spar. Preliminary flight tests indicate that the fuel temperature can reach 115°F (46.1°C) due to heating by the ACMs. The temperatures of the tank walls are lower due to the thermal mass of the adjacent fuel in the wing tanks and the top surface of the tank is cooler due to heat transfer from the cabin air conditioning system. These nonuniform conditions complicate determining the effective fuel concentration and composition within the tank. This is considered in more detail in Section 10.

The airplane was climbing at approximately 1000 ft/min after takeoff from JFK. As the pressure decreases within the CWT, air and fuel vapor flows out of the tank vents. There are four vents within the tank, two from the rear compartments and two in the front, see Fig. 10. At an altitude of 14 kft, the pressure is about .585 bar (8.6 psi) and approximately 40% of the fuel-air mixture originally in the tank ullage at sea level was

been vented. However, vapor will evaporate from the hot fuel to replace the vapor that is being vented. In addition, as the fuel-air mixture is vented from the tank, the remaining gas expands and cools. Heat transfer from the warm walls and hot lower surface compete with this cooling process. The preliminary flight test measurements indicate that the heat transfer between the tank and the fuel-air mixture is very efficient. As a consequence of both the nonuniform state of the tank and the rate processes associated with venting, the resulting locus of conditions within the CWT ullage during the climb cannot be represented in the conventional flammability diagram (Fig. 3).

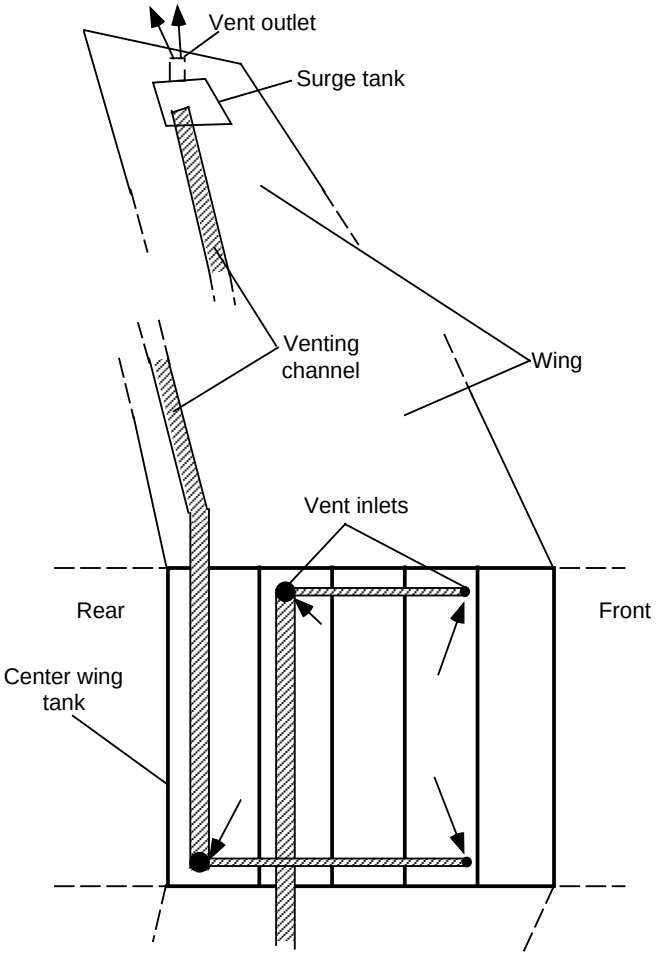

Figure 10: Schematic of 747-100 CWT venting arrangement.

A better representation of the ullage conditions can be obtained by considering the fuel/air mass ratio in the ullage. As mentioned above, a mixture is considered flammable if this ratio exceeds a minimum value, equal to about 0.019 to 0.026 for Jet A. This value is relatively independent of the fuel-air mixture temperature and pressure. Since fuel vapor and air are vented in equal proportions during the climb, this ratio remains unchanged if the fuel evaporation and mixing occur slowly compared to the venting process. The other extreme is if the fuel evaporation and mixing occur rapidly compared to the venting

process, then the fuel-air ratio will increase with increasing altitude. These two extremes are shown on Fig. 11. Hence if the evaporation occurs rapidly, the mixture may change from an inert condition to a flammable one with an increase in altitude. This situation may have occured in TWA 800.

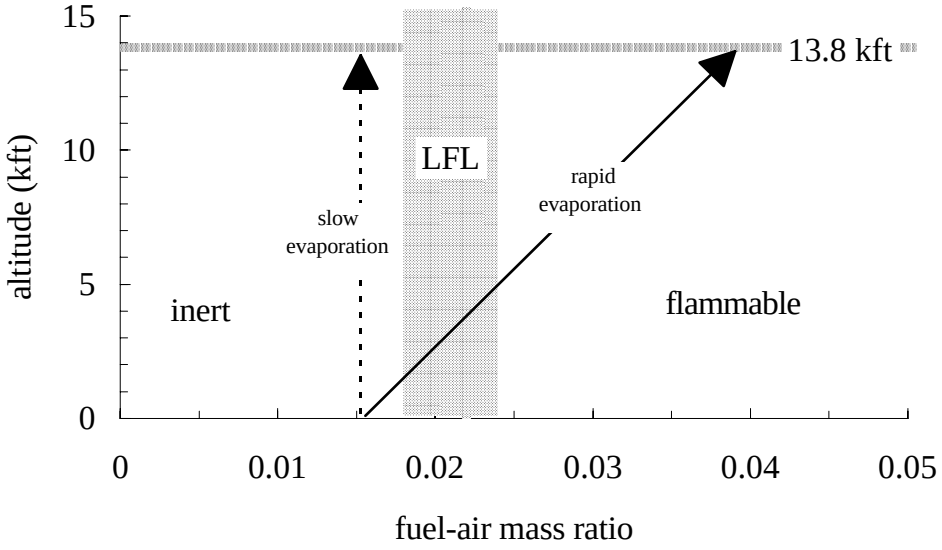

Figure 11: Flammability limit and possible ullage states during the climb of TWA 800.

At present, the issues relating to fuel temperature, flight conditioning and venting during climb are unresolved. There are several steps that must be taken in order to complete the analysis of the ullage condition at the time of the explosion. First, the temperature history of the fuel must be defined through flight test measurements and analysis of the thermal environment in the tank. Second, the effect of flight conditioning and evaporation during the gate hold must be determined through laboratory flammability experiments with fuel conditioned by the appropriate environmental changes. Third, the effect of venting must be examined through a combination of experiment and analysis. Finally, combustion testing must be carried out using parameters that correspond to the conditions in TWA 800. In the next section we describe combustion experiments designed to examine one of these parameters, the limited fuel mass present in the tank.

3 Combustion Testing

We have carried out experiments in the HYJET explosion test facility located in the Graduate Aeronautical Laboratories, California Institute of Technology.

3.1 HYJET Facility

The HYJET experimental facility is built around two pressure vessels, as shown in Fig. 12. The driver vessel has a 127-mm (5 in) inner diameter and is approximately 1.8-m (72

in) long (including the extension into the receiver vessel), with a volume of 0.028 m^3. The receiver vessel is a 0.86-m (34 in) internal diameter cylinder closed by semi-elliptical heads, with a length of approximately 1.6 m (64 in) between head seams and a volume of 1.18 m^3. Both vessels are of heavy construction, rated to withstand internal pressures of up to 70 bar (1030 psi). The receiver vessel is equipped with electrical heaters and digital controllers that enable the temperature of the receiver to be adjusted between room temperature and about 100°C.

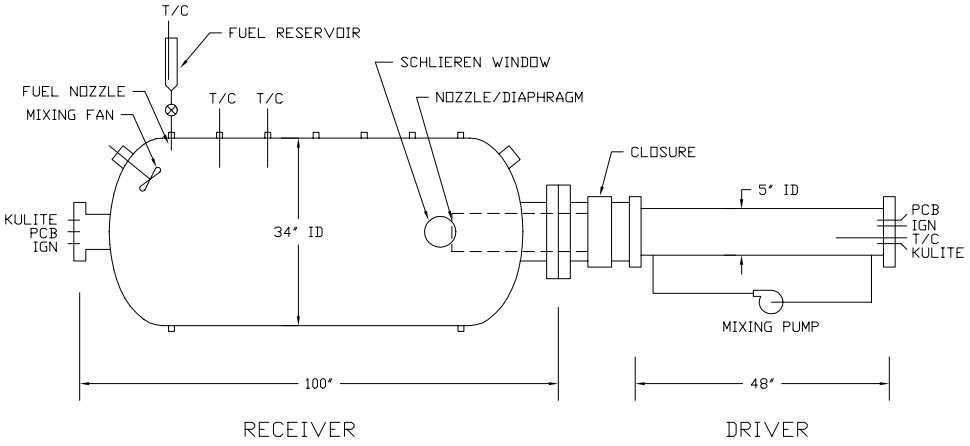

Figure 12: Elevation view of HYJET facility.

The driver vessel is used as a jet or torch igniter[2] in the present tests. A mixture of hydrogen and air or hydrogen and oxygen is ignited by an electrical spark to produce a torch of hot products, which ignites the mixture in the receiver tank. Such a torch is an extremely effective ignition source and eliminates problems with inadequate ignition energy that often arise in flammability limit testing with electrical igniters. The small volume of the driver vessel relative to the receiver ensures that negligible pressure rise in the receiver occurs due to the flow of gas from the driver into the receiver. This makes it very easy to identify when combustion takes place. An example of the pressure signals in the driver and receiver are shown in Fig. 13 for a case in which combustion was successfully initiated.

The torch enters the receiver when the combustion in the driver ruptures a membrane or diaphragm that initially separates the driver and the receiver vessels. The diaphragm and nozzle used to control the size of the torch are located at the end of the driver, which protrudes about 0.l63 m (25 in) into the tank. A removable nozzle adapter/diaphragm holder is located at the end of the driver. Six nozzle diameters from 6.35 to 92 mm (0.25 to 3.625 in) are available. The diaphragms used in these tests are 0.125-mm (0.005 in) thick mylar. When the facility is closed, the end of the driver is located so it can be observed by the schlieren system through 118-mm (4-5/8 in) diameter windows in the side of the tank (see Fig. 14).

[2]Other ignition sources will be tested in a subsequent phase of these experiments.

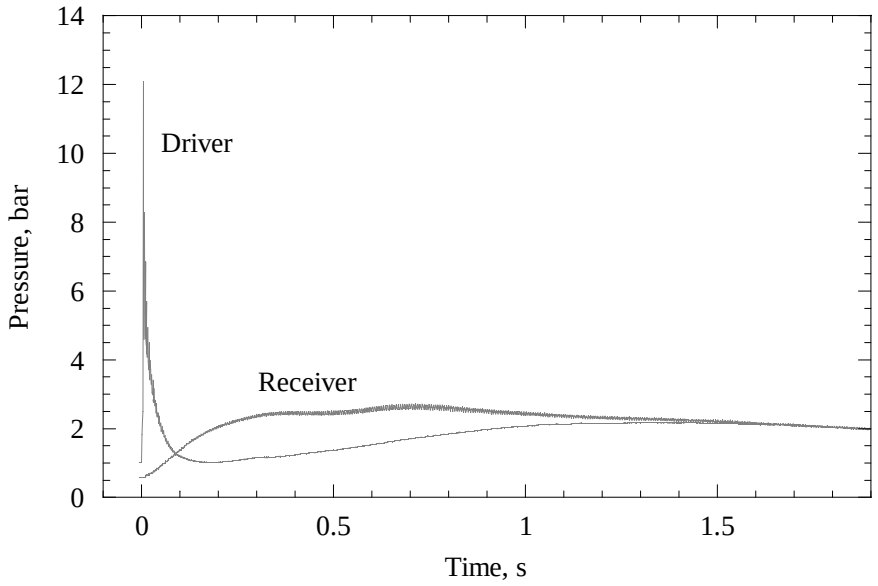

Figure 13: Pressure signals in the driver and receiver for test 305. Successful initiation of combustion, 300 ml of Jet A, 40°C.

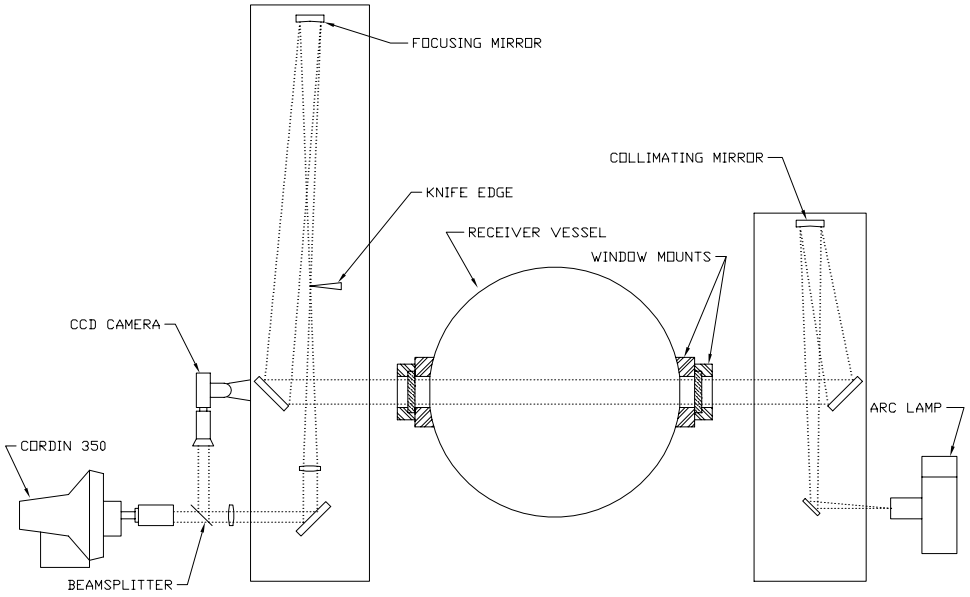

Figure 14: Plan view of HYJET facility, illustrating light path for schlieren system.

The driver and receiver vessels are instrumented with pressure and temperature transducers. The pressure transducers are Kulite brand strain gauge instruments with a thermal protection system constructed of sintered metal. The temperature transducers are type-K thermocouples. The thermocouple bead is rather large so that these measurements are not indicative of true gas temperature and are only used to evaluate the presence or absence of combustion. Data are recorded on a PC-based data acquisition

system after being amplified and filtered. Typical acquisition rates are 10^3 Hz and data are recorded for about 4 s. The schlieren system uses a continuous arc-lamp source. After passing through the optical system, the image is split between a Pullnix CCD video camera and a Cordin 350 framing camera. In the present tests, the windows were often covered with soot and only low-contrast video recordings were obtained in many cases.

3.2 Test Conditions, Procedures, and Results

The test procedure is to install the mylar diaphragm, evacuate both vessels and then fill to the desired gas composition using partial pressures as measured by precision mechanical gauges (Heise). A circulation pump is used to mix the gases in the driver and a 16-inch diameter, two-bladed fan is used to stir the contents of the receiver tank. The pump and fan are turned off before igniting the mixture in the driver vessel.

In the present tests, the liquid fuel, either kerosene or Jet A, was injected into the receiver tank through a commercial simplex atomizer (McMaster-Carr Part No. 3178K41). A few preliminary tests were done without an atomizer. The fuel is contained in a small vessel constructed of a short length of commercial pipe that is electrically heated. A quick-release coupling and a valve on the liquid container allow the liquid supply to be connected and disconnected from the receiver multiple times during the experiment. In this fashion, arbitrary amounts of fuel can be injected even though the capacity of the container is limited to about 140 ml. The fuel volume was measured with a graduated cylinder at room temperature, about 22°C. The fuel mass density was measured by weighing a sample of known volume and found to be approximately 0.80 g/cm^3 for both kerosene and Jet A at room temperature.

Testing with kerosene determined that the maximum injection time required to disperse a quantity of 100 ml was about 2 min, and examination of the container after this time revealed that very little fuel (less than 2 ml) remained behind. We do not have any data or measurements of the droplet size created by the nozzle but we would characterize it as a very fine mist. The exit diameter of the nozzle was measured to be 450 μm (0.018 in). Using the correlation of Lefebvre (1983), we estimate the Sauter mean diameter (SMD) of the droplets to be 25 μm.

The temperature of the pipe and the fuel are measured with type-K thermocouples and an Omega indicator with an electronic ice point. The power to the heaters is manually adjusted with a variable transformer. Compressed air (90 psi) is used to force the liquid fuel through the nozzle. The liquid fuel was either hardware store kerosene (ASTM D 3699 1-K grade) or Jet A obtained from LAX. Two samples of Jet A were used, both were drawn at random from available stores.

Detailed test conditions, peak pressures, liquid amounts, driver composition and driver jet nozzle sizes are given in Table 4 of Appendix A. Various driver mixtures were used in the course of these tests. Some preliminary work was done with stoichiometric H_2-air mixtures and later studies used rich H_2-O_2 mixtures. Various size driver jet nozzles were also used in an effort to ignite near limit mixtures. The effectiveness of the driver was optimized by using rich driver mixtures when the receiver contained a lean mixture

and lean driver mixtures when the receiver contained a rich mixture.

We have carried out several series of tests to explore the issues related to flammability in Jet A and kerosene. Each of the various test series are described in detail in subsequent sections.

3.2.1 Preliminary Tests

Tests 197 to 205 of Table 4 were exploratory and were carried out to determine the feasibility of doing tests with kerosene and Jet A in the HYJET facility. The fuel was heated to a high temperature (over 100°C) and injected into the tank through a 1/2-inch opening without any atomization. We have mentioned these tests only to indicate the nature of the data and no further analyses of these results will be presented.

Tests 206 to 231 were part of another test program. Tests 232 to 253 should also be considered as preliminary. During these tests, the effect of using different composition drivers, driver jet nozzle size and fuel type were examined. Many of these tests were carried out with kerosene. These tests indicated that at low temperatures substantial differences in combustion behavior were found between kerosene and Jet A. Tests 254 and later used either kerosene at high temperatures or Jet A.

Tests 232 and later (except 268 and 269) were carried out with the simplex atomizer and regulated fuel temperatures. The condition of the fuel within the tank was not as well characterized in tests 232 to 253 as it was in later tests. The procedure in 232 to 253 was to inject the fuel with the mixing fan on, continue to mix for 10 min and then to ignite while the fan was operating. Apparently this resulted in some fraction of the fuel being suspended as a mist since for Jet A, higher peak pressures were obtained in tests 250 to 253 than in later tests (269 to 274) in which a much longer time (30-40 min) elapsed between injection and ignition.

Comparison of results with Jet A (252 and 253) and kerosene (245 and 246) at 40°C indicates that higher peak pressures were obtained with kerosene under these test conditions. Pressure traces from two tests (245 and 246) with kerosene are shown in Fig. 15. The substantially higher peak pressures (1.5 to 3 bar) in comparison with Jet A (1 bar) indicate that much more mass of fuel is participating in the combustion in the case of kerosene than in Jet A. This suggests that the vapor pressure of kerosene is higher than Jet A at temperatures less than 60 to 80°C. Less likely are gross differences in liquid behavior (viscosity, surface tension) that would result in aerosol drop size differences. On the other hand, at a temperature of 100°C, essentially identical peak pressures are obtained, indicating that the energy released from hardware-store kerosene and Jet A is very similar.

3.2.2 Tests at 100°C

Tests 254 to 265 used kerosene; tests 288 to 300 used Jet A. In these tests, the fuel and air were both at 100°C and at a pressure of 0.585 bar. The fuel was injected through the simplex nozzle and allowed to vaporize for 10 minutes with the mixing fan running.

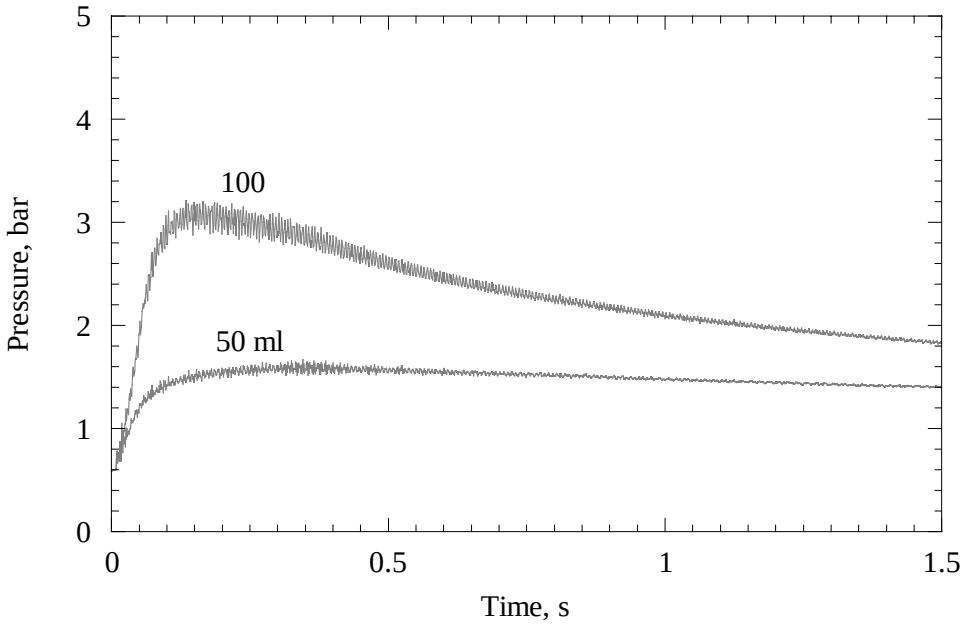

Figure 15: Pressure histories for combustion of kerosene, tests 245 and 246. Air temperature of 40°C, pressure 0.585 bar (14 kft equivalent). Driver jet 1-in diam., 80% H_2, 20% O_2.

Pressure histories for near-limit cases are shown in Fig. 16. These results indicate that for fuel at this temperature, the flammability limit is approximately 25 g/m^3.

These tests were carried out to determine the combustion overpressure as a function of fuel concentration under conditions where the fuel would be completely gaseous. The peak pressures are given as a function of fuel amount in Fig. 17.

3.2.3 Variable Temperature series

Tests 271 to 287 were carried out with a fixed amount of liquid (50 ml) and temperatures between 21 and 100°C for both fuel and air. The fuel was injected through the simplex nozzle, and the mist was allowed to evaporate and settle for 30 minutes. The mixing fan was run for 10 minutes before ignition. Pressure histories for selected cases are shown in Fig. 18. The peak pressures are summarized in Fig. 19.

3.2.4 Variable volume series at 40°C

Tests 301 to 308 were carried out with larger amounts of fuel, up to 700 ml, at a temperature of 40°C. The fuel was injected at a lower pressure (0.239 bar, equivalent to 35 kft), allowed to evaporate for 30 minutes, the tank was filled with air to a pressure of 0.585 bar (14 kft equivalent), the contents were mixed for 10 minutes and then burned. The test was carried out in this fashion to minimize the amount of liquid fuel that was suspended in the form of a mist within the tank. A 10 μm radius droplet has a terminal velocity of

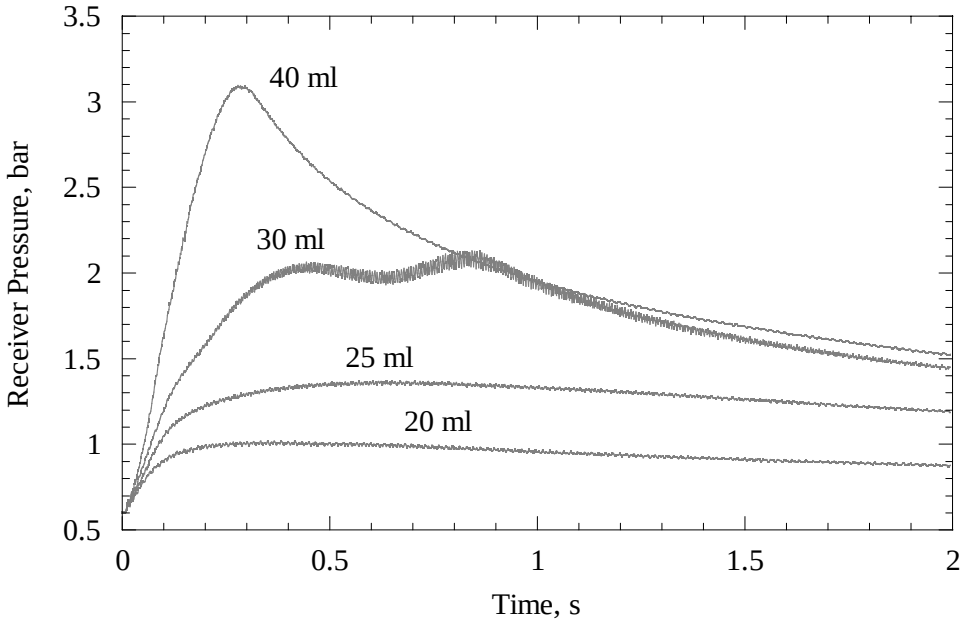

Figure 16: Pressure histories for combustion near the lean limit of gaseous Jet A in air at a temperature of 100°C, pressure 0.585 bar (14 kft equivalent). Tests 288, 298, 289, and 290.

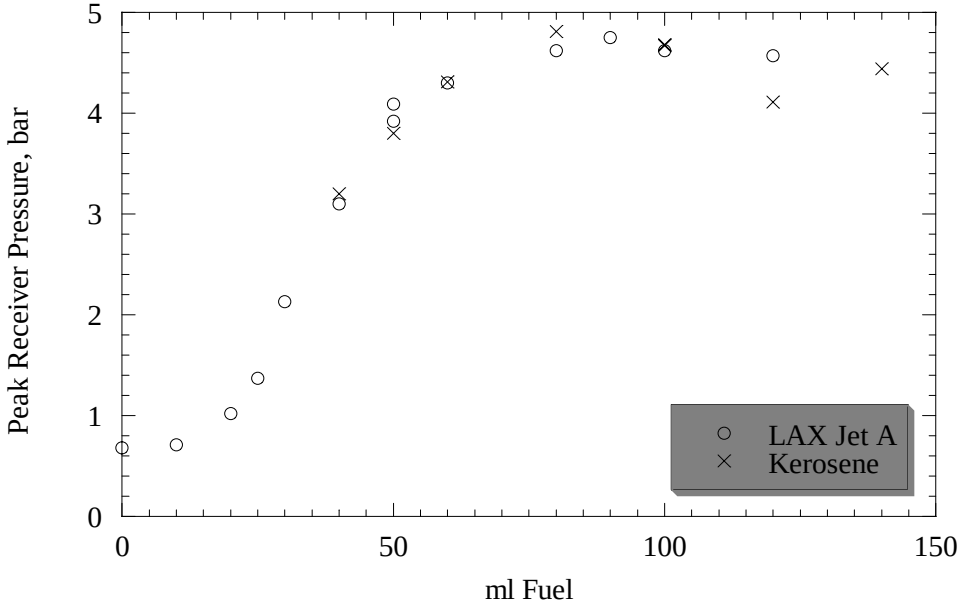

Figure 17: Peak pressure as a function of fuel amount for gaseous kerosene and Jet A. Fuel and air temperature 100°C, pressure 0.585 bar (14 kft equivalent). Tests 255 to 265 and 288 to 300.

about 10 mm/s in still air, yielding a characteristic time of about 86 s for the droplets to settle out of the atmosphere of the tank onto the tank walls. By waiting approximately

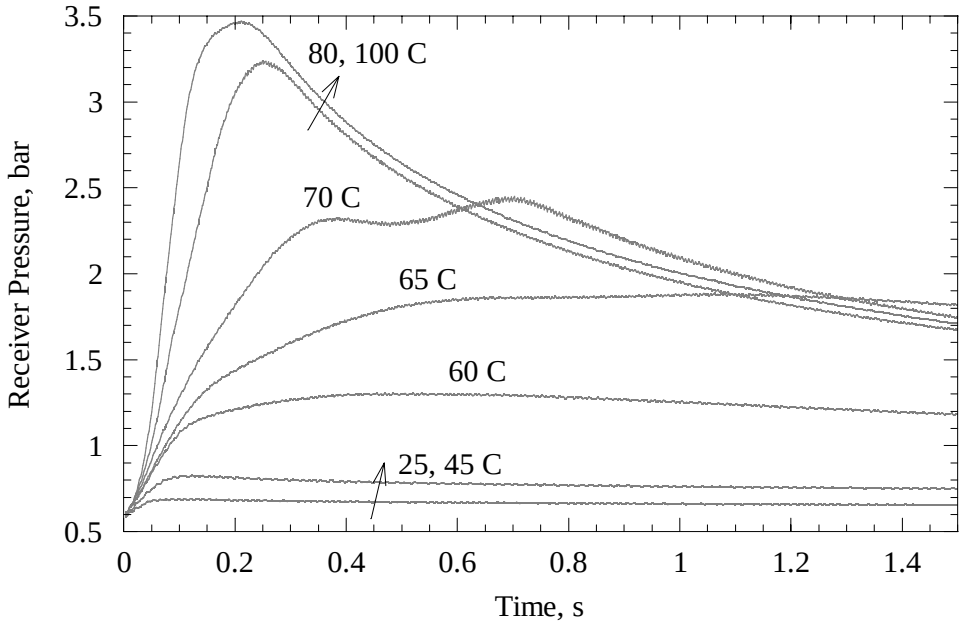

Figure 18: Pressure histories for combustion of Jet A in air at temperatures between 21 and 100°C, pressure 0.585 bar (14 kft equivalent). The volume of liquid fuel injected was 50 ml in all cases. Tests 271 to 281.

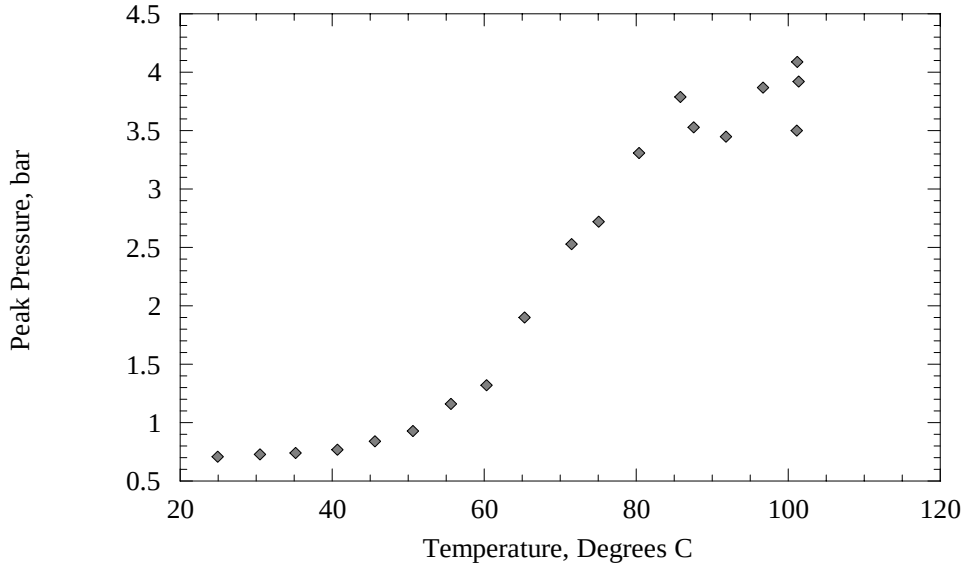

Figure 19: Peak pressures for combustion of gaseous Jet A in air at temperatures between 21 and 100°C, pressure 0.585 bar (14 kft equivalent). The volume of liquid fuel injected was 50 ml in all cases. Tests 271 to 281.

20 characteristic settling times prior to filling with air, we expect that all of the droplets except those less than 2 μm in diameter have settled out of suspension. Comparisons with Ott's results (Fig. 26) indicate that this strategy was successful at minimizing the

mass of suspended liquid.

Pressure histories for fuel volumes between 150 and 700 ml are shown in Fig. 20. As shown in Fig. 21, the pressure at which the fuel is injected has little influence on the peak pressure. The difference between the two pressure traces suggests a slightly slower flame speed for the 14 kft injection case but this could simply be test-to-test variability.

These tests indicate that the quantity of liquid fuel used has a marked effect even though the combustion is taking place in the gas phase. At 40°C, only about 10% of the fuel is actually vaporized and participates in the combustion. This is shown in Fig. 22, where the results for 30 ml at 100°C is shown to be comparable to those obtained with 300 ml of fuel at 40°C.

These results explain why we had so much difficulty attempting to get ignition in earlier tests with only 50 to 100 ml of fuel at low temperatures (less than 40°C). At these temperatures, large amounts of liquid fuel are required so that a sufficient quantity of vapor will be produced.

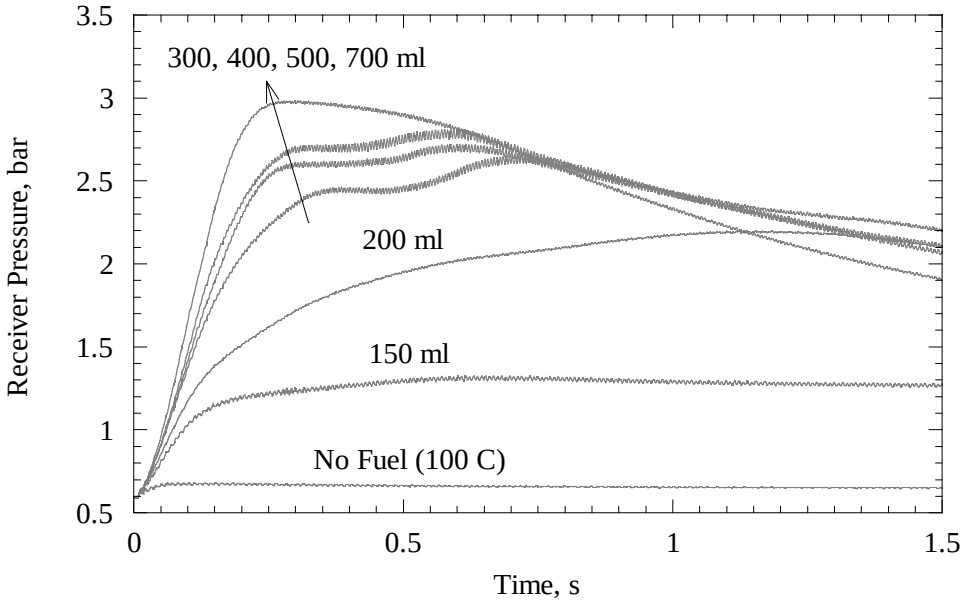

Figure 20: Pressure histories for combustion of gaseous Jet A in air at a temperature of 40°C, and a pressure 0.585 bar (14 kft equivalent). Fuel was injected at a pressure of 0.239 bar, equivalent to 35 kft. Tests 300 to 307.

3.3 Peak Pressure Estimates

The peak pressure obtained in an explosion can be estimated by computing the equilibrium products for a constant-volume, adiabatic, complete combustion process. Experiments with pure substances as fuels show that measured values are consistently lower than adiabatic estimates due to heat transfer during the burn (Shepherd and Ratzel 1985) and in the case of lean mixtures, incomplete combustion. Some relevant properties of pure fuels are given in Tables 1 and 2.

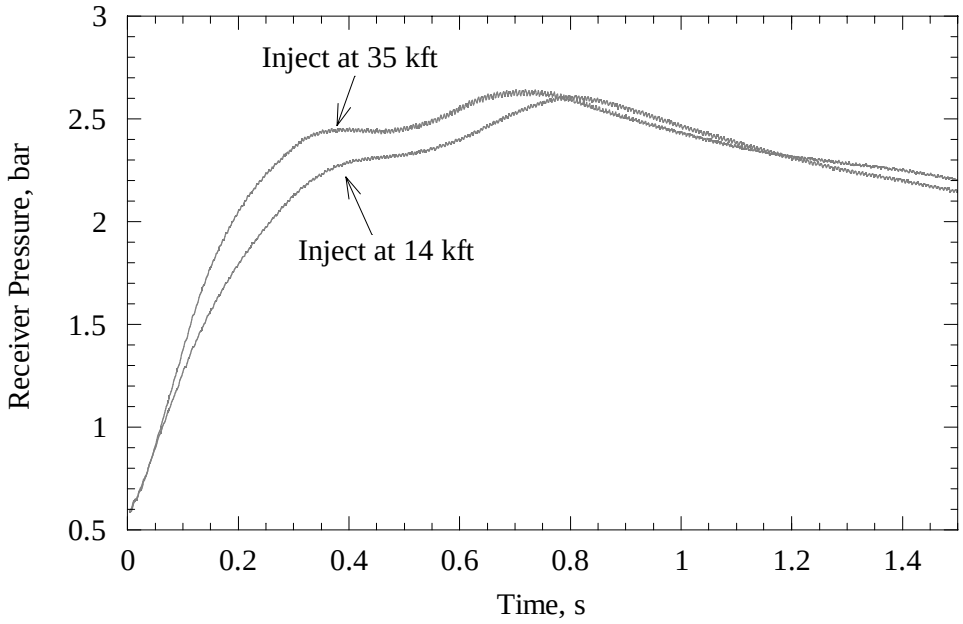

Figure 21: Pressure histories for combustion of gaseous Jet A in air at a temperature of 40°C, and a pressure 0.585 bar (14 kft equivalent). Fuel was injected at a pressure of 0.239 bar, equivalent to 35 kft in test 305 and 0.585 bar, equivalent to 14 kft in test 310.

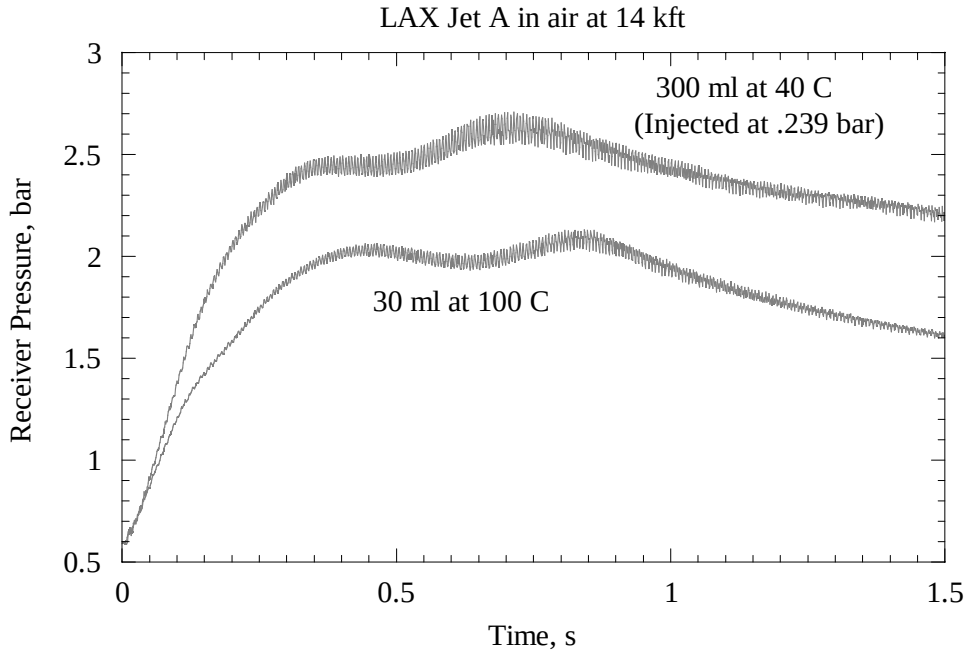

Figure 22: Pressure histories for combustion of gaseous Jet A demonstrating the effect of fuel amount and ambient temperature. Tests 305 and 289.

Table 1: Physical properties of single component hydrocarbon fuels (Reid et al. 1987; Kuchta 1985).

Fuel	Formula	W (g/mol)	T_c (K)	P_c (bar)	T_b (K)	ΔH_{lv} (kJ/mol)	ρ_l (g/cm^3)
			Alkanes				
hexane	C_6H_{14}	86.18	507.4	29.3	341.9	28.9	0.659
octane	C_8H_{18}	114.2	568.8	24.5	398.8	34.4	0.703
decane	$C_{10}H_{22}$	142.3	617.6	20.8	447.3	39.3	0.730
dodecane	$C_{12}H_{26}$	170.3	658.3	18	489.5	43.6	0.748
			Aromatics				
benzene	C_6H_6	78.1	562.1	48.3	353.3	30.8	0.885
methylnapthalene	$C_{11}H_{10}$	142.2	772	35.2	517.8	46.0	1.02
diphenylmethane	$C_{13}H_{12}$	168	767	29.4	537.5	-	1.006

Table 2: Combustion properties of single component hydrocarbon fuels (Reid et al. 1987; Kuchta 1985). X indicates molar or volume fraction at NTP.

Fuel	ΔH_f° (kJ/mol)	Q (kJ/mol)	q (MJ/kg)	e_{LFL} (MJ/kg)	X_{LFL} (%)	X_{ST} (%)	X_{UFL} (%)	f_{LFL} (kg/kg)
				Alkanes				
C_6H_{14}	-167.4	3890.	45.1	1.61	1.2	2.16	7.4	.036
C_8H_{18}	-208.5	5120.	44.8	1.68	0.95	1.65	6.5	.038
$C_{10}H_{22}$	-249.9	6350.	44.6	1.64	0.75	1.33	5.6	.037
$C_{12}H_{26}$	-290.9	7620.	44.7	1.58	0.6	1.12	-	.036
				Aromatics				
C_6H_6	82.9	3170.	40.6	1.42	1.3	2.72	7.9	.036
$C_{11}H_{10}$	116.8	5650.	39.8	1.56	0.8	1.53	-	.040
$C_{13}H_{12}$	89.2	6660.	39.6	1.61	0.7	1.29	-	.041

Adiabatic explosion pressures are computed by using conservation of energy

$$E_{reactants}(T_1) = E_{products}(T_2) \tag{1}$$

to determine the explosion temperature T_2 and the ideal gas law to determine the explosion pressure P_2

$$P_2 = P_1 \frac{R_2 T_2}{R_1 T_1} \tag{2}$$

For the most realistic solutions, the composition of the products is simultaneously determined by a chemical equilibrium computation. We use the computer code STANJAN (Reynolds 1986) for this purpose. A simple approximation to the peak pressure in lean mixtures can be found by equating the energy released in the fuel to the temperature rise in the products, which is mainly air for lean mixtures

$$M_{air} c_v \left(T_2 - T_1\right) \approx M_{fuel} q \tag{3}$$

where c_v is the specific heat capacity of the air and q is the specific heat of combustion. Combining this with the ideal gas law, we have

$$P_2 - P_1 \approx P_1 \frac{M_{fuel}}{M_{air}} \frac{q}{c_v T_1} \tag{4}$$

This indicates that the two main factors are fuel/air mass ratio and the energy content of the fuel. For Jet A, $q = 42.8$ MJ/kg and for hot air, $c_v \approx 850$ J/kg·K, yielding a value

$$\frac{q}{c_v T_1} = 158. \tag{5}$$

for $T_1 = 40°$C. We compare "exact" solutions (using the pseudo-Jet A substance model with W = 160) to the energy balance, Eq. 1, with the approximate model, Eq. 4 for lean mixtures in Fig. 23. Clearly, this simple model is only appropriate for mixtures with $M_{fuel}/M_{air} \leq 0.040$. As the fuel/air ratio increases above this value, the increasing amount of dissociation and increase in heat capacity of the products causes the "exact" values to increasingly fall below the idealized model predictions.

We have compared our measured values with computations for both pure fuels and a pseudo-Jet A substance. On a mass basis, kg fuel per kg of air, the comparison depends on two fuel properties: 1) the ratio of hydrogen to carbon atoms in the molecule; 2) the heat of combustion or equivalently, the heat of formation of the fuel. The extremes in composition are given by paraffins, which have twice as many H-atoms as C-atoms, and aromatics, which have approximately the same number of H-atoms and C-atoms. The specification for Jet A (ASTM 1665) has the maximum concentration of aromatics to be 20%. A preliminary GC-MS analysis reported in Appendix B verifies that some aromatics are present although the majority of the compounds are straight or branched alkanes.

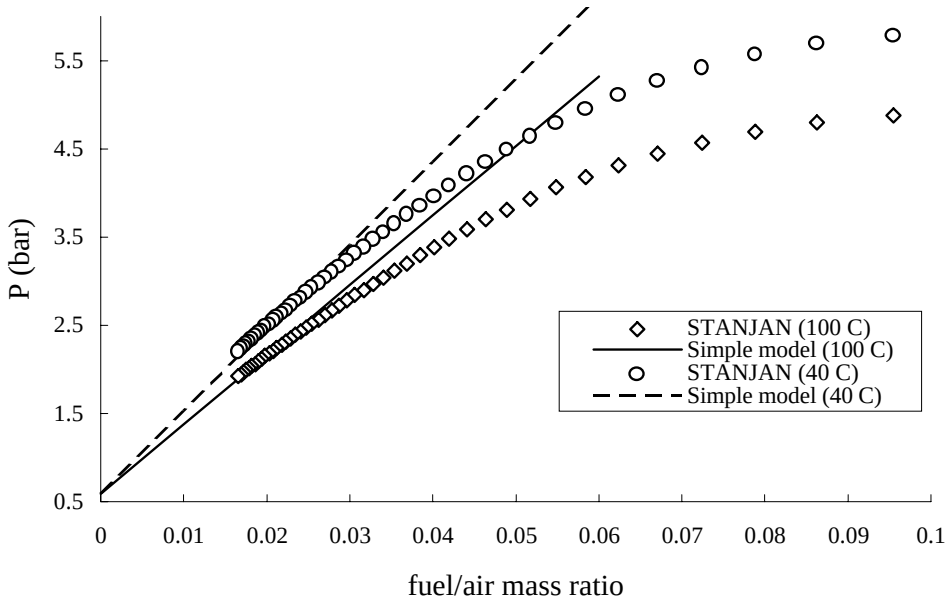

Figure 23: Comparison of "exact" solutions to adiabatic explosion pressure with the approximate model of Eq. 4. Pseudo-Jet A substance (160 g/mol) at two initial temperatures (40 and 100°C) and an initial pressure of 0.585 bar.

Computed results (using STANJAN) for paraffin hydrocarbons (alkanes, C_nH_{2n+2}) and some aromatics are given in Fig. 24. These results are given at initial conditions of .585 bar and 100°C in order to compare with our high-temperature experimental results.

From these comparisons, it is apparent that Jet A has a composition that is intermediate to these extremes. An approach to this issue is to compute combustion adiabats for a series of compounds with a fixed heat of combustion, $q = 42.8$ MJ/kg and a variable H/C ratio. The effective heat of formation $\Delta_f H^\circ$ of these compounds was determined by solving the enthalpy balance equation. Consider a stoichiometric reaction of a generic hydrocarbon fuel. The oxygen-balanced reaction is

$$C_nH_m + (n + \tfrac{m}{4})O_2 \longrightarrow nCO_2 + \tfrac{m}{2}H_2O$$

The heat of combustion per mole of fuel is

$$Q = \Delta_f H^\circ_{fuel} - n\Delta_f H^\circ_{CO_2} - \frac{m}{2}\Delta_f H^\circ_{H_2O} \tag{6}$$

and the specific heat of combustion q is

$$q = \frac{Q}{W_{fuel}} \qquad W_{fuel} = 12n + m \tag{7}$$

The fuel-air mass ratio f for a stoichiometric mixture is only a function of the ratio m/n of hydrogen to carbon atoms. From the oxygen-balanced reaction given previously, we have

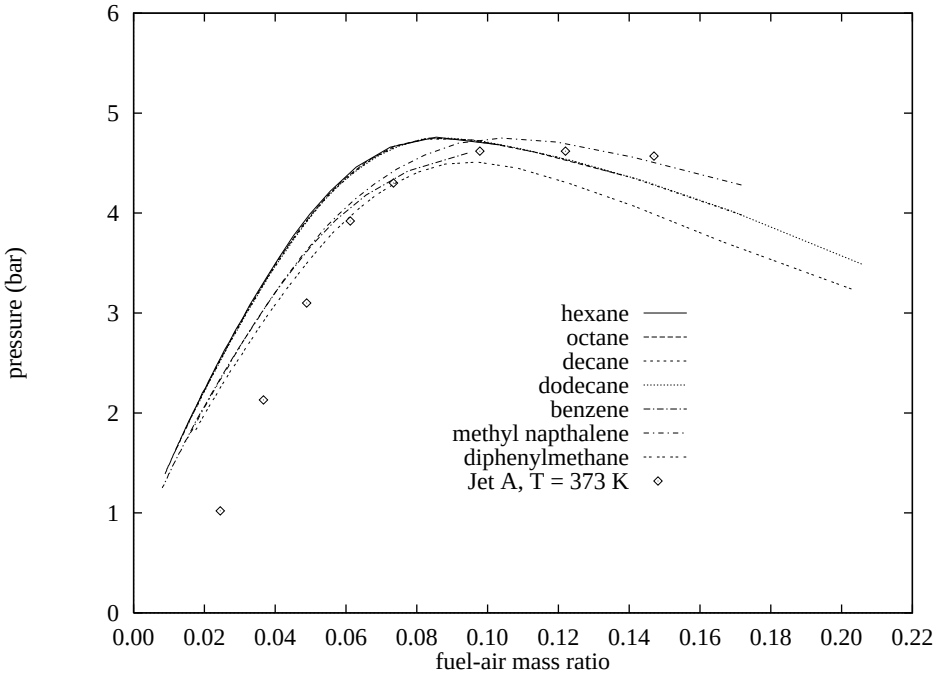

Figure 24: Comparison of computed adiabatic, constant volume explosion pressures for alkanes and aromatics with experimental results for Jet A at 0.585 bar, 100°C.

$$f_{st} \equiv \left(\frac{M_{fuel}}{M_{air}}\right)_{st} = \frac{12 + m/n}{137.3(1 + m/4n)} \tag{8}$$

When m/n =2 (case of alkanes), $f_{st} = 0.068$ and for m/n =1 (case of aromatics), $f_{st} = 0.076$.

A series of computations of this type are shown in Fig. 25a. For these cases, the number of carbon atoms was fixed at 12 and the number of hydrogen atoms was varied. The effect of initial temperature is shown in Fig. 25b. The peak pressure is lower at higher initial temperatures since fractional change in thermal energy is smaller when starting at a higher initial temperature.

The peak pressure observed by Nestor and Ott are consistent with our value of 3 bar (45 psi) observed at 40°C. The values of ΔP_{max}, the maximum pressure rise, obtained by Ott in his static tests were correlated approximately by a scaled vapor pressure curve. This can be justified by observing that the lean combustion energy balance can be rewritten in terms of the fuel vapor partial pressure P_{fuel} as

$$P_2 - P_1 = \frac{W_{fuel}}{W_{air}} \frac{q}{c_v T_1} P_{fuel} \tag{9}$$

If we assume that the fuel vapor is in equilibrium with fuel liquid, which is the case in Ott's tests, then the fuel vapor partial pressure is equal to the fuel vapor pressure P_σ,

resulting in a peak pressure rise of

$$\Delta P_{max} = \alpha P_\sigma(T_1) \qquad \alpha = \frac{W_{fuel}}{W_{air}} \frac{q}{c_v T_1} \tag{10}$$

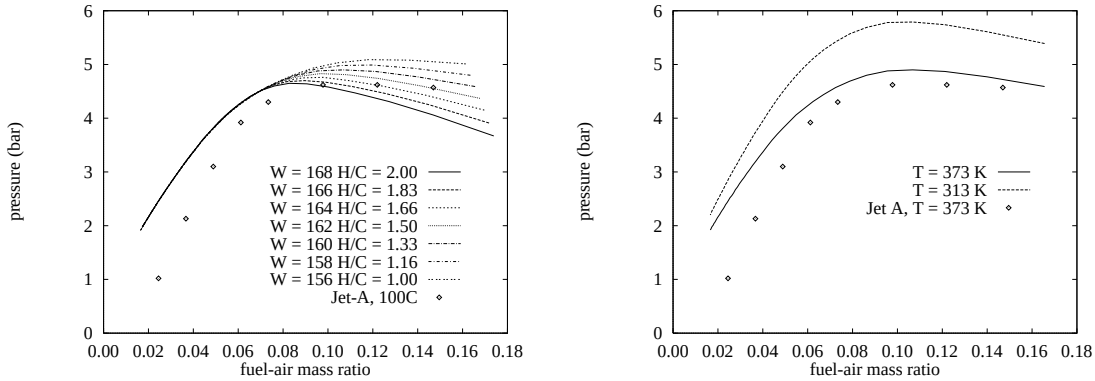

(a) (b)

Figure 25: Comparison of computed adiabatic, constant volume explosion pressures for a pseudo-fuel of fixed heat of combustion with experimental results for Jet A at 0.585 bar, 100°C. (a) results for variable H/C ratio at T = 373 K. (b) results for a fixed H/C ratio for T = 313 K and 373 K.

Note that this result indicates that for lean combustion, the peak pressure rise is independent of the initial pressure, as found experimentally by Ott. Ott's curve fits and the present data are shown together in Fig. 26.

Equation 10 depends on the fuel molar mass W_{fuel}. Therefore, we need to know both the vapor pressure $P_\sigma(T)$ and the molar mass W_{fuel} as a function of temperature in order to predict the combustion pressure rise. As discussed below, there is substantial uncertainty associated with reported values of the vapor pressure of Jet A and the molar mass has not been quantified as a function of temperature. The vapor pressure estimate of Ott results in a value of $\alpha = 460$, implying a fuel molar mass of 84, substantially lower than the value of 144 obtained by Kosvic et al. (1971) or the value of 170 estimated by the API gravity correlation (p. 333 of Lefebvre 1983). In fact, the composition and molar mass of the vapor are functions (unknown at present) of the fuel temperature. Some preliminary chemical analyses of liquid and vapor Jet A are reported in Appendix B. These results indicate that the vapor does have an average molar mass substantially less than the liquid but this has not been quantified at this time.

4 Pressure Trace Analysis

The pressure-time histories observed in the present experiments contain information about the growth of the explosion in time. These data may find application to predicting the duration of the CWT explosion. However, there are significant aspects of the

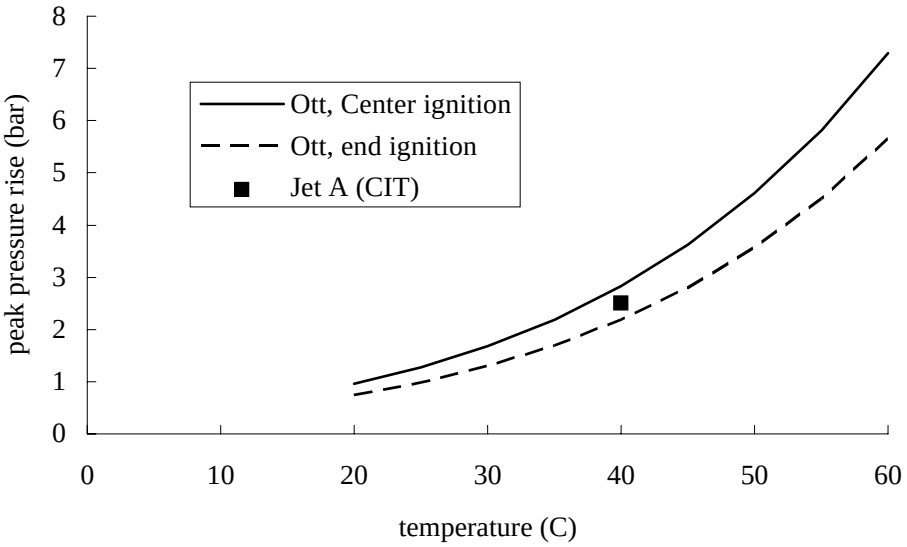

Figure 26: Comparison of Ott's measured peak explosion pressure rise with present experimental results for Jet A at 0.585 bar and 40°C .

CWT that are not modeled in the present tests. These include the much larger size of the CWT (50 m^3), subdivision of the CWT into compartments with connecting passageways, the presence of vents between the tank and the atmosphere, the liquid layer on the floor of the tank and the deformation and failure of the CWT structure during the explosion. These differences are so substantial that we feel that larger-scale testing with more prototypic tanks is required to obtain reliable insight and quantitative evaluation of these effects.

However, it is useful to pursue the analysis of the explosion event and develop some simple models for the pressure-time history. These models serve to illustrate some of the difficulties in explosion analysis and motivate the need for more prototypic experiments and also more sophisticated numerical analyses. In general, modeling and prediction of explosions require a numerical solution of the governing partial differential equations of fluid dynamics together with a model for the chemical reactions in the flame. For a complex structure such as the CWT, this is very challenging since the simulation must be carried out in three space dimensions and requires substantial computation resources. In the case of a structure such as the CWT, structural response and failure may also have to be simultaneously considered. There are research groups who are presently solving problems of this type, a summary of the state of the art in numerical modeling is given by Hjertager (1993) and validation of the results against experiments is given in Popat et al. (1996).

4.1 Simple Explosion Modeling

Simple models of explosions are based on assuming a geometry for the flame front, low-speed flow and laminar flame propagation. Analytical approaches are summarized by Bradley and Mitcheson (1976) and numerical methods are described by Ural and Zalosh (1988). Other issues associated with modeling explosions are turbulence (Tamanini and Chafee 1990), heat loss by radiation and convection (Ural and Zalosh 1988; Shepherd and Ratzel 1985), acoustic waves (Tamanini and Chafee 1992), incomplete combustion and buoyancy (Ural and Zalosh 1988; Nagy et al. 1971). Venting into the atmosphere (NFPA68 1994; Bradley and Mitcheson 1978; Cummings et al. 1984) and venting to another tank (Mulpuru and Wilkin 1982) have been extensively discussed in the context of hazard analysis and safety studies.

The basis for all simple models is conservation of energy for an adiabatic, constant volume system: $E =$ constant. This provides a unique relationship between the average pressure P and the amount of burned gas M_b. For an ideal gas with a constant ratio of specific heats γ and specific heat of combustion q, this relationship is

$$E = \frac{pV}{\gamma - 1} - M_b q \tag{11}$$

where V is the total volume of the vessel. The peak or maximum pressure P_m is obtained when all of the gas is burned $M_b = M_\circ = \rho_\circ V$.

$$\Delta P_m = P_m - P_\circ = (\gamma - 1)\frac{qM_\circ}{V} \tag{12}$$

The constancy of the energy E leads to the following ordinary differential equation for pressure

$$\frac{\mathrm{d}P}{\mathrm{d}t} = \Delta P_m \frac{1}{M_\circ}\frac{\mathrm{d}M_b}{\mathrm{d}t} \tag{13}$$

The rate at which gas is being burned can be computed by considering the flame as having an area $A_f(t)$ which is consuming unburned gas of density ρ_u with a laminar burning speed of S_u.

$$\frac{\mathrm{d}M_b}{\mathrm{d}t} = A_f \rho_u S_u \tag{14}$$

The effect of turbulence is to distort the flame front and increase the product $A_f S_u$ substantially, in some cases up to 100 times larger than the laminar values. The distortion of the flame front occurs over a wide range of length scales, determined by the nature of the turbulent flow and the interaction of the flame with the flow. Engineering models usually treat turbulent flame propagation by replacing the laminar burning speed with an effective "turbulent" value S_T and interpreting the area A_f as the area of a smooth surface passing through the average location of the turbulent flame. Turbulent burning speeds can be up to a factor of 20 higher than the laminar values and increase with increasing turbulent intensity.

Note the distinction between burning speed and the apparent velocity that a flame is observed to propagate with during an explosion. The flame velocity $\mathbf{V}_f$ is locally the vector sum of the fluid velocity $\mathbf{u}$ and the burning speed directed along the normal $\hat{\mathbf{n}}$ to the surface defined by the flame front

$$\mathbf{V}_f = \mathbf{u} + \hat{\mathbf{n}} S_u \tag{15}$$

Since the volume occupied by the combustion products is larger than the volume of the reactants, the flame propagation always results in displacement of the surrounding reactants, inducing a flow $\mathbf{u}$. Therefore the apparent laminar flame speed is higher than the laminar burning velocity by up to a factor of ρ_u/ρ_b, where ρ_u is the mass density of unburned gas and ρ_b is the mass density of burned gas.

As the flame propagates through a closed volume, the pressure increases uniformly in space, compressing both burned and unburned gases. This is an approximation that is valid as long as the flame speed is small relative to the acoustic speed. Fast flames will produce spatial variations in pressure that are manifested as acoustic waves and in extreme cases, shock waves. The flame speed is sufficiently low in current tests so that such pressure oscillations are not observed.

If we neglect the effects of heat transfer during the burn, the unburned gases are spatially uniform and conditions can be predicted by using the isentropic relationships

$$T_u = T_\circ \left(\frac{P}{P_\circ}\right)^{\frac{\gamma-1}{\gamma}} \qquad \rho_u = \rho_\circ \left(\frac{P}{P_\circ}\right)^{\frac{1}{\gamma}} \tag{16}$$

For a given fuel concentration, the flame speed is dependent on both temperature and pressure. For the purposes of engineering studies, the dependence is usually taken to be (Gaydon and Wolfhard 1979)

$$S_u = S_u^o \left(\frac{P}{P_\circ}\right)^n \left(\frac{T}{T_\circ}\right)^2 \tag{17}$$

where the parameter n is substance specific.

Flame speed is also known to be a function of the the fluid motion (strain rate) but this is beyond the present considerations. The laminar flame speed at standard conditions is a function of the fuel concentration and must be determined experimentally, along with the exponent n. Typical hydrocarbon-air flame laminar flame speeds have a maximum value of about 30 to 40 cm/s for stoichiometric mixtures. A compilation of older data is given in Gibbs and Calcote (1959), Davis et al. (1997) discuss the issue of strain rate corrections for toluene and benzene, data for fuels similar to octane are summarized in Heywood (1988). The leaner the mixture, the lower the flame speed. Near the flammability limit, the flame speed decreases to about 4 to 5 cm/s. There is no data available in the literature on Jet A flame speeds other than a range of 0.3 to 0.6 m/s quoted in CRC (1983). There is some data available (Richards and Lefebrve 1989) on turbulent flame speeds in kerosene sprays but this is probably only relevant to later stages of the explosion if the liquid layer is lofted and dispersed. Estimates of the flame

speed in Jet A vapor-air mixtures will be made in a later phase of the present research program.

Given a suitable expression for flame speed, the key remaining issue is the flame area dependence on time $A_f(t)$. This requires experimental data or simplifying assumptions about the shape of flame. However, before considering specific cases, the pressure equation can be reduced to a form that clearly indicates the key parameters:

$$\frac{\mathrm{d}P}{\mathrm{d}t} = \frac{S_u^\circ \Delta P_m}{V^{1/3}} \frac{S_u}{S_u^\circ} \frac{\rho}{\rho_\circ} \frac{A_f(t)}{V^{2/3}} \tag{18}$$

From this, we infer that a characteristic value (such as the maximum) of the pressure time derivative must scale as

$$\left(\frac{\mathrm{d}P}{\mathrm{d}t}\right)_{max} \propto \frac{S_u^\circ \Delta P_m}{V^{1/3}} \tag{19}$$

Based on this notion, the conventional way (NFPA68 1994) to analyze explosion pressure traces is to compute a *pressure rise coefficient* K_g defined as

$$K_g \equiv V^{1/3} \left(\frac{\mathrm{d}P}{\mathrm{d}t}\right)_{max}. \tag{20}$$

Values of K_g for various gases and vessel volumes V are tabulated in NFPA68 (1994). Although the simple scaling relationship indicates that K_g should be independent of volume,

$$K_g \propto S_u^\circ \Delta P_m \tag{21}$$

the influence of scale on the turbulent flame propagation causes a weak dependence on the size of the vessel $K_g \sim \ln V$. The exact dependence is substance dependent and data is available for selected fuels in NFPA68 (1994). In a 1 m^3 vessel, typical values for stoichiometric hydrocarbon-air fuels are $K_g = 100$ bar-m/s. The value of K_g depends also on the fuel type, concentration, vessel shape and initial turbulence level in the vessel. Experimental measurement is the only reliable guide in unusual situations such as the 747 CWT.

For simple geometries, the area of the flame can be related to the fraction of burned gas, which in turn can be related to the instantaneous pressure. This leads to expressions for the scaled area as a function of pressure and the pressure equation becomes an ordinary differential equation. This is the basis for many approximate solution methods for the pressure history during an explosion. Dimensional analysis leads to the following expression

$$\frac{\mathrm{d}P}{\mathrm{d}t} = \frac{S_u^\circ \Delta P_m}{V^{1/3}} \frac{S_u}{S_u^\circ} \quad F(P/P_\circ, P_m/P_\circ, \gamma) \tag{22}$$

The function F depends on the exact choice of model. Three simple geometries and one common ad hoc model are described subsequently. All of these models use the

relationship (Eq. 13) between burned gas mass fraction and pressure. Since the products of combustion are in a spatially nonuniform state, it is easier to work with the compressed reactants or unburned volume in the computation. Integration of Eq. 13 yields

$$\frac{P - P_\circ}{P_m - P_\circ} = \frac{M_b}{M_\circ} = 1 - M_u/M_\circ = 1 - \frac{\rho_u V_u}{\rho_\circ V_\circ} \tag{23}$$

The relationship of unburned volume to flame surface area has to be separately determined for each geometrical case.

Spherical The vessel is a sphere of radius R and at any time the flame is assumed to be a sphere with radius r. The function F for this case can be computed to be

$$F = 3\left(\frac{4\pi}{3}\right)^{1/3}\left(\frac{P}{P_\circ}\right)^{1/\gamma}\left[1 - \left(\frac{P_\circ}{P}\right)^{\frac{1}{\gamma}}\left(\frac{P_m - P}{P_m - P_\circ}\right)\right]^{2/3} \tag{24}$$

Spherical propagation is characteristic of the initial phase of any explosion and can be used to determine the initial pressure history. Integration of the pressure rise equation for early times ($P \leq 2P_\circ$) yields (Nagy et al. 1971) a cubic relationship

$$P(t) \approx P_\circ + \Delta P_m \left(\frac{P_m}{P_\circ}\right)^2 \left(\frac{S_u^\circ t}{R}\right)^3 \tag{25}$$

which has been used to determine initial flame speeds S_u° (or S_T in the turbulent case). The maximum value of F occurs at the end of the burn and is

$$F_{s,max} = 3\left(\frac{4\pi}{3}\right)^{1/3}\left(\frac{P_m}{P_\circ}\right)^{1/\gamma} \tag{26}$$

which has a numerical value of 15.5 for $P_m = 3$, $P_\circ = 0.585$ and $\gamma = 1.4$.

Cylindrical In this case, the container is cylinder of length L and radius R. The function F is

$$F = 2\left(\frac{\pi L}{R}\right)^{1/3}\left(\frac{P}{P_\circ}\right)^{1/\gamma}\left[1 - \left(\frac{P_\circ}{P}\right)^{\frac{1}{\gamma}}\left(\frac{P_m - P}{P_m - P_\circ}\right)\right]^{1/2} \tag{27}$$

This case is relevant to jet initiation along the axis of a cylindrical vessel where the initiation occurs rapidly compared to the flame propagation. The maximum value of F occurs at the end of the burn and is

$$F_{c,max} = 2\left(\frac{\pi L}{R}\right)^{1/3}\left(\frac{P_m}{P_\circ}\right)^{1/\gamma} \tag{28}$$

which has a numerical value of 11.9 for $P_m = 3$, $P_\circ = 0.585$, $L/R = 2$, and $\gamma = 1.4$.

Planar The planar case is appropriate to a planar flame front moving axially along a tube of radius R and length L. This situation is appropriate to ignition at the end of a tube. In this case, the function F is

$$F = \pi^{1/3} \left(\frac{R}{L}\right)^{2/3} \left(\frac{P}{P_\circ}\right)^{1/\gamma} \tag{29}$$

The maximum value of F occurs at the end of the burn and is

$$F_{p,max} = \pi^{1/3} \left(\frac{R}{L}\right)^{2/3} \left(\frac{P_m}{P_\circ}\right)^{1/\gamma} \tag{30}$$

which has a numerical value of 5.9 for $P_m = 3$, $P_\circ = 0.585$, $L/R = 2$, and $\gamma = 1.4$.

Kinney and Graham Kinney and Graham (1985) have proposed an ad hoc relationship for F which is based on the analysis of experimental pressure-time histories. They present their model in terms of an empirical coefficient C_r which can be related to K_g. The original Kinney-Graham model is

$$\frac{\mathrm{d}P}{\mathrm{d}t} = C_r \left(\frac{A}{V}\right) (P - P_\circ)(P_m - P) \tag{31}$$

where the coefficient C_r is determined from the maximum rate of pressure rise and A/V represents the surface to volume ratio of the vessel. Using the definition of K_g we find that

$$K_g = C_r \frac{(\Delta P_M)^2}{2} \frac{A}{V^{2/3}} \tag{32}$$

Kinney and Graham suggest that for stoichiometric fuel-air mixtures a value $C_r \approx 0.6$ to 0.7 (m /bar s) is appropriate and go on to propose a correlation of C_r with S_u which is dimensionally incorrect. Including the dependence of ΔP_m in this correlation, we propose a modified correlation

$$C_r \approx \frac{10 S_u}{\Delta P_m} \tag{33}$$

This leads to a formulation in terms of the function F as

$$F = 30 \left(\frac{4\pi}{3}\right)^{1/3} \left(\frac{P - P_\circ}{P_m - P_\circ}\right) \left[1 - \left(\frac{P - P_\circ}{P_m - P_\circ}\right)\right] \tag{34}$$

These four functions are compared in Fig. 27.

For the idealized models, the maximum value of the pressure rise occurs at the end of combustion while the ad hoc model of Kinney and Graham has the maximum pressure rise occuring when one-half of the mixture mass has been consumed. It is clear that a wide range of values of the maximum pressure rise coefficient can be obtained simply by choosing different flame geometries. This emphasizes the importance of experimental studies and more realistic flame simulations in determining pressure history during the explosion.

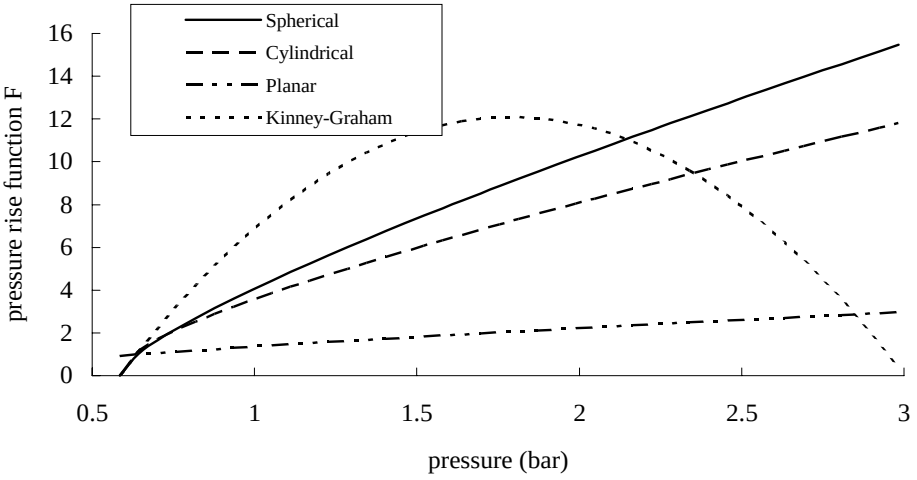

Figure 27: Nondimensional pressure rise functions for $P_\circ$ =0.585 and $P_m = 3.0$, $L/R = 2$, $\gamma = 1.4$

4.2 Experimental Parameters

We have not compared any of the models in detail with the present measurements since the model assumptions are not particularly realistic. The multiple pressure peaks observed in many of the lean mixtures is a characteristic signature of buoyancy and the flame shape cannot be simply described in such situations. Furthermore, the effect of heat loss during the burn is quite important in determining the peak pressure in these situations.

The pressure trace for test 308, 700 ml of Jet A at 40°C, has been analyzed to illustrate the issues that arise in interpreting pressure histories to obtain effective burning velocities. Figure 28 shows the pressure-time trace for the duration of the burn only. The rate of pressure rise is estimated by smoothing the original data and then approximating the derivative with the differences between adjacent points:

$$\frac{\mathrm{d}P}{\mathrm{d}t_n} \approx \frac{P(t_n) - P(t_{n-1})}{t_n - t_{n-1}} \tag{35}$$

The resulting derivative, shown in Fig. 29 is rather noisy but has a clear maximum of about 14.3 bar/s which yields a value of K_g equal to 15 bar-m/s.

The value of K_g observed in the present experiments can be compared with values obtained in similar studies on single substance hydrocarbon fuels. Values of $K_g = 100$ to 200 are typically quoted (NFPA68 1994; Tamanini and Chafee 1990) for stoichiometric mixtures of methane and propane in 1 m^3 vessels. Using the scaling of Eq. 21, this indicates that the effective burning velocity was about 20 to 40 cm/s in test 308, consistent with a lean mixture.

The nondimensional pressure rise function F defined in Eq. 22 can be computed by smoothing the numerical derivatives shown in Fig. 29. The results are plotted in

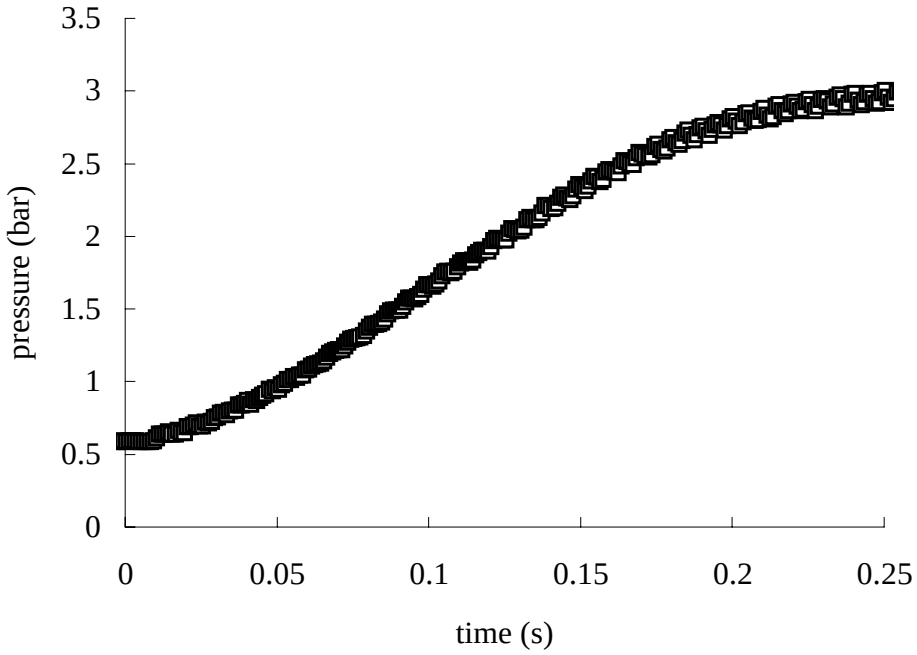

Figure 28: Pressure history during combustion for test 308.

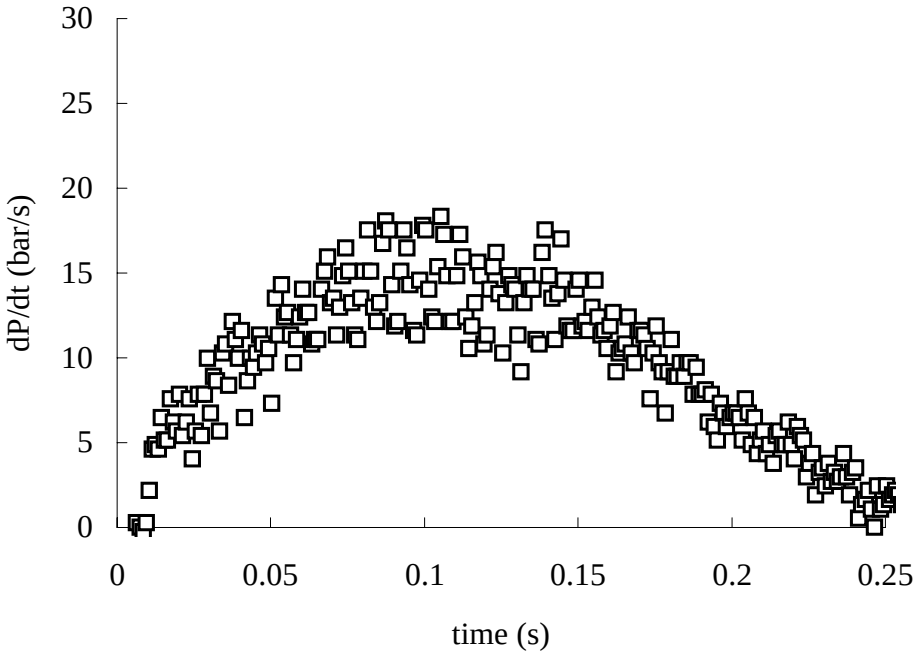

Figure 29: Pressure derivative dP/dt during combustion for test 308.

Fig. 30 after choosing a reference flame speed of 0.5 m/s. The choice of burning velocity is motivated by the apparent similarity between the F function shape and that of the Kinney-Graham model. A burning velocity of 0.5 m/s results in matching the maximum value of F=12 for the Kinney-Graham model.

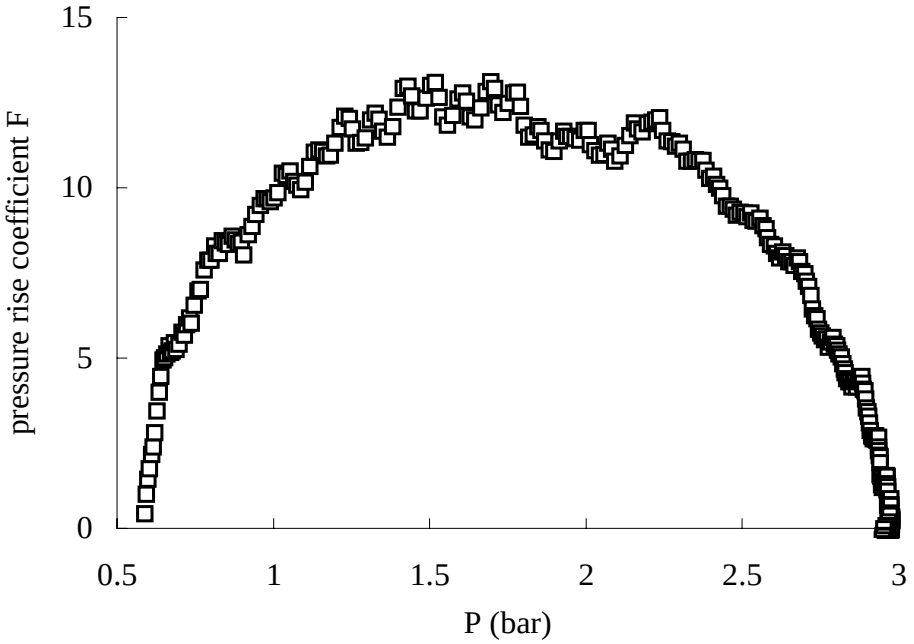

Figure 30: Nondimensional pressure derivative F vs pressure P during combustion for test 308.

Another estimate of the burning velocity can be obtained by using the early-time result of Eq. 25. The standard method of reducing the data with this equation is to plot ΔP^3 vs. time over a short interval after ignition as shown in Fig. 31. Fitting a straight line to the data in these coordinates, the slope of the line can be interpreted using Eq. 25 to obtain the initial burning velocity. For test 308, the result is about 1.2 m/s, higher than the estimates obtained from either the K_g or Kinney-Graham models. These differences reflect both the high turbulence level in the jet used to initiate the combustion and the nonspherical nature of the initial flame kernel produced by jet initiation.

Clearly, all of the methods discussed above are indirect methods of determining flame speeds and the approximations introduced have a substantial effect on the results. This accounts for the range of effective burning speed values of 0.2 to 1.2 m/s inferred from these tests. This values are not necessarily representative of the laminar burning velocity since the effects of turbulence, flame instability and vessel geometry all play a role in determining the effective burning speed. Future tests will use optical observations and spark ignition to obtain more precise measurements of the laminar burning speed.

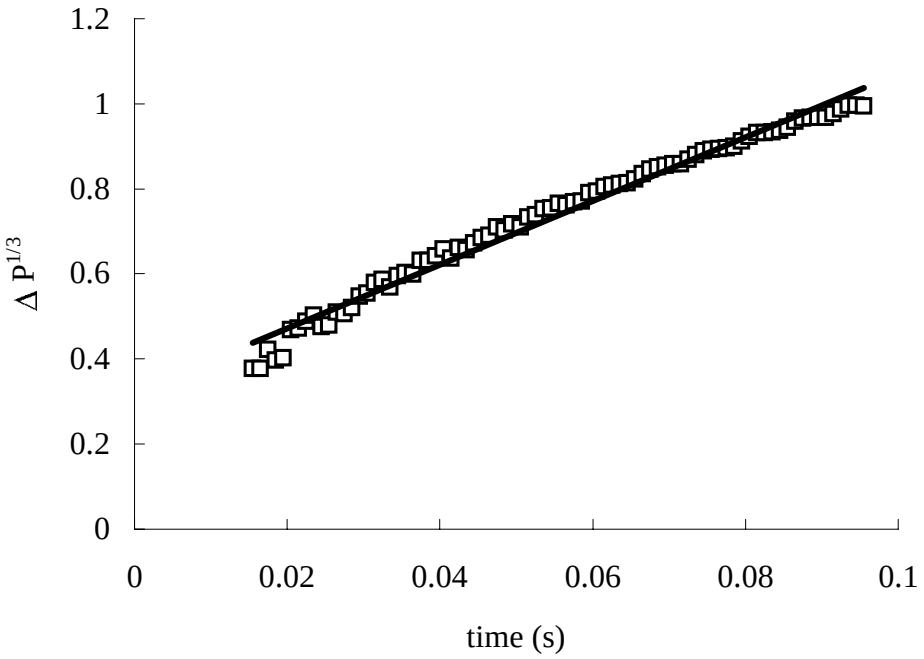

Figure 31: $\Delta P^{1/3}$ vs time for an interval just following ignition in test 308.

5 Flammability Limits

A fuel-air mixture is considered flammable when it will sustain flame propagation after it is ignited. Flammability limits are conventionally measured in terms of the minimum fuel vapor volume (or mole) fraction X_{LFL} where LFL refers to lower flammability limit and maximum fuel vapor concentration X_{UFL} where UFL refers to upper flammability limit. There are extensive compilations of flammability limits (Zabetakis 1965; Kuchta 1985) and some representative values are given in Table 2.

Note that when the amount of fuel at the LFL is expressed as a fuel/air mass ratio f_{LFL}, the limiting value is very similar for all of the fuels in Table 2, $f = 0.035$ to 0.040. This is consistent with the present measurements (Fig. 17) if we define the flammability limit in terms of the transition in the pressure traces observed in Fig. 16. However, the present pressure measurements at 100°C indicate that incomplete combustion can occur at fuel amounts as low as $f = 0.025$. Measurements with kerosene (Zabetakis and Rosen 1957) vapor indicated a limit concentration of about $f = 0.040$. Another measure of the flammability limit that is independent of substance is the energy content at the LFL, from Table 2 this falls in the range of 1.4 to 1.7 MJ/kg.

For liquid fuels, the conventional way to report flammability is to give a *flash point temperature* as determined by a standardized laboratory test (ASTM D56 1988). For a pure substance, the flash point temperature T_{flash} can be determined from the measured concentration limits of flammability, the vapor pressure relation and molar mass. That relationship is

$$P_\sigma(T_{flash}) = PX_{LFL} = P\frac{f_{LFL}}{f_{LFL} + W_{fuel}/W_{air}} \tag{36}$$

where P is the total pressure. This is straightforward to apply for pure fuel and connects the flash point to flammability limits measured in tubes in vessels. As Nestor (1967) points out, this is not the case for Jet A.

The specification (ASTM 1655) for Jet A calls out a minimum flash temperature of 38°C, and a potential range of 40 to 60°C (105 to 140°F) is given in Kuchta (1973). Flash point values of 53 °C (CRC 1983), 43°C (CRC 1967), 48 to 52°C (Nestor 1967), and 48 to 51°C (Ott 1970) are cited in the literature. This range of values is apparently due to the range in volatility allowed by the specification. The flammability limit temperatures measured by Ott and Nestor appear (Fig. 4) to fall in the range of 32 to 38°C, 10 to 15°C lower than the reported flash temperatures. This is apparently due to the differences in the standardized flash point test and the tube or vessel tests used by Nestor and Ott. The flash point test relies on visual observation of a "flash" in a small quantity of vapor whereas the Ott and Nestor tests used visual flame propagation or temperature and pressure transients in a large volume of vapor.

The flash point of the LAX Jet A used in the present tests was measured at Caltech with the Tag closed-cup flash point apparatus using the procedures described in ASTM D56 (1988). A value of 48°C was obtained for the Jet A without any type of conditioning. This is 8°C higher than the 40°C condition for which explosions were consistently obtained in the Hyjet testing and 13°C higher than the limit temperature of 35°C determined in the Nestor study. After the fuel has been used in the vapor pressure apparatus, the flash temperature *decreased* to 46°C. The significance of the decrease in flash point is not understood but emphasizes that the relationship between flash point and fuel handling is not obvious. The hardware store kerosene used in the preliminary CIT tests has a flash point of 56°C.

The fuel-air mass ratio measured by Kosvic et al. (1971) at a temperature of 120°F (49°C) and a pressure of 1 atm was about 0.070. This is close to a stoichiometric mixture and a factor of two higher than the flammability limit estimate of 0.035 discussed previously. The temperature flammability limits obtained by Ott and Nestor (Section 2.1) can be interpreted in terms of a fuel-air mass ratios by using Eq. 36, the measured vapor pressure discussed in Section 7 and an assumed fuel molar mass of 86. Using a range of 32 to 38°C for the limit temperature at 1 bar initial pressure, we compute a fuel-air mass ratio between 0.019 and 0.026. Clearly, this computation is sensitive to the value chosen for the vapor molar mass and further characterization of the vapor is required to sharpen up our estimates. Until that is done, it is unclear how much significance should be given to the difference between the inferred limit values of f for Jet A and the value of 0.035 found for pure substances.

Finally, there have been a number of studies on mists and sprays (Ott 1970; Nestor 1967; Zabetakis and Rosen 1957) that indicate the flammability limit temperature can be greatly reduced and the peak pressure rise substantially increased by suspending the fuel in the form of a spray or mist of liquid droplets. In this fashion, flammable mists of

kerosene and Jet A can be created at even lower temperatures.

The flammability of sprays and vapors for a wide range of hydrocarbon compounds was studied by Burgoyne (1963). He found that if the drop size was sufficiently small (less than 20 μm), a mist has similar flame propagation and limit properties as the pure vapor substance. Flammability limits were actually decreased with increasing droplet sizes, up to 200 μm diameter, at this size the limit fuel-air mass ratio was less than 0.005. For sufficiently large droplets, 1 to 1.5-mm diameter, flame propagation becomes impossible.

These results are relevant to an airplane environment since a certain amount of vibration will occur during takeoff and in flight. In addition, the explosion process itself can cause lofting and atomization of the fuel, possibly resulting in a secondary explosion.

For the purposes of hazard assessment, it is apparent that the flash point is not a reliable guide to explosion hazards of aviation fuels. Explosion testing in vessels or tubes with the appropriate fuel loading is required to evaluate the minimum temperature associated with flammability. In addition, the possibility of mists or sprays widens the flammability envelop even further.

6 Ignition Source and Energy

The source of ignition in the TWA 800 explosion is not the focus of the present study although future experiments are planned on determining ignition energy for spark-type ignition sources in Jet A-air mixtures. The present study has been carried out with a torch or jet ignition in order to study flammability rather ignition. Ignition energies for mixtures of Jet A vapor and air are apparently not known. Previous studies on ignition energy have focused almost exclusively on fuels consisting of a pure substance.

The standard technique (Lewis and von Elbe 1961) for measuring ignition energy is to create an electrical discharge with the electrical energy stored in a capacitor. The stored energy and discharge electrode spacing are varied in order to determine the minimum ignition energy (MIE) required to start a propagating flame. The MIE is found to be a function of fuel type, concentration, and electrode spacing. For hydrocarbon fuels, the smallest value of the MIE is typically about 0.25 mJ (Lewis and von Elbe 1961; Kuchta and Clodfelter 1985; Ballal and Lefebvre 1981) for an optimum electrode spacing of 3 to 4 mm.

The smallest value of the MIE does not occur for a stoichiometric composition but rather for a rich mixture. The heavier the fuel molecule, i.e., the larger the molar mass, the richer the mixture at which the smallest MIE is found. For example, with hexane-air mixtures, the smallest MIE (0.29 mJ) is found for a mixture with 3.7% (molar) hexane in hexane-air; a stoichiometric mixture contains 2.2% hexane. As the composition is made progressively leaner, the MIE increases with decreasing equivalence ratio. For example, a stoichiometric mixture of hexane in air has a MIE of about 1 mJ. It is not known how the MIE for multicomponent fuels such as Jet A vary as a function of equivalence ratio. This issue is being addressed in ongoing studies at Caltech.

Ignition energies for fuel sprays are higher than for homogeneous gas mixtures. The MIE is a function of droplet size distribution (Dietrich et al. 1990) and depends strongly

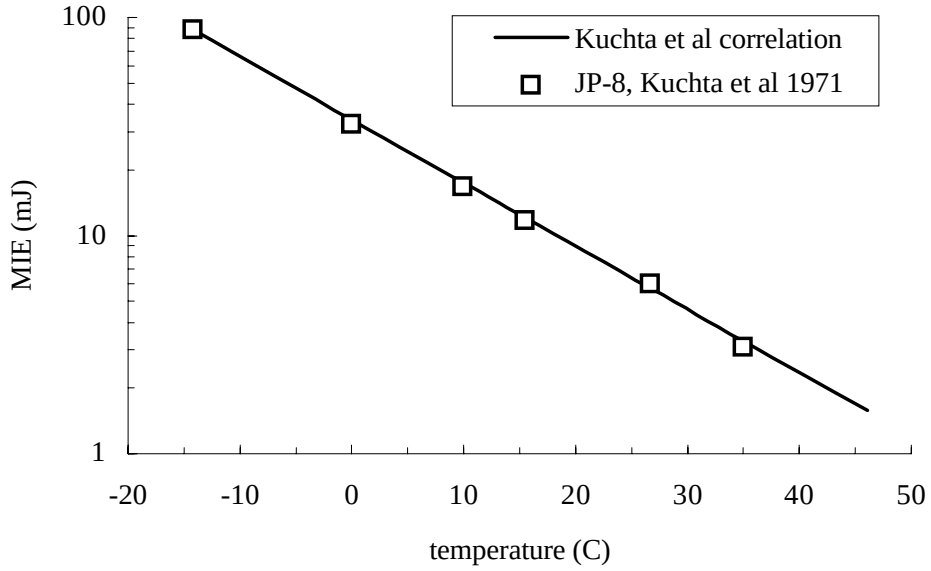

Figure 32: Minimum ignition energy of JP-8 sprays in air as a function of ambient temperature. from (Kuchta et al. 1971)

on temperature (CRC 1983). The ignition energy of JP-8 sprays has been measured (Kuchta et al. 1971) and is found to be a decreasing function of fuel and air temperature. The results of Kuchta et al. (1971) are shown in Fig. 32. These were obtained in a 4-in diam. tube with the fuel dispersed through a pneumatic spray nozzle, estimated drop size of 5 to 10 μm. The reported energy is the stored energy in the capacitor that was discharged through a transformer to produce the arc. Electrode location and spacing are not given but Kuchta et al. state that optimum values were used to give the minimum ignition energy. Extrapolating to 115°F, an ignition energy of less than 2 mJ is predicted. Based on the findings of Burgoyne (1963), this suggests that the ignition energy of a fuel vapor-air mixture is comparable to this value. Tests are in progress to examine this conjecture.

7 Vapor pressure

The vapor pressure of Jet A has seldom actually been measured but rather most of the "data" have been estimated based on distillation curves (ASTM D86 1990) and extrapolating measurements (ASTM D2889 1990) or (ASTM D-93) at a single temperature. The extrapolations (CRC 1983; Barnett and Hibbard 1956; CRC 1967) are conventionally based on the Clausius-Clapeyron equation for the slope of the saturation line σ

$$\left(\frac{\mathrm{d}P}{\mathrm{d}T}\right)_\sigma = \frac{\Delta H_{lv}}{T\Delta v_{lv}} \tag{37}$$

This can be approximated as

$$\frac{\mathrm{d}P}{\mathrm{d}T} = \frac{\Delta H_{lv}}{RT^2} P \tag{38}$$

by assuming the vapor specific volume is much greater than the liquid, $\Delta v_{lv} \approx v_v$ and that the vapor is an ideal gas, $Pv = RT$. For constant heat of vaporization ΔH_{lv} this integrates to

$$lnP = A - \frac{B}{T} \tag{39}$$

The coefficients A and B are usually estimated (CRC 1967) by correlations with the distillation curve slope and the Reid vapor pressure. The resulting vapor pressure estimates vary widely. We compare in Fig. 33 vapor pressures reported in the literature (Lefebvre 1983; Ott 1970; Rose and Cooper 1977; CRC 1983; Tsoovkun et al. 1985) with experimental data obtained at Caltech. We suspect that all of the values reported in the literature (the origin of the Russian values is unknown) are simply evaluations of the approximate vapor pressure formula, Eq. 39 with different sets of parameters A and B.

Some of the differences between the reported vapor pressures certainly are a reflection of variations in refining processes for kerosene, Jet A, and Russian fuels. The specification (ASTM 1655) for Jet A allows for some latitude in fuel volatility. Another source of variation is the uncertainty associated with the prediction or extrapolation method for vapor pressure. Since the distillation curve measurements are generally rather sparse, every 5 to 10°F, and the slope appears to change rapidly near the 10% distillation point, the slope cannot be accurately determined from conventional (ASTM D 86) data.

There appears to be almost no actual experimental data for vapor pressure and no previous efforts to reconcile the various predictions. One measurement that is described in detail (ASTM D323 1990) is the Reid method, which measures vapor pressure with a mechanical pressure gauge at a temperature of 100°F and a vapor:liquid volume ratio of 4:1. The vapor pressure of Jet A at this temperature is so low that this technique is not very reliable but one such data point (quoted in CRC 530) is shown in Fig. 33. Additional comparisons with single component hydrocarbons are shown in Fig. 34.

The relationship (Eq. 36) between vapor pressure and molar mass at the flammability limit can be used to estimate the molar mass of the fuel vapor. An example using the data of Nestor is shown in Fig. 35. The relationship (Eq. 10) between peak explosion pressure rise and vapor pressure can also be used to estimate the molar mass of the fuel vapor. An example using the data of Ott is shown in Fig. 36. Note that both the data and these estimates imply that the molar mass is substantially less than the bulk liquid mean of 160 and molar mass increases with increasing temperature. This is in agreement with the trends expected on the basis of the simple model described in the next section.

Finally, the relationship of Eq. 36 can be used to estimate the range of vapor pressure to expect at the flammability limit given some bounds on the molar mass of the vapor. Nestor estimates a mean molar mass of 75 using a correlation based on a 5% distillation temperature (ASTM D86) of 185°F. On the other hand, Ott estimates (various methods) a molar mass of between 162 and 164 for JP-8. Using these as bounds, we compute that

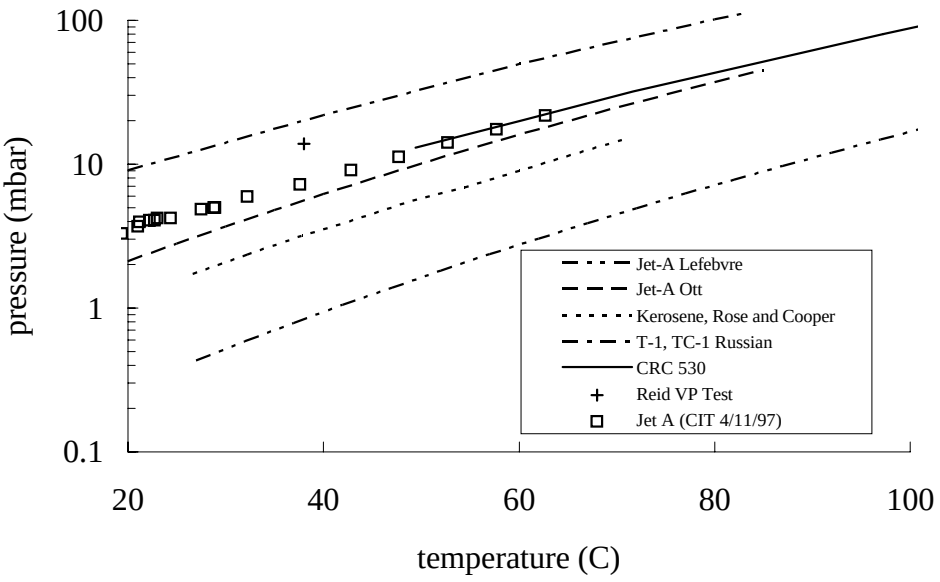

Figure 33: Estimated and measured vapor pressure of Jet A. Measurements reported in the literature contrasted with CIT data.

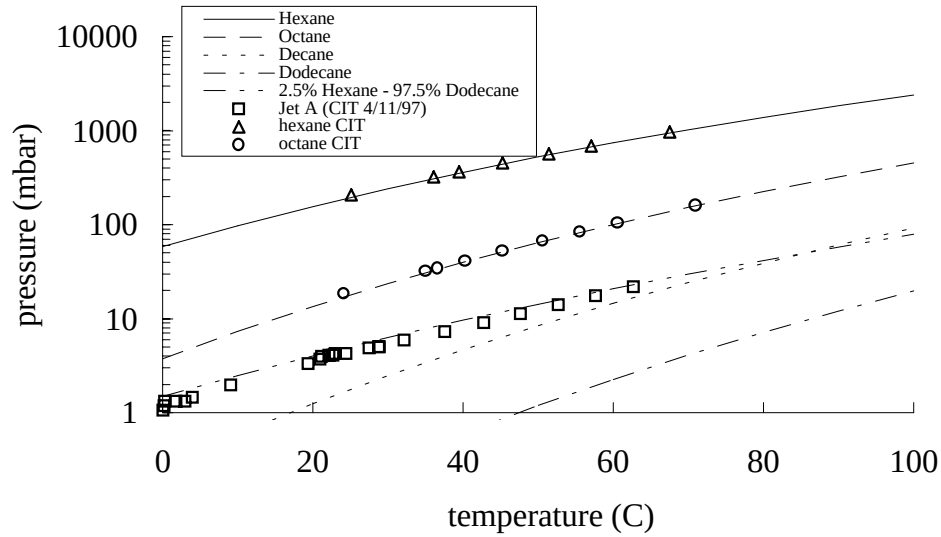

Figure 34: Estimated (Reid et al. 1987) and measured vapor pressure of single component hydrocarbons compared with Jet A.

vapor pressure should be between 5.5 and 11 mbar for temperatures between 35 and 40°C. The measurements described below give values between 7.1 and 8.9 mbar over this temperature range.

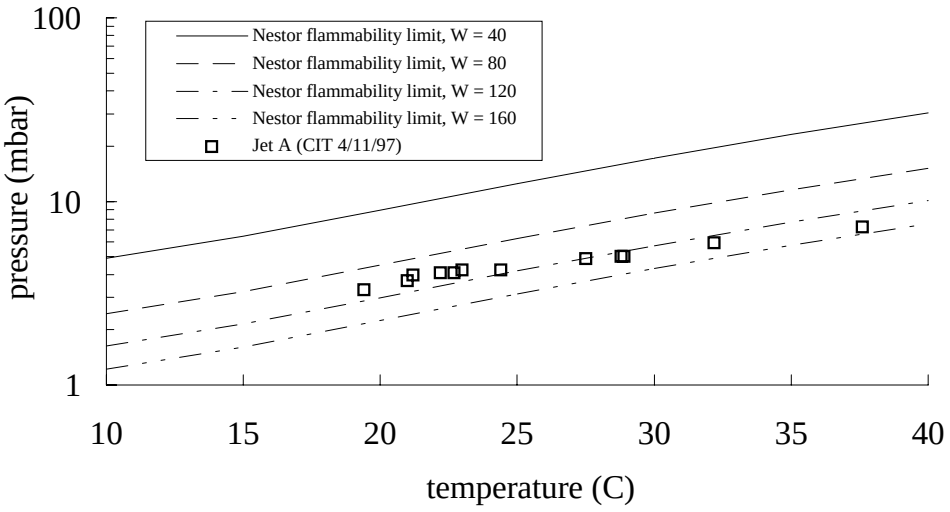

Figure 35: Vapor pressure of Jet A estimated from flammability limits and combustion peak pressure rise. Estimated based on Nestor's flammability limit measurements compared with CIT data.

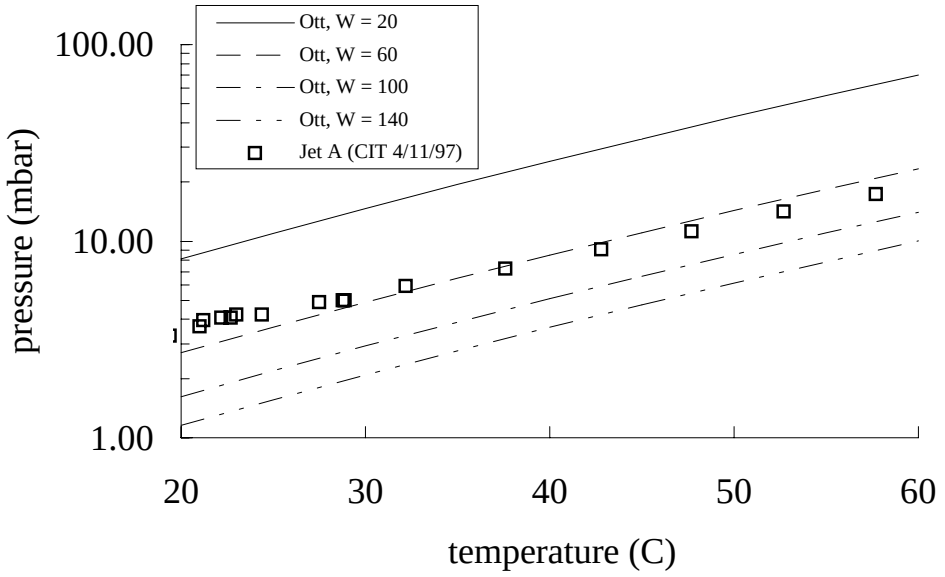

Figure 36: Vapor pressure of Jet A estimated from flammability limits and combustion peak pressure rise. Estimates based on Ott's peak pressure rise compared with CIT data.

7.1 Vapor Pressure Measurements

Vapor pressure measurements were undertaken at Caltech using a simple apparatus (Fig. 37) which consisted of a volume of 1700 ml that could be connected to a fuel reservoir of 860 ml, a precision pressure gauge (MKS Baratron) and a vacuum system.

The main vessel was immersed in a stirred bath of ethylene glycol which was heated with electrical heaters controlled by a feedback system connected to a thermocouple immersed in the bath. The output of the pressure gauge was recorded on a chart recorder and a computer. The fuel temperature is measured by an Omega digital readout attached to a thermocouple that is immersed into the fuel within the main vessel.

Before making a set of vapor pressure measurements, the main vessel was evacuated, closed off and checked for leaks over a period of hours. Since a set of measurements takes place over a day-long period and some of the fuels have very low vapor pressures, the leak rate must be less than 1 mbar over 10 hours. The main vessel was made from a section of 4-in diameter stainless steel pipe with a closure welded on one end and a flange with an o-ring seal welded to the other end. A removable closure mates to the flange with an o-ring seal and is bolted in place. Swagelok o-ring seal fittings are used for the various penetrations into the removable closure. The fuel reservoir was attached to a main vessel using Swagelok fittings and a ball valve. The reservoir can be filled completely full of fuel (no air) and the ball valve closed off before attaching to the main vessel. At the bottom of the vessel, a two-inch diameter magnetic stirrer (teflon coated) is placed in a recess machined to accommodate a circular restraint. The reservoir and ethylene glycol bath are placed on top of the stirrer drive mechanism so that the fuel can be constantly stirred during the test.

The fuel is degassed before making vapor pressure measurements. This is very important for accurate measurements. The procedure is to fill the fuel reservoir, attach the fuel reservoir to the main vessel, evacuate the main vessel and cool it to 0°C by immersing it in an ice water bath. The valve between the fuel reservoir and the main vessel is opened and after some time elapses, the pressure of the evolved air is measured. For 860 ml of Jet A, a pressure of about 66 to 72 mbar is measured, consistent with the estimates given below. This gas is then pumped out of the vessel by connecting the main vessel for the vacuum line for about one minute. The vessel is then sealed off and heated to approximately 30°C. The temperature bath and fuel are stirred constantly during this process. The system is allowed to equilibrate (this is determined by observing the pressure on the chart recorder) and the pressure is measured. The vessel is then cooled to 0°C and the pressure recorded again. Repeated cycles of cooling, evacuation, heating and cooling are performed until the vapor pressure is repeatable at a given temperature. An incomplete degassing process is indicated by hysteresis in the pressure, i.e., the pressure will increase at 0°C after a cycle of heating and cooling even though the vessel remains closed. Since the vapor pressure is quite low (1 to 20 mbar) at the temperatures of interest, even a very small amount of dissolved air can lead to a substantial error in the measured vapor pressure.

The purpose of cooling with the ice bath before evacuation is to minimize the preferential evaporation of the light components of the fuel during the degassing. By lowering the temperature, the vapor pressure is decreased substantially compared to room temperature. However, the outgassing appears to be much slower at low temperature so that cycling between low and high temperatures is needed for effective outgassing. To confirm the effectiveness of this procedure, the total amount of fuel lost to the vacuum system is

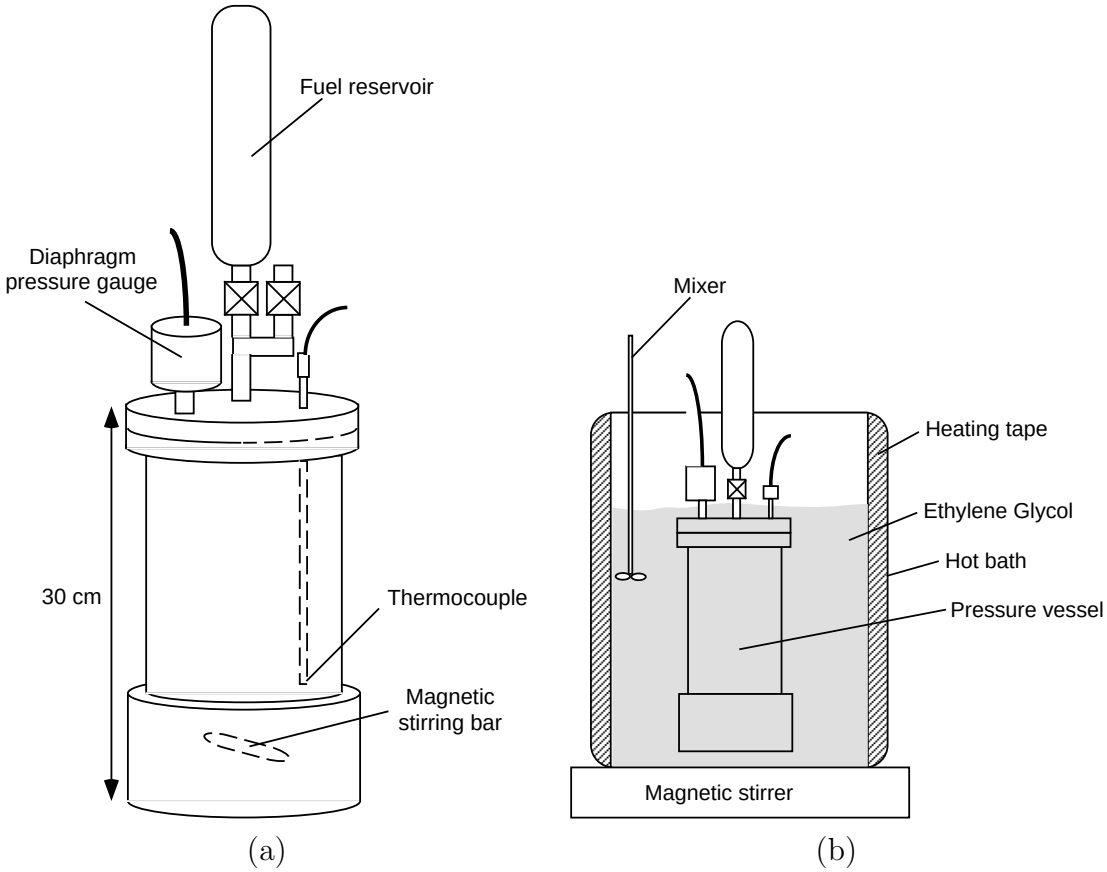

Figure 37: Vapor pressure apparatus. a) Main volume with attached fuel reservoir. b) Assembly immersed in the temperature bath.

determined by measuring the fuel recovered at the end of the measurement and having previously determined the capacity of the fuel reservoir. The measurements are made with graduated cylinders. In this fashion, we have found that less than 0.6% (5 ml out of 860 ml) of the Jet A fuel is lost during the entire measurement process.

A substantial length of time (45 to 60 minutes) is needed to reach a steady or equilibrium value of vapor pressure at a given temperature despite the action of the stirrer and the temperature bath. Some of the equilibration time is associated with the thermal mass of the system but the multicomponent nature of the liquid also plays a role. Preferential evaporation of the light components will create concentration gradients within the liquid. Unless these gradients will be reduced by convection, the vaporization process will slow down and the resulting vapor concentration will be far from equilibrium. This is a concern both in vapor pressure tests and combustion experiments in which the vapor is created by evaporation from a stagnant pool (Ott and Nestor experiments). Convection is required because diffusion within the liquid is extraordinarily slow. The binary mass diffusivity of liquid hexane in liquid dodecane is $D = 2.73 \times 10^{-5}$ cm^2/s at 25°C (Reid et al. 1987). The characteristic time for diffusion across a layer of thickness δ is

δ^2/D. For example, the time required for hexane to diffuse through a 4-in thick layer of dodecane is 3.6 $\times 10^6$ s or about 1 month! In our vapor pressure experiment, the liquid is continuously stirred to minimize the gradients and in the combustion experiments, the dispersal of fuel through the nozzle drastically reduces the diffusion distance and corresponding times.

Once the dissolved gas is removed, the vessel is removed from the ice water bath and placed into the ethylene glycol. The vessel is allowed to warm up to room temperature and then the heater controller is energized. The controller temperature is increased in increments of 5°C and the vapor pressure and actual fuel temperature are recorded after the pressure history indicates that equilibrium has been reached. It typically takes about 10 hours to complete the entire process and measure vapor pressure up to 60°C. The apparatus is allowed to cool down overnight and then further cooling is obtained by placing frozen bottles of water into the bath. The vapor pressure is measured during the cool down process as a check on the measurements made during heating. The stirrer is run constantly during the entire process to prevent stratification of the light component in the liquid. Note that with 860 ml of fuel in a volume of 1700 ml, the mass loading is about 400 kg/m^3 which should be sufficient to yield a "true" vapor pressure measurement.

Measurements have been taken on hexane, octane and LAX Jet A. The hexane and octane measurements were made to verify our technique. The comparisons shown in Fig. 34 with the Reidel vapor pressure correlation (Reid et al. 1987) indicate that the maximum deviations from the correlations are 4% for hexane and 6% for octane. The results for Jet A shown in Fig. 33 agree with the industry proposed values (CRC 1983) between 50 and 60°C and appear to be a reasonable extrapolation for lower temperatures. The data are given in Table 3.

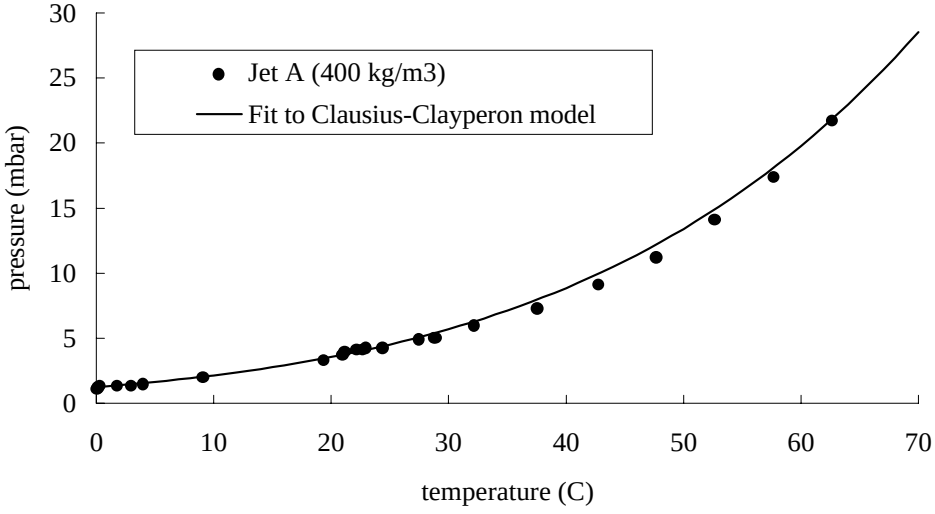

Figure 38: Measured vapor pressure and least squares fit to functional form of Eq. 39.

The observed dependence on temperature can be compared with the standard representation, Eq. 39, of jet fuel vapor pressure. A least squares fit to this representation has

Table 3: Measured vapor pressure of LAX Jet A using the Caltech apparatus and procedure. Estimated uncertainty in pressure is ± 0.2 mbar. Estimated uncertainty in temperature is ± 0.6°C.

$M/V = 400$ kg/m^3				$M/V = 3$ kg/m^3			
T (°C)	P_σ (mbar)	T (°C)	P_σ (mbar)	T (°C)	P_σ (mbar)	T (°C)	P_σ (mbar)
0.1	1.0	23.0	4.2	0.0	0.8	31.8	4.0
0.2	1.2	24.4	4.2	0.6	1.5	41	5.5
0.3	1.3	27.5	4.9	0.9	1.5	41.5	5.7
1.8	1.3	28.8	5.0	1.6	1.6	52	8.0
3.0	1.3	28.9	5.0	2.1	1.6		
4.0	1.4	32.2	5.9	9.2	2.0		
9.1	2.0	37.6	7.2	10.3	2.0		
19.4	3.3	42.8	9.1	15.7	2.4		
21.0	3.7	47.7	11.2	16.3	2.4		
21.2	4.0	52.7	14.1	21.1	2.8		
22.2	4.1	57.7	17.4	23.7	3.0		
22.7	4.1	62.7	21.7	25.2	3.0		

a correlation coefficient of 0.996 and plotting the data in the appropriate coordinates indicates a reasonable fit to this simple form. The resulting relationship for the 400 kg/m^3 case can be expressed as:

$$P_\sigma = 5.75 \times 10^6 \exp(-4191/T) \qquad P \text{ in mbar} \qquad T \text{ in K} \tag{40}$$

Apparently, the analytical representation of the vapor pressure is not too dependent on the function form of the multi-component nature of Jet A. Previous work on crude oil vapor pressure (Woodrow and Seiber 1988) indicates that the vapor can be treated as a mixture of simple compounds. As shown in Fig. 34, a mixture of 2.5% hexane and 97.5% dodecane (mole fractions) provides an approximate match for vapor pressures between 0 and 60°C. This model is tentative and will be refined when a better chemical characterization of Jet A is obtained.

7.2 Mass Loading Effect

Limited experimentation has been carried out on the effect of mass loading. By introducing 6 ml of Jet A into the existing apparatus, data were obtained for a mass loading of 3 kg/m^3. Since such a small quantity of material is used in these tests, only a single degassing exposure of about 1 minute was used at 0°C. Over a period of 10 hours the vapor pressure was measured during a heating cycle of the apparatus. Leak tests indicated that an increase in pressure (due to leaks or additional outgassing) of about 0.26 mbar in 6 hours was initially observed and no measurable leak was noticed between 6 and 20

hours. The results are shown on Fig. 39 and in Table 3. Fitting the data to Eq. 39 yields

$$P_\sigma = 4.971 \times 10^4 \exp(-2868/T) \qquad P \text{ in mbar} \qquad T \text{ in K.} \tag{41}$$

Both sets of data, 400 and 3 kg/m^3, are compared with the predictions of the binary liquid model discussed subsequently. Reasonable agreement is observed between the measurements and the model. A better model composition and more detailed observations are needed to complete this study.

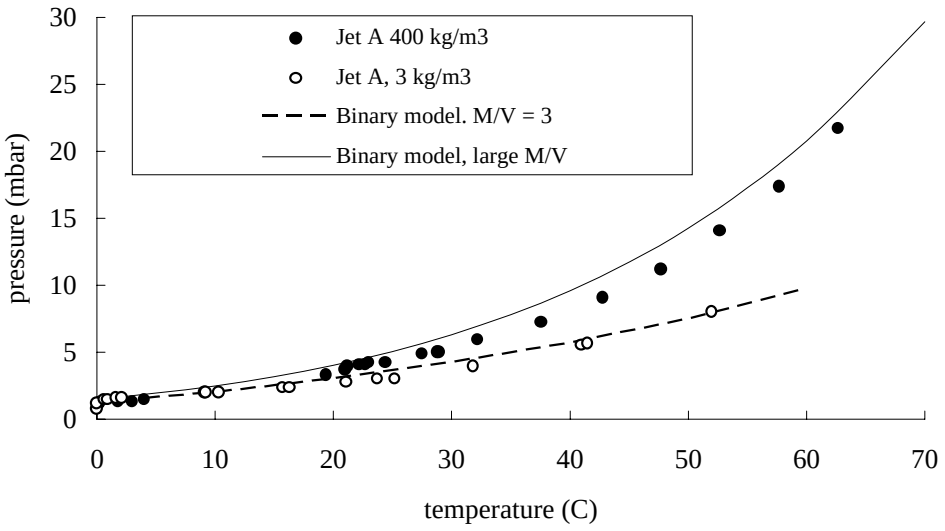

Figure 39: Vapor pressure vs temperature for two mass loadings. Comparison with binary model using 2.5% hexane (molar) and 97.5% dodecane composition.

8 Dissolved Air

A problem with experimental measurements of vapor pressure and an issue in modeling the vapor space composition in the aircraft fuel tank ullage is the influence of dissolved air in the fuel. It is well known that O_2 and N_2 will be released from fuels like Jet A when the pressure is decreased. Preliminary experiments using the Caltech vapor pressure apparatus indicate that a significant amount of air is evolved when the pressure is reduced in the vapor space above the liquid.

Unless the experiment is carefully designed and appropriate corrections are carried out, this effect can seriously distort low-temperature vapor pressure measurements. The conventional treatment for pure substances, degassing the fuel by heating and vacuum exposure, is problematic for multi-component fuels. Such processes can result in removal of the light components from the mixture and an uncontrolled shift in the composition of the fuel. Prolonged exposure to high temperatures can cause chemical changes (Pickard 1996) or cracking of the fuel. All of these factors need to be considered in designing vapor pressure experiments.

One standard parameter for describing gas solubility is the *Ostwald coefficient* β defined as the maximum volume of gas (at a given gas pressure P_g and temperature T) that can be dissolved in a unit volume of liquid. Treating the gas as ideal, the total number of moles of gas N_g dissolved in a volume V_l of liquid are

$$N_g = \frac{\beta V_l P_g}{\tilde{R} T} \tag{42}$$

The total mass of dissolved gas is therefore

$$M_g = \frac{\beta V_l P_g}{RT} \qquad R = \frac{\tilde{R}}{W_g} \tag{43}$$

Ostwald coefficients are a function of temperature $\beta(T)$ and are measured by standardized test procedures (ASTM D 2779). For Jet A between 20 and 40°C, $\beta \approx 0.17$ (CRC 1983).

As an example, the maximum or saturated amount of dissolved air in 50 gallons of Jet A is about 40 g. In the case of the CWT tank of a 747-100, the total tank volume is about 50 M^3, which corresponds to an air mass of 61 kg at sea level. The amount of dissolved air is negligible (less than 10^{-3}) compared to the air present in the ullage. Even if all of this dissolved air were to come out of the solution at 14 kft, it would have no noticeable effect on the vapor space composition. In fact, the air comes out of the solution at a finite rate (see the discussion in Kosvic et al. (1971)) and a maximum of about 40% will come out of the solution at 14 kft due to the air pressure in the CWT ullage. When the air comes out of the solution rapidly, a foam or froth can be formed on the surface. However, visual inspection of fuel samples about 1 inch in depth did not reveal any substantial foam when the fuel was suddenly depressurized. Nestor (1967) also considered this effect and did not find any evidence of foaming under simulated climb conditions.

The ullage volume in the vapor pressure experiments is much smaller than in the combustion experiments so that the effect of dissolved air is much greater. Consider a volume of liquid V_l saturated with air at pressure $P_\circ$ and suddenly introduced into an evacuated container with an ullage volume V_g. Accounting for the air that remains in solution after the system reaches equilibrium, the partial pressure of air in the ullage will be

$$P_{air} = \frac{\beta \frac{V_l}{V_g} P_\circ}{1 + \beta \frac{V_l}{V_g}} \tag{44}$$

In order to measure "true vapor pressure", the volume V_g should be as small as possible relative to V_l so that the "light ends", i.e., low molar mass constituents, are not depleted from the liquid fuel. However, this will exacerbate the problem of dissolved air since the pressure measurement does not distinguish between species. In practice, vapor volumes vary from 1 to 4 times the liquid volume. For $V_g/V_l = 2$, this will result in an air partial pressure of 70 mbar, which will obscure the Jet A vapor pressure at the temperatures of interest. This implies that Jet A has to be almost completely degassed in

order to obtain a reliable vapor pressure measurement when using conventional methods. One technique (Woodrow and Seiber 1988; Woodrow and Seiber 1990) that avoids some of these problems is head space gas chromatography (GC). Fuel vapor composition is measured by the GC and then the vapor pressure is computed using an ideal solution model, as described in the next section. Since the GC technique can discriminate between hydrocarbons and air, the computed vapor pressure will approximate the air-free value.

8.1 Dissolved Water

Water can also be present in Jet A. The solubility is much lower than for air. The handbook (CRC 1983) gives a maximum solubility of .005% by volume at 20°C. The pressure due to this amount of water coming out of solution will be negligible in our vapor pressure experiments.

9 Binary mixture model

The unexpected variation of peak pressure with fuel amount at 40°C (Fig. 40) motivated us to consider the effect of multiple components in the fuel on the vapor composition. To this end, a simple model using two components, one light and one heavy, is developed in this section.

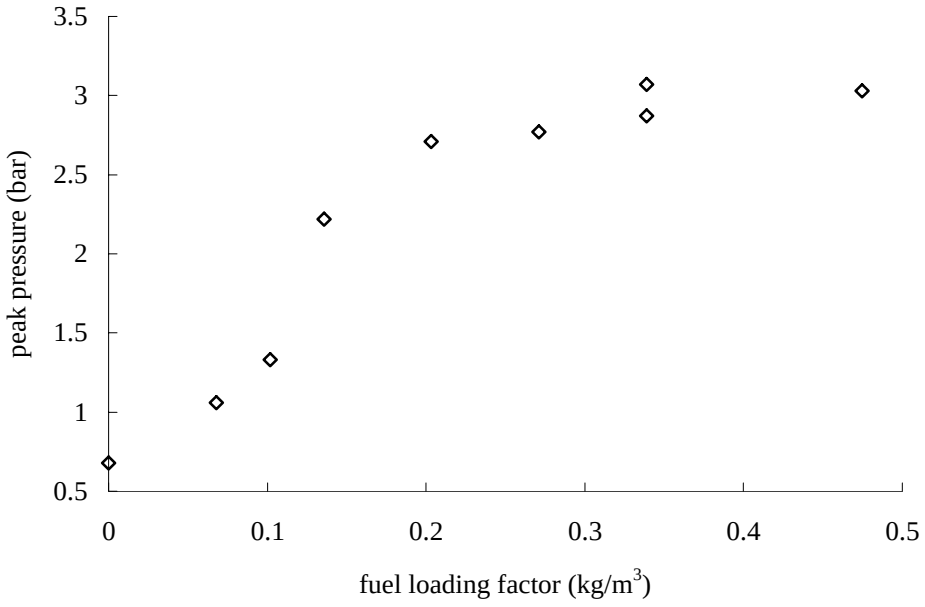

Figure 40: Measured peak pressures as a function of fuel amount for Jet A at 0.585 bar and 40°C .

Determining the partial pressure P_i of component i in a vapor in equilibrium with a liquid mixture is in general a complex task. The simplest sort of model (Abbott and

van Ness 1989) assumes that the liquid and vapor are ideal mixtures, and that activity coefficients, molar volumes and fugacities are independent of pressure. In that case, *Raoult's law* gives the partial pressure as

$$P_i = x_i P_{\sigma i} \tag{45}$$

where $P_{\sigma i}$ is the pure substance saturated vapor pressure and x_i is the mole fraction of species i in the liquid mixture. If the amounts x_i of each component were known, then the vapor pressure of the fuel could be computed as

$$P_\sigma = \sum_{i=1}^{I} x_i P_{\sigma i} \tag{46}$$

Consider a two-component mixture ($I = 2$) inside a container of total volume V. The container ("fuel tank") is partially full of liquid and the vapor above the liquid is in equilibrium with the liquid. The total mass of the mixture within the tank is M and the a total number of moles of each component are N_1° and N_2°. The initial mass M_1 and M_2 of each component can be computed from the number of moles and the molar masses W_1 and W_2:

$$N = N_1^\circ + N_2^\circ \qquad M_1 = W_1 N_1^\circ \qquad M_2 = W_2 N_2^\circ \qquad M = M_1 + M_2 \tag{47}$$

The moles of each component in the liquid are N_1 and N_2 and in the vapor phase n_1 and n_2. These are related by the conservation of the amount of each substance for a closed system

$$n_1 = N_1^\circ - N_1 \qquad n_2 = N_2^\circ - N_2 \tag{48}$$

The partial pressure of each species can be computed using the ideal gas law

$$P_1 = n_1 \frac{\tilde{R}T}{V'} \qquad P_2 = n_2 \frac{\tilde{R}T}{V'} \qquad V' = V - V_l \tag{49}$$

where V_l is the volume occupied by the liquid. Equating the partial pressures as computed by the gas law to the partial pressures computed by Raoult's law and eliminating the variables N_i in favor of n_i, we have:

$$n_1 = \frac{N_1^\circ - n_1}{N^\circ - n_1 - n_2} \frac{P_{\sigma 1} V'}{\tilde{R}T} \tag{50}$$

$$n_2 = \frac{N_2^\circ - n_2}{N^\circ - n_1 - n_2} \frac{P_{\sigma 2} V'}{\tilde{R}T} \tag{51}$$

where $N^\circ = N_1^\circ + N_2^\circ$ is the total number of moles of mixture present in the container. If the amount of liquid present is small compared to the volume of the tank, $V' \approx V$, which is the case of the TWA 800 situation and the CIT experiments. Otherwise, the volume of liquid can be computed as

$$V_l = \frac{W_1(N_1^\circ - n_1) + W_2(N_2^\circ - n_2)}{\rho_l} \tag{52}$$

where ρ_l is the liquid mass density. Note that although we have proceeded as though the tank were closed, the total pressure does not enter into our considerations. Therefore, these results will apply to a vented tank as long as we correct for the loss of substance through the vents, i.e., we need to reduce the amounts N_i° appropriately. Given initial amounts of substance and a temperature T, Eqs. 50-51 can be solved numerically to find the moles n_i of each component in the vapor phase. If we use nondimensional variables, the solution will be a function of the choice of substances and the following parameters

$$T \qquad \frac{M}{V} \qquad \frac{N_1^\circ}{N^\circ} \quad \frac{N_2^\circ}{N^\circ} \tag{53}$$

As an example we have computed the solution for a mock jet fuel mixture consisting of 97.5% dodecane and 2.5% hexane by molar amount. The total vapor pressure as a function of the mass loading factor M/V is shown in Fig. 41 for temperatures of 30, 40 and 50°C.

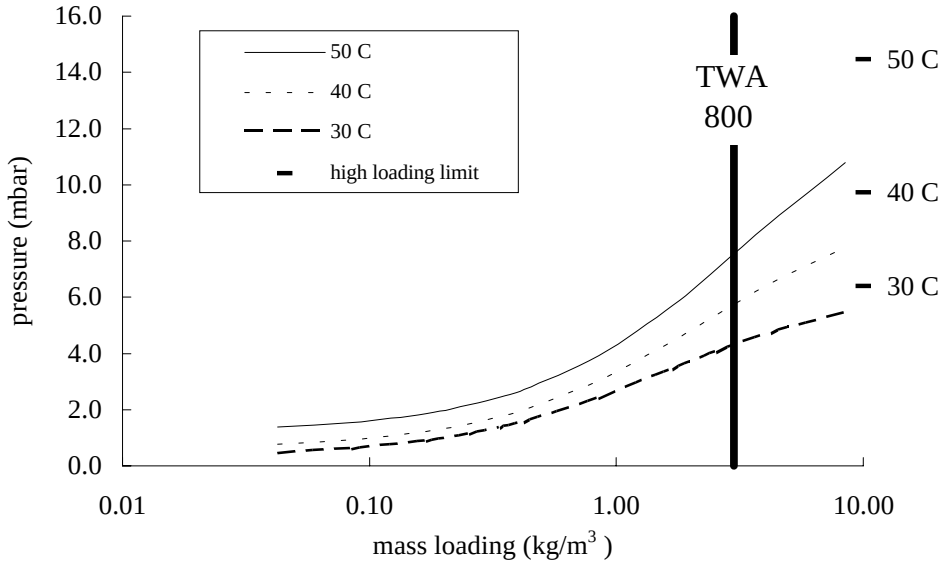

Figure 41: Vapor pressure as a function of fuel loading factor for the ideal binary mixture model with 97.5% dodecane and 2.5% hexane (molar) at 30, 40 and 50°C.

This figure illustrates the effect of depletion of the light component by evaporation. For small values of loading, $M/V \to 0$, the partial pressure of hexane is limited by the decrease of hexane in the liquid with evaporation. As the mass loading M/V is increased, evaporation of hexane results in less depletion and the partial pressure of hexane vapor increases. The partial pressure of dodecane is almost independent of the loading since the effects of depletion are negligible until the mass loading of liquid becomes so small (< 5 g/m^3) that the dodecane is almost all vaporized.

For high loading, $M/V \to \infty$, the partial pressure of hexane and the total vapor pressure approaches limiting values which are given by Raoult's law (Eq. 45) with the mole fractions of liquid given by the initial composition of the mixture. These limiting values are shown as the points labeled "high loading" on Fig. 41. This example illustrates both the importance of having a high loading value in vapor pressure measurements and the importance of the low loading factors in determining hazards in nearly empty fuel tanks. In the CIT combustion experiments, a maximum loading factor of 0.5 kg/m^3 was used. The loading factor in the CWT of TWA 800 was about 3 kg/m^3. The loading factor was 120 kg/m^3 in Nestor's experiments and was 100 kg/m^3 in Ott's experiments. In the CIT vapor pressure experiments, the maximum loading factor is about 400 kg/m^3.

As the loading factor increases, the composition shifts toward the light component. The fraction of hexane in the vapor as a function of loading factor is shown in Fig. 42. As the temperature increases, the composition shifts toward the heavier component. These shifts are reflected in the behavior of the mean molar mass, illustrated in Fig. 43. These results indicate the extreme sensitivity of the behavior of fuel vapor to liquid composition at low temperatures. Although the liquid is 97.5% dodecane, the vapor is almost 100% hexane at temperatures less than 50°C and modest (≥ 1 kg/m^3) fuel loading factors. This dramatically illustrates the importance of understanding the fuel composition, including the apparently "minor" amounts of light species.

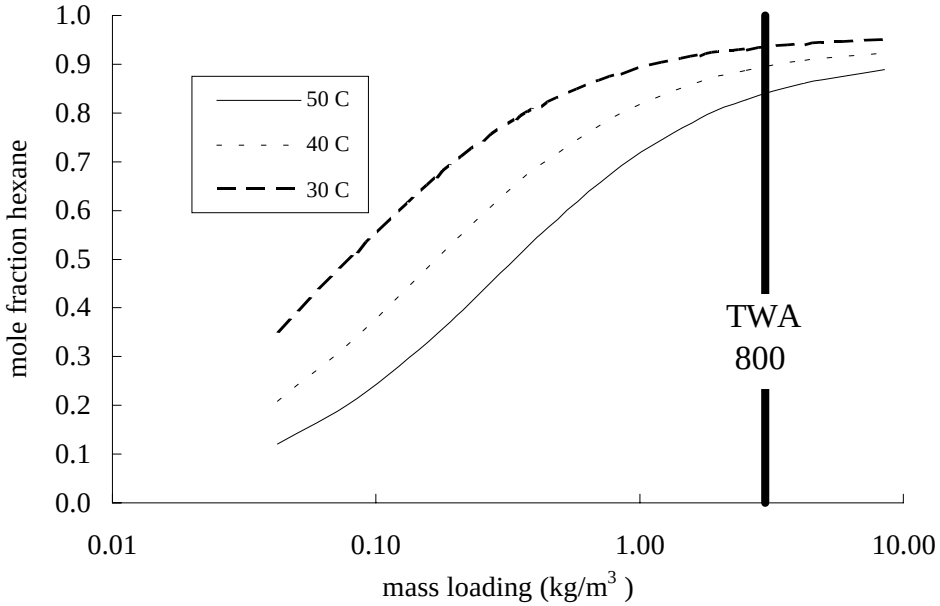

Figure 42: Hexane fraction as a function of fuel loading factor for the ideal binary mixture model with 97.5% dodecane and 2.5% hexane (molar) at 30, 40 and 50°C.

The flammability of these mixtures can be estimated by computing the fuel-air mass ratio f and comparing it with the estimated lower limit range for Jet A of 0.019 to 0.026. In terms of the fuel vapor pressure P_σ and mean molar mass W_{fuel},

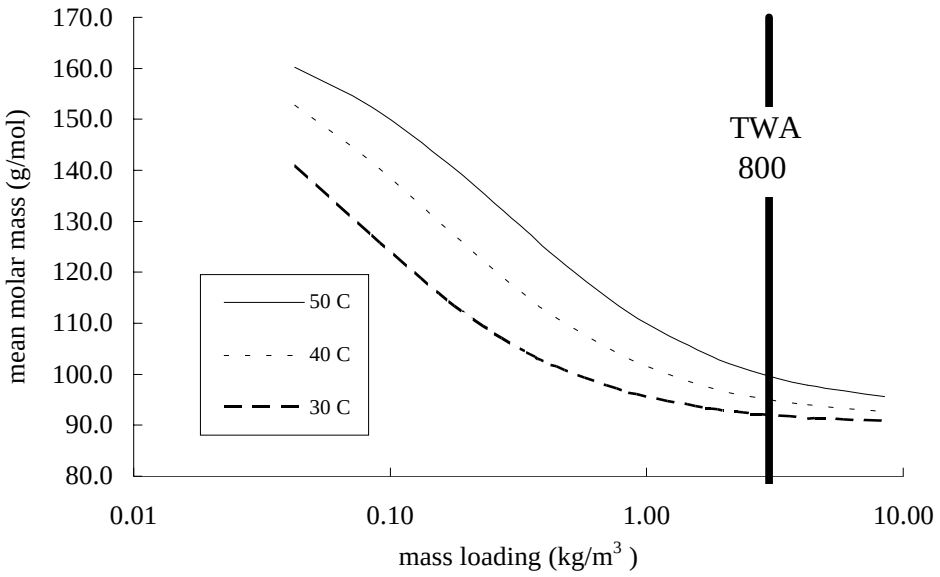

Figure 43: Mean molar mass as a function of fuel loading factor for the ideal binary mixture model with 97.5% dodecane and 2.5% hexane (molar) at 30, 40 and 50°C.

$$f = \frac{P_\sigma}{P_{air}} \frac{W_{fuel}}{W_{air}} \approx \frac{P_\sigma}{P} \frac{W_{fuel}}{W_{air}} \tag{54}$$

where P is the total mixture pressure and the approximation is that P_σ is much less than P. The results are shown in Fig. 44. These results indicate that at a fixed temperature, the vapor will reach a flammable condition as the mass loading is increased, provided that T is high enough.

The model choices of hexane and dodecane and the 2.5% hexane amount were motivated by the vapor pressure measurements but can not be considered realistic. A large number of other possibilities exist and these choices simply serve to illustrate the trends that are a consequence of this model. A realistic model of Jet A will require quantitative chemical analysis to define the appropriate model compounds and composition.

10 Application to TWA Flight 800

In order to evaluate the implications for TWA 800, an estimate of the fuel and air conditions in the CWT at the time of the explosion are needed. First, we will consider the effect of the flight from Athens and the gate hold on the fuel composition. Second, we will consider the effect of the ACM operation and climb out from JFK on the composition of the tank ullage at the time of the explosion.

One issue that has been raised and discussed briefly in Section 2.2, is the problem of flight conditioning of the fuel. The situation is shown in Fig. 45. The fuel tank is vented to the atmosphere through two vent stringers (Fig. 10) which extend the length of the

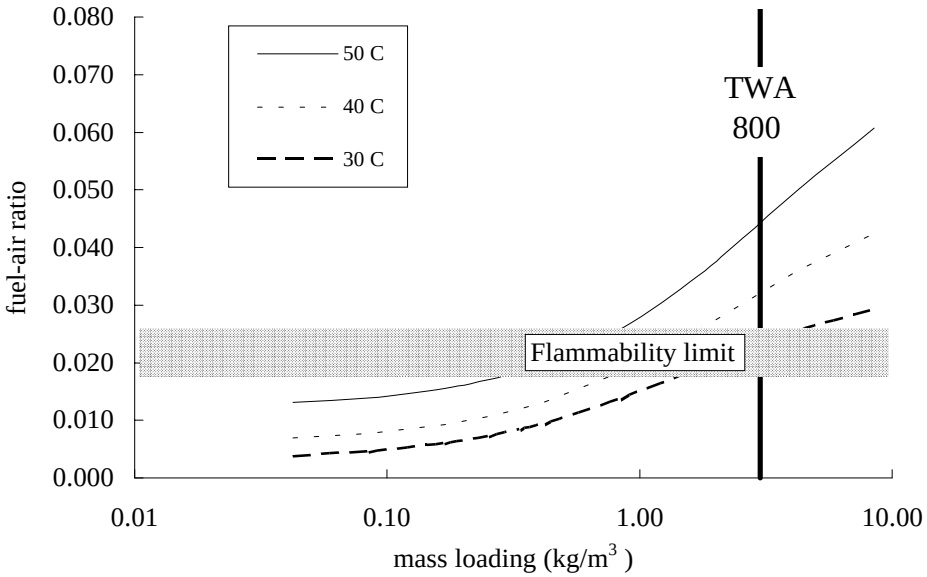

Figure 44: Fuel-air mass ratio as a function of fuel loading factor for the ideal binary mixture model with 97.5% dodecane and 2.5% hexane (molar) at 30, 40 and 50°C.

wing. The path from the tank to the atmosphere is therefore about 100 ft. Each stringer has a nominal cross-section of 4.75-in by 2.75-in. During level flight or ground operations,

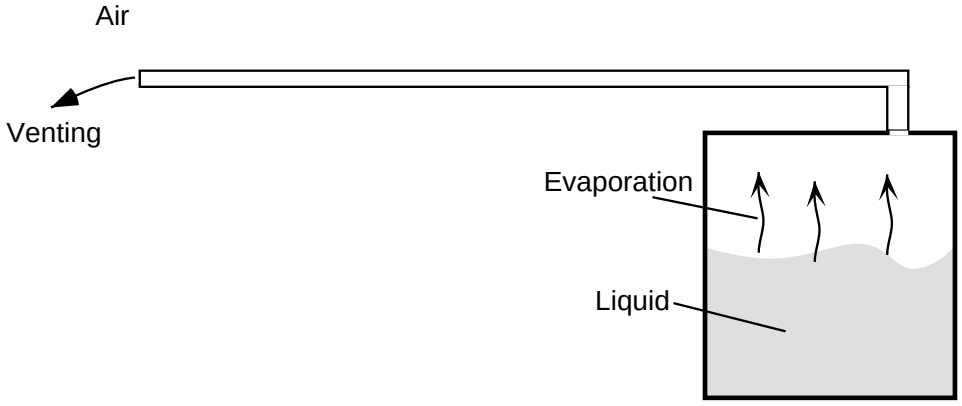

Figure 45: Problem definition for evaporation losses through the vent stringer.

there is no mean flow through the vent stringer. Fuel can only be lost by diffusion along the vent due the concentration gradient between the tank and the atmosphere. The flux J of fuel vapor is determined by Fick's law

$$J = -\mathcal{D}\frac{\partial C}{\partial x} \tag{55}$$

where $\mathcal{D}$ is the mass diffusion coefficient and C is the concentration of fuel per unit volume. For hexane vapor in air at 1 atm and 306 K, the mass diffusion coefficient is

equal to (Reid et al. 1987) 9×10^{-6} m^2/s. The mass diffusion coefficient is proportional to the inverse pressure so that at 0.25 atm (corresponding to 35 kft altitude), $\mathcal{D} = 3.6\times10^{-5}$ m^2/s.

The fuel mass loss associated with diffusion can be estimated by approximating the gradient in concentration as linear. Substitution into Fick's law yields

$$\frac{\mathrm{d}M}{\mathrm{d}t} = AW_{fuel}\mathcal{D}\frac{C_{tank}}{L} \tag{56}$$

where C_{tank} is the concentration (moles/m^3) of fuel in the tank, L is the stringer length and A is the combined area of the two vent stringers. Using a vapor pressure of 7.5 mbar and a total pressure of 0.25 atm, we estimate a fuel loss rate of 1.4×10^{-7} g/s, which over a period of 16 hours would result in the loss of 8 mg of fuel, an inconsequential amount. Of far greater importance is what happens during the climb from JFK to 14 kft.

The issue of the thermal environment produced by the ACM operation during the gate hold must addressed through flight test and thermal modeling. A preliminary flight test was carried out by Boeing (8-26-97) and temperatures at 5 locations within the CWT were measured as a function of altitude. At takeoff, temperatures within the tank ranged from 85 to 96°F (29 to 35°C). After takeoff, a fuel temperature of 115°F (46°C) was measured at the rear spar for altitudes above 7 kft. The air temperatures within the tank decreased with increasing altitude up to about 10.5 kft and then returned to the takeoff values above 12 kft. This is an indication of the role of heat transfer since if the gas within the tank expanded adiabatically (no heat transfer) during climb, the temperature would drop by 44°C.

Both fuel and air temperatures are above the flammability limit temperatures of 25 to 28°C measured by Ott and Nestor at a pressure of 0.585 bar, equivalent to 14 kft. Since the fuel and atmosphere are at different temperatures, it is not clear what the resulting average fuel vapor concentration would be. Experiments and/or models of the heat and mass transfer within the tank are required to address this issue.

A simple approach to the problem of effective fuel composition in the CWT is to consider the analogy between heat and mass transfer in turbulent flows. The situation within the CWT during the gate hold corresponds to the physical problem of natural convection in an enclosure driven by the temperature difference between the bottom and the top, see Fig. 46. Hot gas (a mixture of fuel vapor and air) will rise from the bottom of tank, reach the top, cool off and flow downwards. Fuel evaporated at the bottom will mix with the adjacent air, rise to the top of the tank, partially condense on the cooler upper surface, and drip off or re-evaporate. In this manner, a circulation or convection pattern is set up within the compartment of the CWT. The resulting distribution of fuel vapor depends on the flow pattern and the strength of the convection. Convective flows are conventionally characterized by a nondimensional parameter, the Rayleigh number Ra, which is defined as

$$Ra = \frac{g\alpha\Delta T H^3}{\nu\kappa} \tag{57}$$

where $g = 9.81$ m/s^2 is the acceleration of gravity, α is the coefficient of thermal expansion

for ai is the
therm

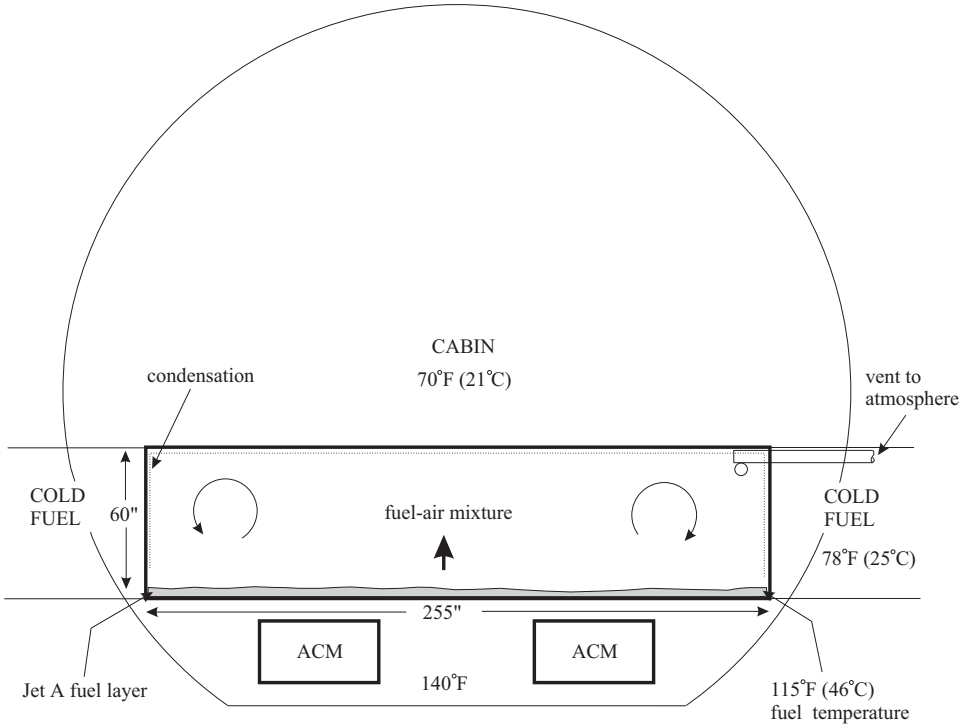

Figure 46: Location of the ACM units that provide the heat sources for fuel vaporization, conduction and natural convection within the CWT. There are three ACM units, only two are visible in this view.

Given the temperature difference $\Delta T = 25°\text{C}$ between the bottom and top of the tank and characteristic height $H = 1.5$ m, the Rayleigh number can be estimated to be $9{\times}10^8$, which will result in highly turbulent flow. In this situation, most of the heat transfer will occur in thin layers (less than 10% of the height of the tank) near the upper and lower surfaces and the bulk of the ullage will be at a uniform temperature which is the average of the upper and lower surface temperatures. This simple picture is supported by experimental measurements (Catton 1978; Thomas and Townsend 1957) but the exact conditions of the CWT have not been examined in laboratory testing. This model suggests that the average air temperature in the tank is about 33.5°C (92°F). This is comparable to the average air temperature measured in the preliminary flight tests (85 to 95°F).

The distribution of fuel vapor is expected to be similar to the temperature profile in a turbulent flow. The mass diffusivity $\mathcal{D}$ of fuel vapor is slightly smaller than the thermal diffusivity κ of the air, so that the concentration boundary layers will be slightly thinner than the temperature boundary layers. The ratio $\kappa/\mathcal{D}$ (Lewis number) for hexane vapor diffusing in air is 2.26 at sea level. The average fuel concentration (expressed as

fuel-air mass ratio) will be the average of the concentrations at the upper and lower surfaces. Assuming that fuel vapor is in equilibrium with the fuel liquid at the upper and lower surfaces, the vapor pressure can be computed from the estimated temperatures of 21°C (corresponding to the 70°F cabin floor temperature) for the upper surface and 46°C for lower surface (corresponding to the fuel temperature of 115°F measured in the preliminary flight tests). If we use the $M/V = 400$ kg/m^3 vapor pressure data obtained at Caltech, the resulting average vapor pressure will be 7.55 mbar. Using a vapor molar mass of 86 g/mol implies a fuel-air mass ratio $f = 0.022$ at sea level and for rapid evaporation during climb, a value of 0.038 at 14 kft. These values should be compared with the flammability limit range of 0.019 to 0.026 estimated from the Nestor experiments discussed in Section 2.1.

Since there was only a limited amount (50 to 100 gallons) of fuel present in the tank, the issue of fuel fractionation must be considered. Fifty gallons of Jet A in the CWT corresponds to a loading of about 3 kg/m^3. Our preliminary measurements and the binary mixture model both indicate a decrease in fuel vapor pressure with a decrease in the loading factor. At a loading of 3 kg/m^3, we estimate a fuel-air mass ratio $f = 0.015$ at sea level and for rapid evaporation during climb, a value of 0.027 at 14 kft, if we do not correct for the loss of the light component of the fuel. These values bracket the estimated flammability range and indicate that the mixture would be flammable at an altitude of 14 kft but not at sea level (see Fig. 11)

Simple estimates of the heat transfer and the experiments of Kosvic et al. suggest that rapid evaporation during the climb phase is very plausible. Based on an average fuel partial pressure of 5 mbar, the total mass of fuel vapor present in the CWT at sea level is 0.9 kg. During the climb, equal proportions of fuel vapor and air will be vented out of the tank. At an altitude of 14 kft, 0.373 kg of the fuel vapor originally present would have been vented from the CWT. Since the light component is now partially depleted, the vapor pressure will further decrease. The binary mixture model indicates that the mean vapor pressure of the fuel will decrease about 20% to a value of 4.0 mbar. This decreases the estimated maximum possible fuel-air mass ratio at 14 kft to $f = 0.022$, just within the flammable range.

From the vapor pressure measurements, we can estimate the heat of vaporization from Eq. 38, to be 435 kJ/kg. This implies an energy input of at least 162 kJ is required for fuel evaporation to make up for the vented fuel vapor. Over a period of 15 minutes, this amounts to an average power of 180 W. This is a very modest requirement in comparison to the heat transfer through the CWT structure due to the temperature difference between the bottom and top of the tank.

The limited mass of fuel will also affect the peak explosion overpressure. At 40°C, we found (Fig. 20) that with a loading of .5 kg/m^3, a limiting peak pressure was apparently reached. At this condition, a peak explosion pressure of about 3 bar was obtained. Further combustion tests at lower temperatures (30 to 35°C) are needed to determine to overpressure variation with fuel loading at these conditions.

The maximum combustion pressure rise can be estimated in several ways. The adiabatic estimate from Eq. 9 yields an upper bound of 2.15 bar (31.6 psi) pressure rise. This

value does not include any potential reduction due to heat transfer or venting. A more realistic value can be obtained by correcting Ott's data (Fig. 26) for our value of fuel mass loading and the decrease in light component due to venting during climb. At 33°C, the peak pressure rise is predicted to be between 1.54 and 1.98 bar (22.6 and 29.1 psi) for a fuel loading of about 100 kg/m^3. Based on our binary model results, we expect the vapor pressure and composition to be close to the large loading limit under these conditions. Equation 9 indicates that the peak pressure rise can be corrected for finite fuel loading and depletion by simply multiplying by the ratio of the expected fuel-air mass ratio to the fuel-air mass ratio present in Ott's experiments. This yields an estimate of a peak pressure rise that is 60% of Ott's value, or a range of 0.92 bar (13.5 psi) to 1.19 bar (17.4 psi).

Even higher peak pressures are possible, depending on the nonuniformity of the vapor concentration and the role of mists or sprays created by aircraft vibration and lofting during the course of the explosion. In those cases, observations by Ott and Nestor indicate that peak pressure rise up to 5 bar (73.5 psi) may be possible. Other the other hand, heat transfer and venting effects may result in further reductions of the peak pressure. Further uncertainty is introduced by the multicompartment nature of the CWT. These effects can only be resolved by testing with scale models and actual CWT structures.

However, even without considering these effects, the expected pressures are sufficiently high to pose a threat to the airplane integrity. Portions of the CWT structure are estimated (by Boeing) to fail for overpressures greater than about 20 psi. We conclude that failure of the CWT structure is a credible consequence of the explosion of the fuel-air mixture in the ullage at an altitude of 14 kft.

11 Conclusions

Key findings of our study are:

1. Flammability limits of Jet A are uncertain.

   There is substantial variability in the measured flammability limits of Jet A. In terms of temperature conditions, the lower flammability limit is between 32 and 38°C at sea level, 24 and 29°C at 15 kft. In terms of the fuel-air mass ratio, the lower flammability limit is estimated to fall in the range of .019 to .026. This is substantially lower than the value of 0.035 qouted for pure hydrocarbon fuels. The limits depend on ignition energy and the method of observation.

2. The composition of Jet A is poorly known.

   Jet A is a mixture of hydrocarbons with a broad range of molar masses. Molecules with as few as 5 and as many as 16 carbon atoms (molar mass of 226) are observed in a typical liquid sample (see Appendix B). The low-temperature (20 to 40°C) vapor contains only the lighter components, with 10 carbon atoms or fewer (molar masses less than 130). The precise composition is usually not known or regularly measured for Jet A so this is a difficult issue to discuss in quantitative terms. However,

it is very significant for understanding experimental results on flammability and explosion. Better characterization is needed as a function of temperature and fuel loading factor.

3. Most Jet A vapor pressure data are really unreliable correlations.

   The existing vapor pressure "data" is highly contradictory and probably based on correlations rather than measurement. The vapor pressure is likely to vary from batch to batch and measurements can easily be contaminated by dissolved air. Measurements have been made for one batch of LAX Jet A which agree with the CRC 530 estimate and are slightly higher than the Ott data but disagree with all other reported values.

4. Jet A vapor pressure can be modeled with a binary mixture.

   Experiments and a simple binary mixture model show that for the purposes of estimating vapor pressure, a mixture of 2.5% hexane and 97.5% dodecane produces a vapor pressure very close to the Jet A measured values. Further chemical characterization of Jet A and combustion tests are needed to refine this model.

5. Previous studies on Jet A have not examined the effect of fuel loading (mass of fuel per ullage volume) on flammability and explosion peak pressure.

   Flammability limits for multi-component liquid fuel are not a unique function of temperature but also depend on the total mass of liquid used in the experiment. Flammability of Jet A at low temperatures (40°C) is due to the vaporization of the low boiling point fractions or "light ends" in the fuel. A simple model of Jet A using two components, one light (hexane) and one heavy (dodecane), shows that the partial pressure of the light component in the vapor will be a strong function of the ratio of liquid mass to vapor volume. Experimental measurements at two values of the fuel loading, 3 and 400 kg/m^3 confirm this prediction. Explosion peak pressure measurements demonstrate a strong dependence on fuel loading values.

6. The flash point of Jet A is 10 to 15°C higher than the flammability limit temperature as determined by actual explosion testing.

   The light components of the fuel determine the low-temperature flammability, preparation and handling of the fuel may have a significance to flammability that will not be reflected in the average properties of the fuel. Some evidence of this will be reflected in changes in the flash point. However, the flash point temperatures are not a reliable guide to assessing explosion hazards in multicomponent fuels. Flammability tests in vessels or tubes with the appropriate mass loading factor and instrumentation must be used to determine flammability. Previous tests by Ott and Nestor provide a substantial data base on flammability and the present tests extend this to include the effects of fuel loading factor.

7. It is not sufficient to know the vapor pressure but the vapor composition must also be known in order to predict flammability from pressure and temperature conditions.

   Vapor pressure does not uniquely determine flammability limits and flash points as it does for pure liquids. Our simple binary mixture models illustrate how the composition of the vapor is a function of temperature and the liquid mass/vapor volume ratio. Therefore experiments with different fuel mass/volume ratios will yield different flammability limits. In addition, the minimum mass of fuel required to obtain a flammable mixture will be a strong function of temperature. Chemical characterization and our simple model illustrates that the light fractions of the fuel dominate the vapor composition at low temperatures. Although previous investigators have recognized that the multicomponent nature of the fuel, the consequences have apparently never been carefully examined.

8. The fuel vapor in the ullage of the TWA 800 CWT was flammable at the time of the explosion and the estimated peak pressures are sufficiently high that structural failure is a credible consequence of flame propagation within the tank ullage. However, the magnitude of the peak pressure and the pressure-time history within the CWT cannot be predicted with any certainty given the present data.

   Additional testing is required to understand the effect of fuel and air temperature differences, laminar flame speeds, ignition energies, the size (scaling) of the tank, partitions between compartments and the potential for liquid fuel dispersion by the explosion. Further lab scale testing is in progress and large scale tests are in the planning stages.

References

Abbott, M. M. and H. C. van Ness (1989). *Thermodynamics* (2nd ed.). McGraw-Hill.

ASTM D2889 (1990). *Standard Test Method for Calculation of True Vapor Pressures of Petroleum Distillate Fuels*. American Society for Testing and Materials.

ASTM D323 (1990). *Standard Test Method for Vapor Pressure of Petroleum Products (Reid Method)*. American Society for Testing and Materials.

ASTM D56 (1988). *Standard Test Method for Flash Point by Tag Closed Tester*. American Society for Testing and Materials.

ASTM D86 (1990). *Standard Test Method for Distillation of Petroleum Products*. American Society for Testing and Materials.

Ballal, D. and A. Lefebvre (1981). A general model of spark ignition for gaseous and liquid fuel-air mixtures. In *Eighteenth Symposium (International) on Combustion*, pp. 1737–1745. The Combustion Institute.

Barnett, H. and R. Hibbard (1956). Properties of aircraft fuels. Technical Note 3276, National Advisory Committee for Aeronautics, Washington.

Bradley, D. and A. Mitcheson (1976). Mathematical solutions for explosions in spherical vessels. *Combustion and Flame 26*, 201–217.

Bradley, D. and A. Mitcheson (1978). The venting of gaseous explosions in spherical vessels. *Combustion and Flame 32*, 221–255.

Burgoyne, J. (1963). The flammability of mists and sprays. In *2nd Symp. on Chemical Process Hazards*. Instn Chem. Engrs.

Catton, I. (1978). Natural convection in enclosures. In *Sixth International Heat Transfer Conference*, Volume 6, pp. 13–31.

CRC (1967, May). CRC aviation handbook–fuels and fuel systems. NAVAIR 06-5-504, Naval Air Systems Command.

CRC (1983). Handbook of aviation fuel properties. CRC Report 530, Society of Automotive Engineers, Warrendale, PA.

Cummings, J. C., J. H. S. Lee, A. C. Camp, and K. D. Marx (1984). Analysis of combustion in closed or vented rooms and vessels. *Plant/Operation Progress 3*(4), 239–247.

Davis, S. G., H. Wang, K. Brezinsky, and C. K. Law (1997). Benzene/toulene flames and oxidation kinetics. In *Twenty-Fifth Symposium (International) on Combustion*, pp. 1025–1034. The Combustion Institute.

Dietrich, D., N. Cernansky, M. Somashekara, and I. Namer (1990). Spark ignition of a bidisperse, *n*-decane fuel spray. In *Twenty-Third Symposium (International) on Combustion*, pp. 1383–1389. The Combustion Institute.

Gaydon, A. G. and H. G. Wolfhard (1979). *Flames*. Chapman and Hall.

Gibbs, G. and H. F. Calcote (1959). Laminar burning velocity. *J. Chem. Eng. Data 4*, 226–237.

Heywood, J. B. (1988). *Internal Combustion Engine Fandamentals*. McGraw-Hill.

Hjertager, B. H. (1993). Computer modelling of turbulent gas explosions in complex 2D and 3D geometries. *Journal of Hazardous Materials 34*, 173–197.

Kinney, G. F. and K. J. Graham (1985). *Explosive Shocks in Air* (2nd ed.). Springer.

Kosvic, T., L. Zung, and M. Gerstein (1971). Analysis of aircraft fuel tank fire and explosion hazards. Technical Report AFAPL-TR-71-7, Air Force Aero Propulsion Laboratory, Wright-Patterson Air Force Base, Ohio.

Kuchta, J. M., , J. N. Murphy, A. L. Furno, and A. Bartkowski (1971). Fire hazard evaluation of thickened aircraft fuels. In *Aircraft Fuels, Lubricants and Fire Safety*, Volume 84 of *AGARD Conference Proceedings*, pp. 22–1 to 22–11.

Kuchta, J. M. (1973). *Fire and Explosion Manual for Aircraft Accident Investigators*. Bureau of Mines. AD-771 191.

Kuchta, J. M. (1975). Summary of ignition properties of jet fuels and other aircraft combustible fluids. Technical Report AFAPL-TR-75-70, U.S. Bureau of Mines.

Kuchta, J. M. (1985). Investigation of fire and explosion accidents in the chemical, mining, and fuel-related industries—a manual. Bulletin 680, U.S. Bureau of Mines.

Kuchta, J. M. and R. G. Clodfelter (1985). Aircraft mishap fire pattern investigations. Final Report APWAL-TR-85-2057, Aero Propulsion Laboratory.

Lefebvre, A. H. (1983). *Gas Turbine Combustion*. Hemisphere.

Lewis, B. and G. von Elbe (1961). *Combustion, Flames and Explosions of Gases* (Second ed.)., pp. 323–346. Academic Press.

Moussa, N. (1990). Flammability of aircraft fuels. SAE Technical Paper Series 901949. Aerospace Technology Conference & Exposition, Long Beach, CA Oct 1-4.

Moussa, N., M. Whale, D. Grossmann, and X. Zhang (1996). The potential for fuel tank fire and hydrodynamic ram initiated by uncontained engine debris on commercial aircraft. Draft report for FAA, BlazeTech Corporation, Cambridge, Massachussetts.

Mulpuru, S. R. and G. B. Wilkin (1982, February). A model for vented deflagration of hydrogen in a volume. AECL 6826, Whiteshell Nuclear Research Establishment.

Nagy, J., E. Seiler, J. Conn, and H. Verakis (1971). Explosion development in closed vessels. Report of Investigations 7507, Bureau of Mines, U.S. Department of the Interior.

Nestor, L. (1967). Investigation of turbine fuel flammability within aircraft fuel tanks. Final Report DS-67-7, Naval Air Propulsion Test Center, Naval Base, Philadelphia.

NFPA68 (1994). *Guide for Venting of Deflagrations*. 1 Batterymarch Park, PO BOx 9101, Quincy, MA 02269-9101: National Fire Protection Association.

Ott, E. (1970). Effects of fuel slosh and vibration on the flammability hazards of hydrocarbon turbine fuels within aircraft fuel tanks. Technical Report AFAPL-TR-70-65, Fire Protection Branch of the Fuels and Lubrication Division, Wright-Patterson Air Force Base, Ohio.

Pickard, J. (1996). Kinetics of the autoxidation of a jet-a fuel. *Energy and Fuels 10*, 1074–1077.

Popat, N., C. A. Catlin, B. Arntzen, R. P. Lindstedt, B. H. Hjertager, T. Solberg, O. Saeter, and A. C. V. den Berg (1996). Investigations to improve and assess the accuracy of computational fluid dynamic based explosion models. *Journal of Hazardous Materials 45*, 1–25.

Reid, R., J. Prausnitz, and B. Poling (1987). *The Properties of Liquids and Gases* (4th ed.). McGraw-Hill.

Reynolds, W. C. (1986, January). *The Element Potential Method for Chemical Equilibrium Analysis: Implementation in the Interactive Program STANJAN* (3rd ed.). Dept. of Mechanical Engineering, Stanford, CA: Stanford University.

Richards, G. A. and A. H. Lefebrve (1989). Turbulent flame speeds of hydrocarbon fuel droplets in air. *Combustion and Flame 78*, 299–307.

Rose, J. and J. Cooper (1977). *Technical Data on Fuel* (7th ed.). Wiley.

Shepherd, J. E. and A. C. Ratzel (1985). Heat transfer resulting from premixed combustion. In C. Law, Y. Jaluria, W. W. Yuen, and K. Miyasaka (Eds.), *Heat Transfer in Fire and Combustion Systems*, ASME HTD-45, pp. 191–201.

Tamanini, F. and J. L. Chafee (1990). Turbulent unvented gas explosions under dynamic mixture injection conditions. In *Twenty-Third Symposium (International) on Combustion*, pp. 851–858. The Combustion Institute.

Tamanini, F. and J. L. Chafee (1992). Turbulent vented gas explosions with and without acoustically-induced instabilities. In *Twenty-Fourth Symposium (International) on Combustion*, pp. 1845–1851. The Combustion Institute.

Thomas, D. B. and A. A. Townsend (1957). Turbulent convection over a heated horizontal surface. *Journal of Fluid Mechanics 2*, 473–492.

Tsoovkun, N. et al. (1985). *Physico-Chemical Properties of Jet Fuel*. Cheemeeya, Moscow.

Ural, E. A. and R. G. Zalosh (1988, April). HICCUP: A computer code for hydrogen injection, combustion, and cooldown using phenomenological models. EPRI NP-5721-CCM, Electric Power Research Institute.

Woodrow, J. and J. Seiber (1988). Vapor-pressure measurement of complex hydrocarbon mixtures by headspace gas chromatography. *J of Chromatography 455*, 53–65.

Woodrow, J. and J. Seiber (1990). Evaluation of a method for determining vapor pressures of petroleum mixtures by headspace gas chromatography. Final Report

CARB-RR-90-14, Department of Environmental Toxicology, University of California, Davis.

Zabetakis, M. and B. H. Rosen (1957). Considerations involved in handling kerosine. *Proc. Am. Petrol. Inst. 37*(3), 296–306.

Zabetakis, M. G. (1965). Flammability characteristics of combustible gases and vapors. Bulletin 627, Bureau of Mines.

A Test Conditions

Table 4: Test conditions

Date	Run No	Fuel	Vol. (ml)	Yfuel	T_{FUEL} (C)	P_{AIR} (bar)	T_{AIR} (C)	N_{AIR} (mol)	P_{MAX} (bar)	Driver	Comments
10/19/96	197	Kerosine	90	0.1030	Hot	0.59	71.3	24.1	3.89	30% H2-Air, .9 bar, 0.5-in nozzle	Fuel temp unknown, 1/2 nozzle for 197-205
10/19/96	198	Kerosine	30	0.0345	Hot	0.59	73.2	24.0	-	30% H2-Air, .9 bar, 0.5-in nozzle	NOGO
10/19/96	200	Kerosine	50	0.0576	Hot	0.59	74.0	23.9	3.13	30% H2-Air, .9 bar, 0.5-in nozzle	
10/19/96	201	Kerosine	40	0.0460	Hot	0.59	73.4	24.0	-	30% H2-Air, .9 bar, 0.5-in nozzle	NOGO
10/19/96	202	Jet-A	90	0.1032	Hot	0.59	72.0	24.1	-	30% H2-Air, .9 bar, 0.5-in nozzle	NOGO, LAX fuel used in 202-205
10/19/96	203	Jet-A	180	0.2063	Hot	0.59	72.0	24.1	-	35% H2-Air, .9 bar, 0.5-in nozzle	NOGO
10/20/96	204	Jet-A	90	0.1073	Hot	0.59	86.0	23.1	4.54	35% H2-Air, 1 bar, 0.5-in nozzle	
10/20/96	205	Jet-A	50	0.0596	Hot	0.59	86.0	23.1	3.41	35% H2-Air, 1 bar, 0.5-in nozzle	
1/3/97	232	Kerosine	50	0.0531	61.7	0.59	46.5	26.0	-	30% H2-Air, 1 bar, 0.5-in nozzle	NOGO Runs 232 on used simplex spray nozzle
1/3/97	234	Kerosine	150	0.1591	50.0	0.59	46.3	26.0	-	30% H2-Air, 1 bar, 0.5-in nozzle	NOGO
1/3/97	236	Kerosine	50	0.0520	55.0	0.59	40.0	26.5	-	30% H2-Air, 1 bar, 0.5-in nozzle	NOGO
1/3/97	238	Kerosine	100	0.1106	80.0	0.59	60.0	24.9	-	30% H2-Air, 1 bar, 0.5-in nozzle	NOGO
1/4/97	239	Kerosine	100	0.1109	82.0	0.59	60.8	24.9	4.71	35% H2-Air, 1 bar, 0.5-in nozzle	
1/4/97	240	Kerosine	50	0.0558	84.0	0.59	62.9	24.7	2.80	35% H2-Air, 1 bar, 0.5-in nozzle	
1/4/97	241	Kerosine	40	0.0444	81.3	0.59	60.9	24.9	-	35% H2-Air, 1 bar, 0.5-in nozzle	NOGO
1/4/97	242	Kerosine	70	0.0775	82.4	0.59	60.1	24.9	3.64	35% H2-Air, 1 bar, 0.5-in nozzle	
1/4/97	243	Kerosine	60	0.0666	81.0	0.59	61.1	24.9	2.72	35% H2-Air, 1 bar, 0.5-in nozzle	
1/4/97	244	Kerosine	140	0.1559	80.0	0.59	62.1	24.8	4.85	35% H2-Air, 1 bar, 0.5-in nozzle	substantial condensation on windows, fittings leaking on fuel supply
1/5/97	245	Kerosine	100	0.1046	43.0	0.59	41.7	26.4	3.21	80/20 H2-O2, 1 bar, 1.0-in nozzle	repaired fuel supply
1/5/97	246	Kerosine	50	0.0526	41.2	0.59	43.8	26.2	1.67	80/20 H2-O2, 1 bar, 1.0-in nozzle	
1/5/97	247	Kerosine	50	0.0526	43.5	0.59	43.7	26.2	1.25	80/20 H2-O2, 1 bar, 0.5-in nozzle	
1/6/97	248	Kerosine	100	0.1005	21.4	0.59	29.5	27.4	2.08	80/20 H2-O2, 1 bar, 1.5-in nozzle	cold fuel mist
1/6/97	249	Kerosine	100	0.1011	21.5	0.59	31.3	27.3	1.60	80/20 H2-O2, 1 bar, 1.0-in nozzle	cold fuel mist
1/7/97	250	Jet-A	50	0.0495	21.4	0.59	24.7	27.9	0.98	80/20 H2-O2, 1 bar, 1.0-in nozzle	cold fuel mist, weak burn
1/7/97	251	Jet-A	100	0.0994	22.2	0.59	26.1	27.8	1.04	80/20 H2-O2, 1 bar, 1.0-in nozzle	cold fuel mist, weak burn
1/7/97	252	Jet-A	50	0.0502	41.1	0.59	29.0	27.5	0.99	80/20 H2-O2, 1 bar, 1.0-in nozzle	cold fuel mist, weak burn
1/7/97	253	Jet-A	100	0.1004	42.4	0.59	29.2	27.5	1.08	80/20 H2-O2, 1 bar, 1.0-in nozzle	cold fuel mist, weak burn
1/9/97	254	Kerosene	40	0.0493	106.2	0.59	97.7	22.4	3.20	35% H2-Air, 1 bar, 0.5-in nozzle	fuel should be all vapor for 254 to 265
1/9/97	255	Kerosene	50	0.0616	103.4	0.59	98.0	22.4	3.80	35% H2-Air, 1 bar, 0.5-in nozzle	
1/10/97	256	Kerosene	80	0.0989	102.7	0.59	99.1	22.3	0.64	35% H2-Air, 1 bar, 0.5-in nozzle	NOGO - 5 min wait after injection
1/10/97	257	Kerosene	60	0.0742	104.4	0.59	99.3	22.3	4.31	35% H2-Air, 1 bar, 0.5-in nozzle	
1/10/97	258	Kerosene	80	0.0988	103.0	0.59	98.8	22.3	4.81	35% H2-Air, 1 bar, 0.5-in nozzle	
1/10/97	259	Kerosene	100	0.1238	103.2	0.59	99.7	22.3	0.66	35% H2-Air, 1 bar, 0.5-in nozzle	NOGO
1/10/97	260	Kerosene	120	0.1487	102.2	0.59	100.0	22.3	0.71	35% H2-Air, 1 bar, 1.0-in nozzle	NOGO (driver too weak?)
1/11/97	261	Kerosene	100	0.1234	101.7	0.59	98.4	22.4	4.67	80/20 H2-O2, 1 bar, 0.5-in nozzle	

Date	Run No	Fuel	Vol. (ml)	Yfuel	T_{FUEL} (C)	P_{AIR} (bar)	T_{AIR} (C)	N_{AIR} (mol)	P_{MAX} (bar)	Driver	Comments	
1/11/97	262	Kerosene	120	0.1484	100.0	0.59	99.1	22.3	4.11	80/20 H2-O2, 1 bar, 0.5-in nozzle		
1/11/97	263	Kerosene	140	0.1734	100.0	0.59	99.8	22.3	-	80/20 H2-O2, 1 bar, 0.5-in nozzle	NOGO - driver too rich?	
1/11/97	264	Kerosene	140	0.1726	100.0	0.59	98.1	22.4	4.44	40/60 H2/O2, 1 bar, 0.5-in nozzle	excess O2 in driver	
1/11/97	265	Kerosene	100	0.1245	100.0	0.59	101.6	22.2	4.68	40/60 H2/O2, 1 bar, 0.5-in nozzle	excess O2 in driver	
1/12/97	266	Kerosene	100	0.1074	40.0	0.59	50.2	25.7	3.76	40/60 H2/O2, 1 bar, 0.5-in nozzle	30 min wait post-injection, lean driver	
1/12/97	267	JetA	100	0.1078	50.0	0.59	51.5	25.6	2.26	40/60 H2/O2, 1 bar, 0.5-in nozzle	30 min wait post-injection, lean driver	
1/12/97	268	Kerosene	100	0.1073	50.0	0.59	50.0	25.7	2.57	40/60 H2/O2, 1 bar, 0.5-in nozzle	NO ATOMIZER, 1 hr wait with fan on	
1/13/97	269	JetA	50	0.0506	21.0	0.59	31.4	27.3	0.65	40/60 H2/O2, 1 bar, 0.5-in nozzle	NO ATOMIZER, 1 hr wait with fan on, NO GO	
1/13/97	270	Kero	50	0.0507	21.5	0.59	32.3	27.2	0.65	40/60 H2/O2, 1 bar, 0.5-in	No Atomizer, 1 hr wait fan on, NO GO	
1/14/97	271	Jet A	50	0.0495	20.8	0.59	24.9	27.9	0.71	80/20 H2-O2, 1 bar, 0.5-in nozzle	spray fan on, 30 min fan off, mix 10 min, NO GO	
1/14/97	272	Jet A	50	0.0504	30.5	0.59	30.5	27.4	0.73	80/20 H2-O2, 1 bar, 0.5-in nozzle	spray fan on, 30 min fan off, mix 10 min, NO GO	New Jet A
1/14/97	273	Jet A	50	0.0512	35.0	0.59	35.2	26.9	0.74	80/20 H2-O2, 1 bar, 0.5-in nozzle	spray fan on, 30 min fan off, mix 10 min, NO GO	
1/15/97	274	Jet A	50	0.0521	40.0	0.59	40.7	26.5	0.77	80/20 H2-O2, 1 bar, 0.5-in nozzle	spray fan on, 30 min fan off, mix 10 min, NO GO	
1/15/97	275	Jet A	50	0.0529	45.0	0.59	45.6	26.1	0.84	80/20 H2-O2, 1 bar, 0.5-in nozzle	spray fan on, 30 min fan off, mix 10 min, NO GO	
1/15/97	276	Jet A	50	0.0538	50.0	0.59	50.6	25.7	0.93	80/20 H2-O2, 1 bar, 0.5-in nozzle	spray fan on, 30 min fan off, mix 10 min, NO GO	
1/15/97	277	Jet A	50	0.0546	55.0	0.59	55.6	25.3	1.16	80/20 H2-O2, 1 bar, 0.5-in nozzle	spray fan on, 30 min fan off, mix 10 min, NO GO	
1/15/97	278	Jet A	50	0.0554	60.0	0.59	60.3	24.9	1.32	80/20 H2-O2, 1 bar, 0.5-in nozzle	spray fan on, 30 min fan off, mix 10 min	
1/15/97	279	Jet A	50	0.0562	65.0	0.59	65.3	24.5	1.90	80/20 H2-O2, 1 bar, 0.5-in nozzle	spray fan on, 30 min fan off, mix 10 min	
1/16/97	280	Jet A	50	0.0572	70.0	0.59	71.5	24.1	2.53	80/20 H2-O2, 1 bar, 0.5-in nozzle	spray fan on, 30 min fan off, mix 10 min	
1/16/97	281	Jet A	50	0.0578	75.0	0.59	75.1	23.9	2.72	80/20 H2-O2, 1 bar, 0.5-in nozzle	spray fan on, 30 min fan off, mix 10 min	
1/16/97	282	Jet A	50	0.0587	80.0	0.59	80.4	23.5	3.31	80/20 H2-O2, 1 bar, 0.5-in nozzle	spray fan on, 30 min fan off, mix 10 min	
1/16/97	283	Jet A	50	0.0596	85.0	0.59	85.8	23.1	3.79	80/20 H2-O2, 1 bar, 0.5-in nozzle	spray fan on, 30 min fan off, mix 10 min	
1/17/97	284	Jet A	50	0.0621	100.0	0.59	101.1	22.2	3.50	80/20 H2-O2, 1 bar, 0.5-in nozzle	spray fan on, 30 min fan off, mix 10 min	
1/17/97	285	Jet A	50	0.0614	95.0	0.59	96.7	22.5	3.87	80/20 H2-O2, 1 bar, 0.5-in nozzle	spray fan on, 30 min fan off, mix 10 min	
1/17/97	286	Jet A	50	0.0606	90.0	0.59	91.8	22.8	3.45	80/20 H2-O2, 1 bar, 0.5-in nozzle	spray fan on, 30 min fan off, mix 10 min	
1/17/97	287	Jet A	50	0.0599	85.0	0.59	87.6	23.0	3.53	80/20 H2-O2, 1 bar, 0.5-in nozzle	spray fan on, 30 min fan off, mix 10 min	
1/18/97	288	Jet A	20	0.0249	100.0	0.59	102.2	22.1	1.02	80/20 H2-O2, 1 bar, 0.5-in nozzle	fill, mix 10 min, ignite NO GO	
1/18/97	289	Jet A	30	0.0373	100.0	0.59	100.9	22.2	2.13	80/20 H2-O2, 1 bar, 0.5-in nozzle	fill, mix 10 min, ignite weak GO	
1/18/97	290	Jet A	40	0.0497	100.0	0.59	101.2	22.2	3.10	80/20 H2-O2, 1 bar, 0.5-in nozzle	fill, mix 10 min, ignite	
1/18/97	291	Jet A	50	0.0622	100.0	0.59	101.4	22.2	3.92	80/20 H2-O2, 1 bar, 0.5-in nozzle	fill, mix 10 min, ignite	
1/18/97	292	Jet A	60	0.0748	100.0	0.59	102.3	22.1	4.30	80/20 H2-O2, 1 bar, 0.5-in nozzle	fill, mix 10 min, ignite	
1/18/97	293	Jet A	80	0.0998	100.0	0.59	102.6	22.1	4.62	80/20 H2-O2, 1 bar, 0.5-in nozzle	fill, mix 10 min, ignite	
1/18/97	294	Jet A	100	0.1247	100.0	0.59	102.4	22.1	4.62	80/20 H2-O2, 1 bar, 0.5-in nozzle	fill, mix 10 min, ignite	
1/18/97	295	Jet A	120	0.1494	100.0	0.59	101.8	22.2	4.57	40/60 H2/O2, 1 bar, 0.5-in	fill, mix 10 min, ignite	
1/18/97	296	Jet A	90	0.1121	100.0	0.59	101.8	22.2	4.75	80/20 H2-O2, 1 bar, 0.5-in nozzle	fill, mix 10 min, ignite	

Date	Run No	Fuel	Vol. (ml)	Yfuel	T_{FUEL} (C)	P_{AIR} (bar)	T_{AIR} (C)	N_{AIR} (mol)	P_{MAX} (bar)	Driver	Comments
1/18/97	297	Jet A	50	0.0622	100.0	0.59	101.2	22.2	4.09	80/20 H2-O2, 1 bar, 0.5-in nozzle	fill, mix 10 min, ignite
1/18/97	298	Jet A	25	0.0311	100.0	0.59	101.3	22.2	1.37	80/20 H2-O2, 1 bar, 0.5-in nozzle	fill, mix 10 min, ignite
1/18/97	299	Jet A	10	0.0124	100.0	0.59	101.0	22.2	0.71	80/20 H2-O2, 1 bar, 0.5-in nozzle	fill, mix 10 min, ignite
1/18/97	300	Jet A	0	0.0000	0.0	0.59	99.6	22.3	0.68	80/20 H2-O2, 1 bar, 0.5-in nozzle	baseline for 100 C tests, no fuel
1/27/97	301	Jet A	100	0.1034	40.0	0.59	38.3	26.7	1.06	80/20 H2-O2, 1 bar, 0.5-in nozzle	inject fuel into vacuum, wait 30, add air and mix 10 min NO GO
1/27/97	302	Jet A	500	0.5235	60.0	0.59	42.1	26.3	3.07	80/20 H2-O2, 1 bar, 0.5-in nozzle	inject fuel into vacuum, wait 30, add air and mix 10 min
1/28/97	303	Jet A	500	0.5228	60.0	0.59	41.7	26.4	2.87	80/20 H2-O2, 1 bar, 0.5-in nozzle	inject fuel into 35 kft, wait 30, add air and mix 10 min
1/29/97	304	Jet A	400	0.4188	40.0	0.59	42.1	26.3	2.77	80/20 H2-O2, 1 bar, 0.5-in nozzle	inject fuel into 35 kft, wait 30, add air and mix 10 min
1/30/97	305	Jet A	300	0.3148	40.0	0.59	42.8	26.3	2.71	80/20 H2-O2, 1 bar, 0.5-in nozzle	inject fuel into 35 kft, wait 30, add air and mix 10 min
1/31/97	306	Jet A	200	0.2091	40.0	0.59	41.6	26.4	2.22	80/20 H2-O2, 1 bar, 0.5-in nozzle	inject fuel into 35 kft, wait 30, add air and mix 10 min very weak GO
2/2/97	307	Jet A	150	0.1569	40.0	0.59	41.8	26.4	1.33	80/20 H2-O2, 1 bar, 0.5-in nozzle	inject fuel into 35 kft, wait 30, add air and mix 10 min looks self-sustaining
2/3/97	308	Jet A	700	0.7324	40.0	0.59	41.9	26.4	3.03	80/20 H2-O2, 1 bar, 0.5-in nozzle	inject fuel into 35 kft, wait 30, add air and mix 10 min

B GC-MS Analysis

A preliminary analysis of liquid and vapor Jet A composition was performed to get an appreciation for the typical fuel composition and the differences between liquid and vapor. This analysis was carried out[3] using an HP5890/HP5989A Gas Chromatograph-Mass Spectrometer (GC-MS) with a 30 m-long HP-1 column. A 1 μl sample of the liquid was analyzed and the total ion chromatogram is shown in Fig. 47. Time refers to retention time within the GC column. This has been normalized so that the highest peak is one. The carbon number is shown next to the main peaks in the spectrum. The MS analysis was used to identify a number of these peaks, the major ones are n-alkanes although many branched compounds and some ring compounds were also found. The MS was not set up to analyze for compounds with a molar mass less than 35 and the first observed peak is CO_2. Integration of the TIC yields a median carbon number of 12, corresponding to dodecane, for the liquid composition.

Using the same setup, we analyzed 100 μl of headspace gas from a vial of Jet A heated to 40°C. The normalized total ion chromatogram is shown in Fig. 48. Note that the retention time axis is expanded relative to that shown in Fig. 47. The integrated TIC yields a median composition of C6 to C7, corresponding to hexane or heptane. Since the components lighter than C4 cannot be analyzed by this method, the carbon number of the true median composition is overestimated. The two chromatograms clearly demonstrate the dramatic differences between liquid and vapor composition. The large number of components present in both phases illustrates the challenge of modeling Jet A as a multicomponent fuel.

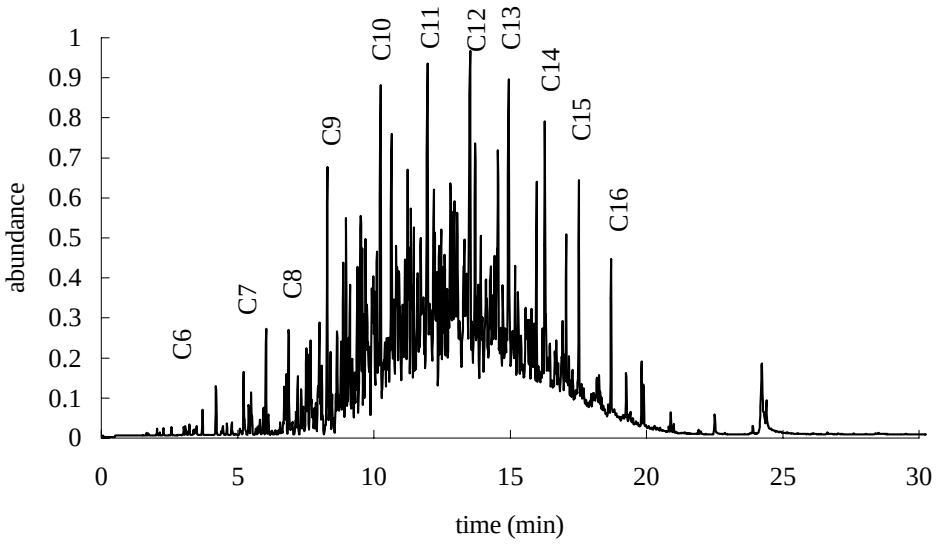

Figure 47: Normalized total ion chromatogram for LAX Jet A liquid.

[3]We thank Peter Green of the Caltech Environmental Analysis Center for setting up the equipment and advising us.

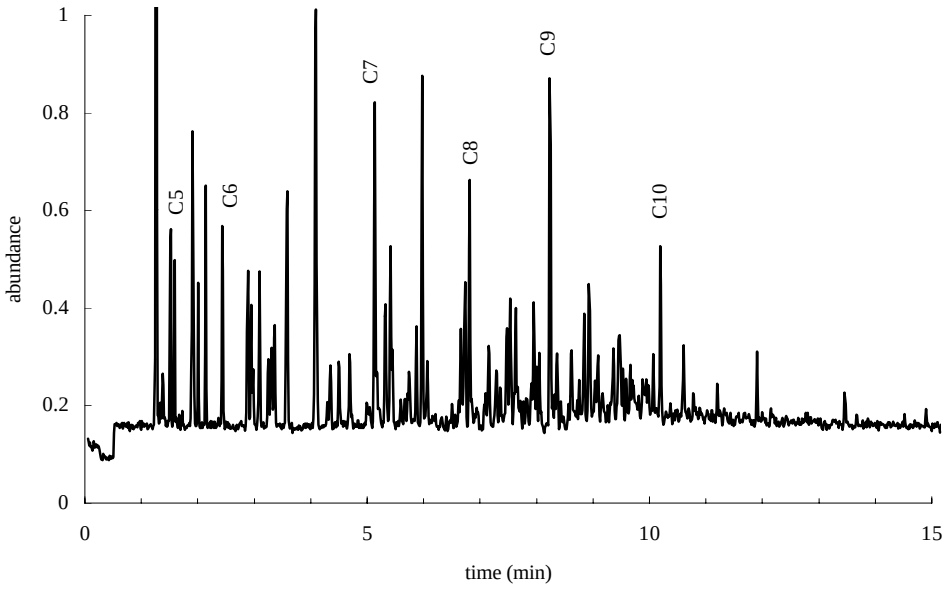

Figure 48: Normalized total ion chromatogram for LAX Jet A vapor. Obtained from the headspace of a 1.88 cc vial at 40°C, mass loading of about 300 kg/m^3.